University of Nottingham
UK | CHINA | MALAYSIA

Division of Molecular Therapeutics and Formulation

School of Pharmacy

Evaluation of cationic lipid-based liposomes as a delivery vehicle for DNA therapeutics into dendritic cells

Freya Leech, BSc., MSc.

Thesis submitted to the University of Nottingham

for the degree of Doctor of Philosophy

February 2024

Table of Contents

Abstract

DNA vaccines have been licenced for various purposes, including a therapeutic canine melanoma vaccine (Grosenbaugh et al, 2011), a prophylactic equine west nile virus vaccine (Davis et al, 2001), and more recently the ZyCov-D SARS-Cov-2 vaccine for humans (Khobragade et al, 2022). DNA vaccines are stable, immunogenic, and provide a safe non-live approach to inducing both humoural and cellular immune responses in immune-rich environments such as the skin. Successful delivery of these vaccines is determined by the carrier since DNA alone fails to initiate immune responses due to rapid clearance *in vivo*. It was theorised that the formulation of a cationic liposome-DNA complex with controlled physicochemical characteristics would result in efficient uptake and expression of encoded proteins by dendritic cells (DCs), an essential step in initiating systemic immune responses.

Cationic lipids interact electrostatically with the negatively charged DNA backbone, resulting in a stable DNA-liposome complex with tunable characteristics. In this thesis, a well characterised liposomal formulation composed of DC-Cholesterol and DOPE was selected for initial evaluation. Liposomes were prepared by the thin film method at different molar ratios of DC-Cholesterol: 25 mol%, 30 mol%, 35 mol%, 40 mol%, and 50 mol%. Formulations were combined with DNA at nitrogen: phosphate (NP) ratios of 3, 6, 9, and 12. Hydrodynamic size, zeta potential, and encapsulation efficiency were all measured alongside morphology by cryogenic transmission electron microscopy and fusion studies using fluorescence resonance energy transfer. Liposomes containing 35 mol% DC-Cholesterol and higher formed stable complexes with 100% encapsulation efficiency regardless of NP ratio. To balance the need for stability, an overall positive complex charge, and DOPE content, liposomes composed of 40 mol% DC-Cholesterol were taken forward into transfection studies.

A panel of cell lines consisting of the human embryonic kidney cell line HEK293T, the murine fibroblast cell line NIH 3T3, and the murine dendritic cell line DC2.4 were selected for *in vitro* transfection studies. Liposomes were labelled with the lipophilic dye DiD and combined with a model plasmid encoding for green fluorescent protein and incubated with each cell line. Cells were stained with a live dead stain and assayed by flow cytometry. Uptake was evaluated by the percentage of live cells positive for DiD-associated fluorescence; more than 90% of live cells showed uptake, regardless of cell line or NP ratio. GFP expression was evaluated by measuring the percentage of live cells positive for GFP. Expression was dependent on both cell line and NP ratio, where the expression was highest in HEK293T cells, moderate in NIH 3T3 cells, and low in DC2.4 cells. Endosomal trapping was investigated as a potential mechanism limiting GFP expression by pretreating cells with chloroquine diphosphate, an endosomal disruptor. No difference in GFP expression was observed, either in population of cells positive for GFP or mean fluorescence intensity, suggesting endosomal trapping is not a limiting factor. In a balb/c murine vaccination study, *in vivo* immune responses to DC-Chol/DOPE liposomes containing 40 mol% DC-Cholesterol and a model SARS-Cov-2 pDNA combined at NP ratios of 3 and 9 were measured. Liposome doses were injected subcutaneously on days 1, 8, and 15 before being sacrificed on day 19. Antigen-specific serum antibody responses were measured by enzyme linked immunosorbent assay (ELISA) and splenocyte responses were measured by ELISpot. No immune responses were detected in response to liposomes formulated with DC-Cholesterol and DOPE.

It was subsequently hypothesised that exchanging DC-Cholesterol with the multivalent cholesterol based lipid GL67 would improve GFP expression in dendritic cells, and that doing so would correlate with better immune responses *in vivo*. It was also hypothesised that inclusion of linolenic acid, a fatty acid that has been shown to directly interact with dendritic cells along with its metabolites, may increase GFP expression. When linolenic acid was included with either DC-Chol/DOPE or GL67/DOPE, no difference in GFP expression was observed when compared to formulations without linolenic

acid. Liposomes formed of 40 mol% GL67 and 60 mol% DOPE initiated strong expression of GFP in DC2.4 cells in a screening study, however, when taken forward into HEK293T and NIH 3T3 cells and three biological repeats carried out in all three cell lines, strong variation was observed in GFP expression. This may be linked to cell toxicity, cell variation, batch variation, temperature, or other unknown variables since the literature rarely describes both technical and biological replicability.

Overall, this study has demonstrated that multivalency is an important and so far underexplored factor in cationic lipid choice for liposomes for dendritic cell delivery. Liposomes formulated with the multivalent cationic lipid GL67 appeared to elicit stronger expression of GFP in DC2.4 cells than liposomes formulated with DC-Cholesterol, although variation between biological replicates impeded conclusive comparisons and highlighted a key gap in the literature in describing replicability. This provides key information for the future development of cationic liposome formulation for dermal dendritic cell transfection and vaccination.

Covid Impact Statement

The work in this thesis was impacted by the restrictions imposed due to the COVID-19 pandemic. From March to September 2020, access to laboratory work at the university was very restricted and research activities primarily consisted of work from home. This prevented any laboratory-based experiments from being undertaken. Between September 2020 and September 2021, strict laboratory occupancy limits were enforced and access to experimental instruments for the work was severely impacted. For example, the cell culture laboratory was limited to single occupancy, and flow cytometry, via my industry partner, was extremely difficult to access. In order to allow users fair access to laboratory space, a booking system was introduced; however due to user competition, experiments were not always able to be completed. Office use was restricted due to air circulation difficulties and non-laboratory work had to be carried out from home, hindering productivity without access to proper working environments and routines. Training on equipment was also delayed due to group size restrictions. Although these restrictions ended in September 2021, the hangover effects of the pandemic continued to affect research for longer due to supply chain issues and shortages. Personal health and wellbeing was also significantly negatively affected by the pandemic and associated events.

As a result of the restrictions, the original aims of this project were adjusted. Initial aims had included investigating dendritic cell activation/maturation by liposomes, measured by cell surface markers using flow cytometry, and progressing to dendritic cell/T cell coculture. Focus was instead shifted to reformulating liposomes. Also, prior to the pandemic, this project focused on evaluating these liposome formulations for a melanoma pDNA vaccine but shifted focus to COVID-19.

Acknowledgements

I would like to thank my supervisors, Dr Maria Marlow, Dr Pavel Gershkovich, and Prof Lindy Durrant. The lessons you have taught me are ones that will last a lifetime, and this thesis would not have been the same without your constant guidance and feedback.

A huge thank you to the Marlow group, my D20 office mates, the D13 cell culture group, and especially the Drs Tejasvi Shivakumar, Fiona Smith, and Abdullah Aljasser. Thank you to Dr Julie Watts at the nmRC, and the entire team at Scancell. Thank you to the BBSRC DTP and Sandra, Farrah, Matthew, and Kirstin, the unsung non-academic heroes. There are too many more to name and I suspect many of you will never know how much you helped, but I appreciate you.

Perhaps most importantly, thank you to my own personal support system. To my two cats, Marley and Socks, who brightened every virtual meeting despite never being invited. My best friend Emilia Copeland, who consistently reminded me at all the perfect moments that life exists outside the PhD and it is there to be lived. My beloved in-laws, the Leechs and the Woods, for whom I am incredibly grateful that I get to call family.

And absolutely most importantly, to my husband Andrew, who has exhibited complete and unwavering faith and patience in me: I could never have done this without you.

List of posters and presentations

1. Poster: Transfection efficiency of DNA-liposome complexes in a dendritic cell line. *UK & Ireland Controlled Release Society, Manchester, June 2020*
2. Presentation: Cationic liposome-DNA complexes induce cellular protein expression in a cell line dependent fashion. *Nottingham BBSRC Doctoral Training Partnership, April 2022*
3. Poster: Cationic liposome-DNA complexes induce cellular protein expression in a cell line dependent fashion. *Academy of Pharmaceutical Sciences, Belfast, September 2022*

List of figures

List of tables

Chapter 1: Intradermal delivery of DNA vaccines

1.1 Nucleic acid-based vaccines; requirements and future potential

Vaccine is a term broadly given to antigenic preparations designed to initiate long-lasting protective immunity against a variety of diseases; historically, this has involved the preparation of attenuated or inactivated forms of the disease which are limited by complexity of preparation, variable efficacy, and potential risks (Lu et al, 2024). For example, the BCG vaccine against mycobacterium tuberculosis is considered to be the globally most widely-used vaccine but is extremely variable in its efficacy, the duration and strength of its effectiveness determined by mycobacterium strain variation and mutation, route of administration, patient age, and geographical location (Dockrell and Smith, 2017). More recently, the COVID-19 pandemic has illustrated the challenge of rapid pathogenic mutation on vaccine design; normal declines in protection over time (Feikin et al, 2022) were exacerbated as formulations against earlier strains suffered from reduction in efficacy against newer mutations (Malik et al, 2022). Immune evasion by antigenic mutation has also been observed in human immunodeficiency virus and influenza (Weisblum et al, 2020) and is a hallmark of cancer progression (Hanahan and Weinberg, 2011).

In addition, challenges to vaccine development include disruptions to global vaccinations and increasing likelihood of encountering new pathogens. The Vaccine Impact Modelling Consortium suggested that disruptions to global vaccination efforts due to the COVID-19 pandemic could be responsible for up to 967,000 additional deaths between the years of 2020 and 2030, but that intensified vaccination regimes may avert up to 79% of these deaths (Hartner et al, 2024). Additionally, a meta-analysis of global historical epidemics dating back to 1600 identified an increasing rate of pandemic occurrence resulting in a 44% chance of reliving another pandemic of a similar intensity experienced in COVID-19 in one's lifetime (Marani et al, 2021). All of these factors illustrate the need for safe and widely effective vaccines, particularly ones with the potential for rapid development.

Nucleic acid vaccines such as DNA or mRNA vaccines attracted global attention in 2020 when several mRNA vaccines against SARS-Cov-2 received emergency use authorisation from the United States Food and Drug Administration (US FDA), less than one calendar year from pathogen identification and sequencing (Bok et al, 2021). Although the speed of the development is partially attributable to expedited logistics in funding grants, collaborations, and other stages of development, nucleic acid vaccines as a technology lends itself to rapid development (Chakraborty et al, 2023). Either mRNA or DNA are modified to encode for a selection of target antigens before being coupled to a carrier, which enhances uptake and protects the nucleic acid from degradation *in vivo* (Conde et al, 2023). Upon delivery, cells translate the genetic transcripts into protein and produce the antigen using innate protein and antigen processing pathways, which then initiates an immune response.

The first nucleic acid vaccines licenced for use in humans were based on mRNA and provided immunity against the spike protein on SARS-Cov-2, notably the BNT162b2 vaccine developed by Pfizer/BioNTech (Polack et al, 2020) and the mRNA-1273 vaccine developed by Moderna (Jackson et al, 2020; Baden et al, 2020). Since the main challenge of delivering mRNA is its inherent instability and susceptibility to degradation prior to translation, both vaccines condensed the mRNA in lipid nanoparticles. Formation of these nanoparticles relies on careful lipid selection and the essential inclusion of lipids that supply positive charges, which form stable electrostatic bonds with the negative charges in mRNA and enable its crossing of cell membranes (Chen et al, 2022). In comparison, the DNA-based vaccine ZyCov-D offered lower but still significant protection against SARS-Cov-2 when the plasmid was delivered intradermally by needle-free injection (Dey et al, 2021; Khobragade et al, 2022). Plasmid DNA offers key advantages over mRNA such as increased stability, ease of manufacture, and lower toxicity, although suffers from the added challenge of needing to cross the nuclear membrane which is not required by mRNA (Liu, 2019).

Currently licenced DNA vaccines attribute their effectiveness to additional adjunctive effects in their formulation. A pDNA vaccine encoding for human tyrosinase was shown to significantly increase survival time in canines with oral malignant melanoma (Grosenbaugh et al, 2011). This effectiveness came from its xenogeneic properties; the canine host cells transcribed human tyrosinase, which is 85% homologous to canine tyrosinase. Its presentation on host cells enabled immune recognition of the protein, while being different enough to elicit an immune response where canine tyrosinase would have induced immune tolerance (Grosenbaugh et al, 2011). Similarly, a pDNA vaccine against West Nile virus yielded immune protection that varied by species; a single intramuscular injection of the pDNA vaccine induced 100% protection in horses but required electroporation to be effective in mice (Davis et al, 2001). In fish crows, a single intramuscular injection prevented death but not infection (Turell et al, 2003). DNA vaccines in humans have encountered challenges initiating immune responses while remaining well-tolerated in terms of toxicity, requiring a broad immune response that includes both cellular and humoural immune cell types capable of both high frequency and high avidity responses (Xue et al, 2016).

1.2 Antigen specific responses for prophylactic and therapeutic vaccination

Therapeutic and prophylactic vaccination differ slightly by method of action; therapeutic vaccines such as cancer vaccines are administered to patients already suffering from the disease with the aim to either cure or simply improve symptoms (Noguchi et al, 2013). Prophylactic vaccines are administered to healthy people with the aim to induce immune memory against an antigen, to prevent or reduce severity of future infections without necessarily requiring an immediate immune response (den Hartog et al, 2019). Both rely on established stages of immune response; innate or passive immunity scans the microenvironment for indications of tissue damage or dangerous pathogens and recruits adaptive or active immunity through antigen presentation (Pradeu and Cooper, 2012). Adaptive immune

cells are then capable of forming immune memory, where innate immune cells are not (Natoli and Ostuni, 2019). Adaptive immunity is a longer-term process involving an exhaustive array of cell types, subtypes, and phenotypes that precisely respond to the antigenic threat based on its origin and location, often in a coordinated response involving what are termed humoral and cell-mediated responses (Zhang et al, 2022).

The type and extent of adaptive immune response is driven by dendritic cells (DCs), which pervade all tissues in a highly endocytic state and constantly sample antigens local to their environment (Carroll et al, 2024). Antigen acquisition involves a series of phenotypic changes, termed "activation", that allow the DCs to initiate nonspecific immune responses and present antigen to naïve T cells for antigen specific adaptive immune responses necessitated by three signals. DCs process and express antigen on major histocompatibility complex (MHC) receptors 1 and 2 (see section 1.3), which interact with the T cell receptor (TCR) (signal one) alongside costimulatory receptors (signal two) and cytokines (signal three) to determine the T cell response (Clark et al, 2019). The presence of costimulatory receptor and cytokines are required for T cell activation and specific types determine type of response; for example, DC recognition of cytoplasmic double stranded DNA occurs through toll-like receptor 9 (TLR9) which induces production of interferon gamma and other proinflammatory cytokines and increases expression of costimulatory receptors (Kis-Toth et al, 2011). This has the downstream effect of activating CD8+ T cells that produce interferon gamma and granzyme, a key protein in cell-mediated target cell death, alongside B cells that produce complement-fixing antibodies including immunoglobulin G1 and G3 (IgG1 and IgG3). The process of activating dendritic cells to selectively deliver the three signals required for T cell activation is referred to as "licencing" and is necessary for sufficient T cell activation (Thaiss et al, 2011).

When innate immune responses are insufficient in resolving the cause of cell damage or infection, the antigen specificity of adaptive immune responses provides a more targeted response. T cells include a variety of

subsets involved in cell-mediated and humoural immunity as well as immune regulation and memory, with some plasticity and functional overlap (Raphael et al, 2015). T cell subsets have historically been defined by their unique cytokine profiles and expression of either CD4 or CD8, receptors that recognise their dendritic cell costimulatory receptor counterparts. T cells expressing CD8 are also called cytotoxic T cells and are characterised by strong interferon gamma production and cell killing ability (Mosmann and Sad, 1996). In contrast, T cells expressing CD4 are generally termed T helper cells, due to their ability to influence and recruit other cells of the immune system. T helper type 1 cells are involved in cell-mediated inflammatory reactions including cytotoxic T cell support, interferon gamma production, and delayed-type hypersensitivity reactions, while T helper type 2 cells are involved in systemic humoural reactions such as B cell help, antibody production, and allergy (Mosmann and Sad, 1996; Raphael et al, 2015). Both CD8 and CD4 are referred to as coreceptors and are responsible for anchoring the TCR to MHC 1 and 2 respectively (Figure 1). These interactions determine the type of T cell-mediated immune response, which requires the simultaneous activation of costimulatory receptors such as CD28 (Brownlie and Zamoyska, 2013). In contrast, coinhibitory receptors such as programmed death receptor 1 (PD-1) or cytotoxic T-lymphocyte-associated protein 4 (CTLA-4) can induce antigenic tolerance in T cells (Rotte, 2019). All of these T cell subsets orchestrate immune responses specific to the antigen which is recognised by their T cell receptor; the mechanism of T cell maturation in the thymus deletes T cells that possess TCRs that either do not recognise self MHC, or are overly reactive to self MHC, effectively ensuring that the only T cells that survive to

maturity are ones that recognise antigens in need of immunogenic clearance (Kosmrlj et al, 2008).

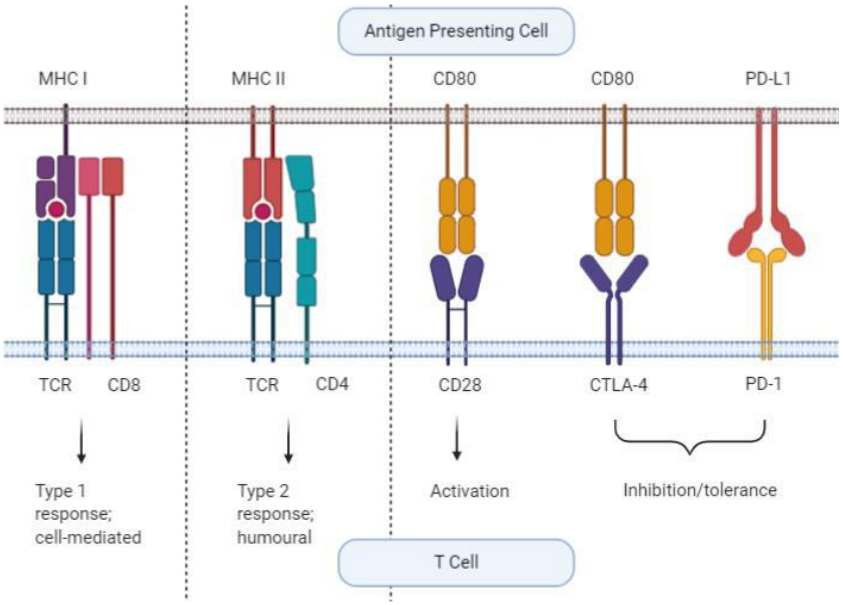

Figure 1. Type and amplitude of T cell-mediated immune response is determined through ligation of the TCR and coreceptors with MHC. Interactions with costimulatory receptors initiate proinflammatory responses, while coinhibitory receptors induce antigenic tolerance.

Uniquely, B cells are capable of presenting antigen to T cells as well as sampling antigen from dendritic cells, but are activated by a combination of antigen engagement and chemokine exposure (Goodnow et al, 2010). Once activated, B cells differentiate into one of three phenotypic fates: antibody-producing plasma cells, germinal centre B cells that proliferate and produce plasma cells, or long-lived circulating memory B cells that retain the antigen specificity alongside differentiation potential. The B cell marker CD40 is also switched off during differentiation, having been linked to the proliferation and survival of B cells and their differentiated counterparts (Lane et al, 1992). The authors demonstrate that its ligand is expressed on 90% of activated CD4+ T cells and its inhibition suppresses B cell proliferation, but also that its expression can be induced by B-T cell interactions. Antibodies themselves possess one of five essential isotypes that operate in distinct places with distinct effector functions. For example, immunoglobulin G (IgG) circulates in blood and extracellular fluid, opsonising pathogens and activating complement, a group of proteins adept at killing dangerous cells such as those infected by SARS-Cov-2 (Noris et al,

2020). Antibodies are generally considered the classical example of humoural immunity due to their diversity in phenotype and effector functions as well as the sensitivity and specificity of detection assays such as the enzyme linked immunosorbent assay (ELISA) (Noval et al, 2021).

Both T cell and B cell function and activation are driven in large part by dendritic cells, which is particularly observable in some immune-altered disease states. Using a human organotypic skin melanoma model, Blasio et al (2020) showed that dendritic cells could have the cluster of differentiation 14 (CD14) marker upregulated by three different melanoma cell lines, indicating influence towards an immunosuppressive phenotype. Although tumour-resident DCs are needed to licence anti-tumour activity of migratory T cells, tumour-mediated immunosuppression is often characterised by a decrease in DC numbers, impacting immunotherapy efficacy (Santana-Magal et al, 2020). This effect could be reversed by intradermal administration of a whole-cell DC vaccine, which increased immune infiltration into tumours and encouraged a systemic humoural and cell-mediated anti-tumour response (Bulgarelli et al, 2019). This has strong implications in developing therapeutic cancer vaccines – the phenotype and activation status of dendritic cells affects not only the local microenvironment but also T and B cell responses. Therefore, the signalling pathways and determining factors that determine antigen expression and DC activation must be considered when investigating nanoparticle vaccine delivery.

1.3 Intracellular uptake and antigen expression pathways

Nonviral gene delivery to any cell type depends on crossing the cell membrane before the complex is processed and translated into protein. This is challenging for most complexes to do passively due to their hydrophilic surface and large diameter, and consequently endocytosis has been observed as the predominant mechanism for complex internalisation (Khalil et al, 2006). Endocytosis pathways include clathrin-mediated, caveolae-mediated, and clathrin/caveolae-independent endocytosis as well as macropinocytosis, which all differ in coat composition and can affect the

fate of the internalised complexes. For example, cationic DNA-chitosan polyplexes transfected in HeLa cells showed highly efficient uptake in clathrin-independent endocytosis as well as endocytic escape into the cytoplasm (Garaiova et al, 2012). Endocytic escape is essential for successful uptake and transfection of many formulations which take advantage of receptor-mediated endocytosis through the inclusion of receptor ligands (Hinuma et al, 2022; Lorenz et al, 2011). Other nanoparticles evade endocytosis entirely, relying on integration with the cell membrane (Li et al, 2017). The specific machinery involved in endocytosis is heterogeneous and cell-dependent, and is experimentally investigated by using pharmacological inhibitors, cell lines with endocytosis proteins knocked down or mutated, or reduction in temperature to suppress endocytosis (Iversen et al, 2011).

Endocytosis is altered in dendritic cells due to their roles in antigen sampling, processing, and presentation on MHC 2 which strongly involve endocytic vesicles (Sabado et al, 2007). Nucleated non-antigen presenting cells are generally only capable of presenting endogenous antigen on MHC 1 and do not constitutively express MHC 2, except in states of dysregulation. MHC 2 expression on tumour cells can suppress anti-tumour immune responses (Johnson et al, 2016) and in hypersensitivity disorders, its induction on mast cells contributes to pathogenesis (Kambayashi et al, 2009). Expression of exogenous antigen on MHC 2 involves delayed acidification of endosomes, reduced acidity of lysosomes, and activation-dependent regulation of MHC trafficking to and from the cell membrane (Roche and Furuta, 2015). This is due to the need for proteolysis of whole antigen into peptides suitable for MHC binding without complete antigen degradation. Processing of exogeneous antigens through the MHC class 2 pathway occurs within the endosome, in which MHC 2 molecules exit the rough endoplasmic reticulum bound to an invariant chain that occupies the antigen binding site. When the MHC-containing endosome fuses with an endosome containing antigenic material, the invariant chain is exchanged for the exogeneous antigen peptide and the final complex transported to the cell membrane for expression (Blum et al, 2013). Although most

endocytosis receptors are recycled through early endosomes, in dendritic cells MHC processing in late endosomes and lysosomes is facilitated by certain endosomal receptors such as the multilectin receptor DEC-205 (Mahnke et al, 2000). This is different to the pathway for endogenous antigen expression on MHC 1; endogenous antigens are processed into peptide fragments in the cytosol before entering the rough endoplasmic reticulum where they are bound to an MHC 1 molecule and transported to the cell surface (Ackerman and Cresswell, 2003). Both of these pathways are utilised when DCs are transfected with immunogenic complexes; an endocytosis receptor ligand conjugated with polyethyleneimine (PEI) and bound to plasmid DNA elicited both MHC 1 and 2 expression in mouse bone marrow-derived DCs (Diebold et al, 2001). However, the high toxicity of PEI *in vivo* has prevented extensive use without additional modifications and the induction of effective DC antigen presentation through plasmid DNA transfection requires a careful balance of toxicity/immunogenicity and safety (Israel et al, 2015).

Delivery of DNA-encoded antigen encounters a challenge in achieving presentation on MHC 2, since this pathway relies on antigen sampling in the microenvironment and DNA delivery induces endogeneous antigen production. However, there are mechanisms by which this can be overcome. Dendritic cells can present antigens released by apoptotic cells (Rovere et al, 1998) or directly from stromal cells such as fibroblasts, which have the additional ability to induce dendritic cell activation or tolerance (Khosravi-Maharlooei et al, 2016). DCs are also capable of cross-presenting exogeneous antigen on MHC 1, albeit through unknown endosomal mechanisms seemingly dependent on cell activation status (Segura et al, 2009; Gutierrez-Martinez et al, 2015). Cross expression of endogenous antigen on MHC 2 is inducible during activation (ten Broeke et al, 2013), largely due to antigen sampling within the cell itself by a process called macroautophagy (Dengjel et al, 2005). Expression level by number of MHC molecules is also determinative of immune response; where individual TCR-MHC receptor interactions are measured by strength of affinity, the overall cell-cell interactions measure total strength across all receptor interactions,

termed “avidity”, and is an important predictor of immune response (Kumbhari et al, 2020; Xue et al, 2016). High avidity TCR-MHC interactions can be achieved by effective antigen processing as well as the careful selection of immunogenic peptide epitopes for encoding on DNA. Although nanoparticle design strongly affects DC expression, the role of dendritic cells in initiating immune responses does not exist in a vacuum and can also be affected by the behaviour and phenotype of neighbouring cells.

1.4 Intradermal cell populations for immune response initiation

DNA delivery to dendritic cells must consider the environment in which they are plentiful. The skin is a rich immune organ, structured into three layers (Nguyen and Soulika, 2019); the outermost layer called the epidermis, the central layer called the dermis, and the innermost layer consisting of subcutaneous fat. The epidermis is divided into layers (Figure 2), the innermost of which is the stratum basale, composed of immune cells such as Langerhans cells and T cells, melanocytes, and basal keratinocytes.

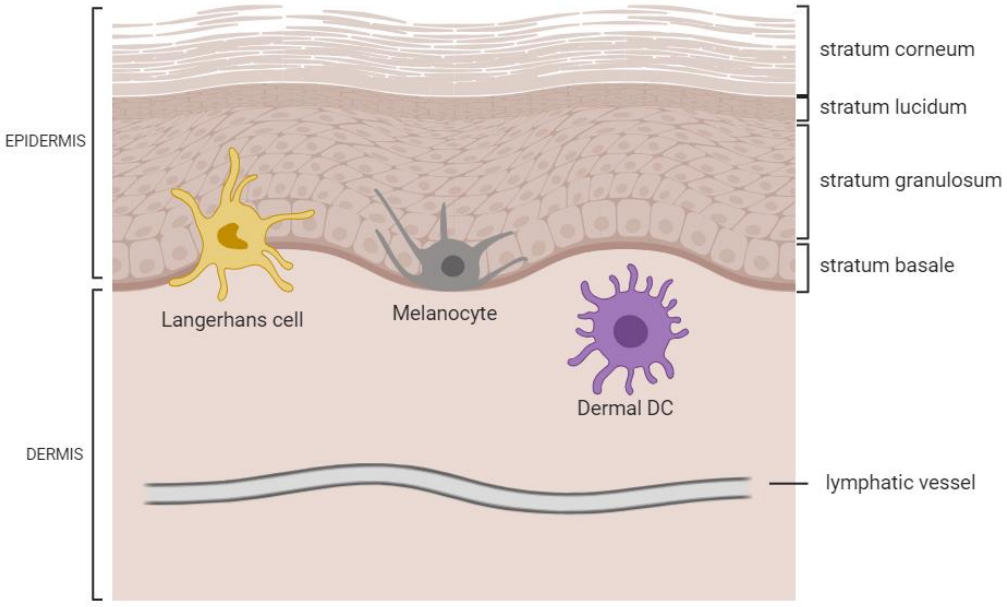

Figure 2. Major structures found within the skin.

The basal keratinocytes continuously supply the layers above with keratinocytes, forming a live keratinocyte layer that produce keratin filaments called the stratum granulosum. As keratinocytes reach the surface of the skin, they form a clear layer of dead cells called the stratum lucidum

and a tough, impermeable outermost layer of terminally differentiated corneocytes called the stratum corneum. Keratinocyte targeting for DNA vaccines have been explored by topical application of peptide complexes (Vij et al, 2015), but the strength of the stratum corneum barrier usually necessitates strategies that involve piercing it (Foldvari et al, 2006; Zakrewsky et al, 2015). The dermis can form extensions that protrude into the epidermis to supply lymphatic drainage and capillary blood supply, called the papillary dermis, while the reticular dermis is composed of immune cells including macrophages, lymphocytes, and mast cells as well as fibroblasts that secrete the supporting extracellular matrix (Nguyen and Soulika, 2019). The immune cell supply in the upper dermis, lower epidermis, and dermoepithelial junction make this zone the preferred target for DNA therapeutics in the skin (Chen et al, 2010; Sun et al, 2019)

Dendritic cells exist both in circulation and in nearly every tissue in the human body but form an essential part of the skin's immune barrier as langerin positive Langerhans cells and as dermal dendritic cells (Romani et al, 2011). A range of dendritic cell phenotypes populate the skin, with varying capabilities of eliciting cytotoxic or T cell responses, categorised by route of differentiation and often correlating with function (Eisenbarth, 2019). Antigen uptake occurs in dermal DCs and is processed and presented on MHC class I and II; activated DCs migrate to the lymph node (LN) where a rich source of naïve T cells are located (Egawa and Kabashima, 2020). Antigens originating in the dermal environment can also migrate to the lymph node before being taken up by lymph node dendritic cells (Tozuka et al, 2016), and involvement of the lymph node is thought to be an essential part of dermal immunity. T cells activated by specific antigens upregulate expression of homing molecules specific to the origin of antigen, such as E-selectin and P-selectin for skin homing (Issekutz and Issekutz, 2002). Upon contact with the target antigen in situ, T cells produce large quantities of proinflammatory cytokines and initiate cell death by production of perforin and granzyme, among other cell-mediated mechanisms (Egawa and Kabashima, 2020). Activated T cells also activate B cells through CD40 and CD40 ligand, which has a reciprocal activating effect on effector T cells and

antigen presenting cells; administration of a CD40 agonist in a murine tumour model resulted in a shift in phenotypes of effector T cells, antigen presenting cells, and secreted cytokines in favour of anti-tumour responses (Byrne and Vonderheide, 2016).

Dermal stromal cells also provide integral immune support and regulation. Keratinocytes are the most dominant cell type in the skin, proliferating and differentiating to continually supply the epithelium with new cells. This proliferation is essential in wound healing and defence; these microenvironments are strongly influenced by keratinocyte secretion of immune-modulating cytokines in response to pathogen recognition by toll-like receptors (TLR) (Piiponen et al, 2020). Furthermore, keratinocytes express the integrins αvβ6 and αvβ8, which allow transforming growth factor beta (TGF-β) to become biologically active. TGF-β is an essential growth factor for Langerhans cell migration to the lymph node upon activation (Mohammed et al, 2016). In inflammatory disease states, keratinocyte autocrine secretion of proinflammatory cytokines drives the dysregulated microenvironment and sustains T cell and Langerhans cell responses (Xu et al, 2021). Conversely, in cases of vitiligo where dermal autoimmunity results in the destruction of melanocytes, keratinocyte production of the chemokines CXCL9 and CXCL10 provide T cell homing signals that results in finely tuned T cell recruitment and localisation within the skin. The pathogenesis of vitiligo was found to be driven almost exclusively by keratinocyte control of the microenvironment, where individual immune cell populations were not essential (Richmond et al, 2017). This kind of cell control is important given the continual remodelling of the skin originating from the basal layer; epithelial basal cell density has been observed to regulate immune cell density and positioning in a regular tiling pattern (Park et al, 2021). Single cell transcriptomic analysis by RNA sequencing identified keratinocyte subsets that correlated with normal epidermal function, but differentially overexpressed MHC 1 molecules and could directly present antigen to T cells when in a psoriatic state (Liu et al, 2022; Klicznik et al, 2018).

Dermal fibroblasts are a heterogeneous cell population responsible for the synthesis and remodelling of the extracellular matrix in the skin with comprehensive roles in immune regulation, both in physiological and disease states. Derived from mesenchymal cells, they are essential in skin structural support and both secrete and respond to cytokines, chemokines, and growth factors. During inflammation, fibroblasts directly communicate with a variety of immune cells including neutrophils, B cells, T cells, and macrophages to increase cell migration, maturation, proliferation, and adhesion (Stunova and Vistejnova, 2018). Similarly to keratinocytes, fibroblasts moderate the pathogenesis of vitiligo through production of CXCL9 and CXCL10 (Xu et al, 2022) and atopic dermatitis through proinflammatory cytokine production (He et al, 2020). However, fibroblast-mediated immune regulation occurs extensively through cell-cell interactions directly with dendritic cells. Fibroblasts interact with dendritic cells via β2 integrins on DCs via CD90 and ICAM-1 on fibroblasts, inducing dendritic cell maturation that upregulates MHC and costimulation receptor expression alongside DC-mediated cytokine secretion more effectively than DC activation by bacterial lipopolysaccharide (Saalbach et al, 2007). During dengue virus infections, fibroblast-activated dendritic cells increased production of type 1 interferons and elicited moderate T cell proliferation despite virally compromised antigen presentation mechanisms (Montes-Gomez et al, 2020). Conversely, cancer-associated fibroblasts can induce strongly immunosuppressive environments by polarising macrophages towards an immunosuppressive phenotype, inducing myeloid-derived suppressor cells, and reducing dendritic cell antigen presentation and activation (Davidson et al, 2021).

Alongside extensive local regulation of innate immunity by fibroblasts, dendritic cells, and keratinocytes, the presence and biology of lymphatic vessels allow for adaptive immune cell recruitment and support (Lane et al, 2018). Not limited to passive transport, lymphatic capillaries and endothelial cells are highly responsive to inflammation, where fluid transport is tightly controlled and adhesion molecules and chemokines upregulated for essential DC trafficking. Following viral infection or

vaccination with viral subunits, lymphatic endothelial cells have been found to scavenge and store antigen dependent on dose and inflammation of the microenvironment for future memory immune responses (Tamburini et al, 2014). This can backfire where autoreactivity is concerned; lymphatic epithelial cells can induce T cell tolerance to neoplasms and reduce immune cell recruitment to the tumour site, but also facilitate tyrosinase-specific T cell autoimmunity in vitiligo (Lund et al, 2016). Regardless, lymphatic vessels support a unidirectional interstitial fluid flow and are lined with highly endocytic and permeable endothelial cells with approximately 100 μm gaps between them. These and their expression of key dendritic cell-specific adhesion molecules and chemokines are essential for DC recruitment into the tissues as well as migration towards local lymph nodes (Randolph et al, 2005). Immunostaining and microscopy of skin obtained from human plastic surgery patients revealed a spatial relationship between dendritic cells and lymphatic vessels, suggested to be linked to dendritic cell behaviour. Dendritic cells that exhibit strongly dendritic morphology less than 30 μm below the dermoepithelial junction had predominantly interstitial locations, suggesting activated and patrolling behaviour. Dendritic cells more than 150 μm below the dermoepithelial junction had a more rounded morphology and perivascular locations, suggesting increased motility (Wang et al, 2014). It is clear that the regulation of immune responses in the skin are regulated by nonimmune bystander cells as well as self-renewing dendritic and Langerhans cell populations and migratory immune cell recruitment. Successful delivery strategies to the skin and the initiation of antigen-specific immune responses will need to consider the dermal environment as a complex system.

1.5 Intradermal DNA delivery

Naked DNA delivered to the skin is prone to degradation at various stages of delivery, from significant tissue degradation to enzymatic degradation in the cytoplasm by DNAses (Elnekave et al, 2011). In a study investigating biodistribution of a multiantigen naked DNA vaccine by quantitative

polymerase chain reaction, researchers compared intravenous, intramuscular, and intradermal delivery of injections containing 200 μg pDNA. The plasmid persisted the longest in situ when administered intradermally and reached all lymph nodes assayed, where only two lymph nodes were reached when administered intramuscularly. The local pressure of the skin resulted in a higher localised concentration for longer than either of the other two administration sites. However, only three out of 36 mice given intradermal DNA were positive for pDNA at 28 days, the threshold at which it was deemed likely to initiate immune responses, and this was 100-fold lower than the original dose (Tuomela et al, 2005). Furthermore, 200 μg pDNA is an unrealistic dose for clinical use when scaled up for human use. Chesnoy and Huang (2002) delivered 20 μg of naked pDNA encoding for luciferase intradermally, aiding delivery by electroporation. They found that expression was transient and highly dependent on the ionic strength of the solution, hypothesising that the elevated level of ions would protect DNA from adsorption and increase availability for epidermal cell uptake. Faurez et al (2010) suggested that since DNA is a polyanion and cannot interact with negatively charged cell membranes, pDNA uptake is likely to be cell dependent and variable but likely requires additional tools or formulations that disrupt the cell membrane. Furthermore, these studies only measure expression and biodistribution; the initiation of immune responses provides an additional hurdle in successful DNA vaccine design.

Mechanistically, delivery to the skin aims to reduce the amount of time pDNA vaccine formulations spend in the tissue or the cytoplasm. Electroporation is a common method to enhance uptake, involving the supply of an electrical charge to temporarily destabilise local cell membranes and increase permeability (Elnekave et al, 2011). A study by Smith et al (2020) intradermally administered 100 μg of pDNA encoding for the SARS-Cov-2 spike protein in guinea pigs with electroporation immediately following injection. Systemic immune responses were observed, including high titers of neutralising antibodies as well as T cell-mediated responses as early as 7 days post single injection. The change in

permeability is not limited to cell membranes, having been observed to induce changes in vascular structures, with dendritic cells leaving the skin through lymphatic vessels within 8 hours of intradermal pDNA immunisation with electroporation (Smith et al, 2014). As well as its role in improving uptake of DNA, electroporation has been found to induce production of pro-inflammatory cytokines in the skin and function as a potential adjuvant, improving dendritic cell migration and augmenting antigen-specific responses immune responses to pDNA encoded antigens (Todorova et al, 2017). This is possibly due to superficial tissue injury which releases cell derived compounds that can in turn activate patrolling dendritic cells and Langerhans cells; however, the discomfort of the initial pulse of electroporation and potential for localised tissue damage may prevent widespread use in the clinic.

Alternatives to electroporation rely on physical gene delivery methods such as biolistics, which precipitates pDNA and directly transfects cell membranes by high velocity acceleration. For example, the Helios “gene gun” involves the complexation of pDNA with the cation spermidine before precipitating that complex on gold microparticles and firing at high velocity to deliver intradermally. The role of spermidine in this preparation can be optimised further; a study replacing it with a cell penetrating peptide preparation delivered intradermally in mice observed splenic T cell responses indicative of systemic cell-mediated immunity, as well as neutralising antibodies to the encoded SARS-Cov-2 spike protein (So et al, 2024). This has been compared to needle free injection which involves high pressure liquid injection with a nozzle diameter smaller than the outer diameter of a standard 21G needle. Auto-reloading needle free injection systems are commonly used in livestock for a variety of drugs, and is less uncomfortable than electroporation or high volume needle injections (Trimzi and Ham, 2021). A study by Nguyen-Hoai et al (2021) intradermally delivered pDNA encoding for the breast cancer antigen HER2, comparing delivery by gene gun and needle free jet injection. In a tumour challenge study where mice were immunised on days 1 and 15 and injected with tumour cells on day 25, pDNA delivered by gene gun provided protection

against tumour growth in 70% of mice compared to only 30% in the jet injection group. Systemic antibody production and T cell responses to the HER2 epitope were only detectable after gene gun, but the authors suggested this limitation may be due to the low immunogenicity of HER2. Indeed, a study immunising rabbits with pDNA encoding for select HIV antigens observed strong immune responses when delivered by needle free injection (Chapman et al, 2023). However, the predominant downside to clinical adoption of the gene gun and needle free injection systems is the requirement for specialist equipment and expertise, potentially limiting widespread use in healthcare.

Microneedle technology attempts to resolve this by manufacturing patches with an array of needle like microprojections attached to a backing plate designed to transiently pierce the stratum corneum to a depth up to 1 μm. This can involve application of the patch followed by topical DNA application, application of DNA-coated patches, or application of dissolving patches that incorporate pDNA within the usually polymeric formulations (McCaffrey et al, 2016). Topical administration of DNA nanoparticles following solid microneedle patch administration may limit pDNA availability, since less than 20% of the DNA may traverse the skin over an 8 hour period (Niu et al, 2019). However, when an anthrax protective antigen-encoding pDNA was condensed to the surface of polymeric nanoparticles composed of poly (lactic-co-glycolic acid) (PGLA), topical administration after the patch resulted in strong systemic immune responses (Kumar et al, 2012). In another study, Seok et al (2017) coated a microneedle patch with PGLA-condensed pDNA encoding for H1N1 strain flu antigens. The titer of neutralising IgG antibodies in sera was approximately fourfold lower than that induced in the study by Kumar et al (2012); this may be explained by potential differences in immunogenicity of anthrax protective antigen and H1N1 flu antigens, as well as a dosing regimen that supplied the mice with half the dose of pDNA in the latter study compared to the former. Both studies elicited immune responses deemed to be statistically significant and protective. The formulations of dissolving microneedles are highly variable, designed in conjunction with the pDNA and associated nanoparticles to

optimise mechanical properties and loading efficiencies (Liao et al, 2017). However, various formulations have been successful in initiating antigen-specific immune responses to pDNA encoded antigens (Li et al, 2023; Liao et al, 2017; Qiu et al, 2014). It is worth noting that all three of these studies examine different encoded antigens, nanoparticle formulations, and microneedle polymers for microneedle preparation which makes direct comparison difficult. Furthermore, many of these mechanical techniques can be used in parallel, such as electroporation of hollow microneedle arrays (Daugimont et al, 2010). The formulation of pDNA nanocarrier has been found to be highly predictive of immune response, and is of primary concern before selecting a method of delivery (Khalid and Poh, 2023).

1.6 Vectors for DNA delivery; viral, nonviral, lipidic and polymeric

Naked plasmid DNA delivery suffers from significant degradation, requiring immense doses to achieve adequate transfection *in vivo* (Tuomela et al, 2005). Complexation with a vector can confer protection from these degradative systems as well as enhance uptake and immunogenicity, depending on the viral or nonviral formulation. Viral vectors take advantage of viral machinery that allows the virion to enter cells and integrate its nucleic acids into the host cell for protein production, with five main classes possessing one of two integration mechanisms. Adenovirus, herpes, and adeno-associated virus vectors persist in the cell nucleus as extrachromosomal episomes, while oncoretrovirus and lentivirus vectors integrate into host chromatin (Thomas et al, 2003). However, the efficacy of these vectors has historically suffered from significant toxicity, skewed immune responses towards antiviral cell-mediated immunity, and a risk of oncogenesis. Newer vectors have also been explored for a variety of cancers, finding mixed efficacy that is largely dependent on choice of antigen (Anderson and Schneider, 2007). The safety concerns and limitations of viral vectors have popularised nonviral alternatives, broadly composed of either lipids or polymers and tailored for the site of delivery and encoded antigen (Travieso et al, 2022; Ramamoorth and Narvekar, 2015). Nonviral vectors make up almost a third of total gene therapy clinical trials, and are

likely to grow in proportion due to continuous improvement in understanding of their limitations (Sharma et al, 2021).

Nonviral polymeric structures have been used to deliver DNA-based gene therapeutics for a range of diseases. Generally, polymer formulations are based on one of a well-characterised library of polymers including poly L-lysine (PLL), polyethyleneimine (PEI), poly (β-amino ester) (PBAE), poly (lactide-co-glycolide) (PGLA) as well as non linear dendrimer structures (Ke et al, 2020). Each of these polymers has unique strengths, varying in size and structure of nucleic acid it can condense, as well as its suitable sites of delivery due to differences in clearance rate and high cytotoxicity. PEI has been used extensively for DNA delivery, possessing a high charge density from three charged amine groups and attributing its success in transfection to its high rate of endosomal escape (Casper et al, 2023). However, PEI alone is significantly cytotoxic and modifications are needed to improve this: for example, the inclusion of a nontoxic copolymer such as polyethylene glycol (Terry et al, 2021). Other strategies take advantage of naturally occurring polysaccharides such as chitosan, which has a similar potential for endosomal escape as PEI (Richard et al, 2013) and maintains significant modifiability for improvements in toxicity and transfection (Mao et al, 2010; Bravo-Anaya, 2019).

Polymer-based and lipid-based nonviral vectors are often compared and share many of the same strengths such as biocompatibility, modifiability, and scalability as well as many of the same limitations such as lack of immunogenicity (Wahane et al, 2020). However, lipid based nanoparticles have been suggested to have an advantage over other particulate systems due to their biodegradability, potential for controlled or modified drug release, and capacity for combination with other systems (Ghasemiyeh and Mohammadi-Samani, 2018). The structure of lipid-based nanoparticles can be altered by preparation method, achieving solid lipid nanoparticles (SLN) or more flexible liposome structures that are characterised by spherical phospholipid bilayers with an aqueous core (Radler et al, 1997). According to the “solid core” structure detailed by Zhigaltsev and Cullis (2023), lipids

must contain a hydrophilic and hydrophobic portion to assemble into liposomal lipid bilayers; any lipids included that are insoluble in a membrane progressively accumulate within the aqueous core depending on the overall composition. SLNs were formed by T-junction mixing a lipid-containing ethanol phase and an aqueous phase; at 10 mol%, the insoluble lipid forms a "bulge" out of the membrane into the aqueous compartment and as content increases, stabilises into an SLN with a micelle-like structure containing a solid lipid core and outer lipid monolayer. Pink et al (2019) used a mixture of small angle neutron scattering and all-atom molecular dynamics to identify a mechanism of SLN formation by a phase inversion method in which non-bilayer forming lipids were heated and rapidly cooled before sonication. The lipids formed liquid aggregates that, at equilibrium, formed ordered solid aggregates that was strongly influenced by the shape of the lipids themselves. However, this method is unsuitable for DNA loading due to DNA denaturation at high temperatures. Francis et al (2020) formed SLNs by solvent emulsification, finding that the addition of DNA yielded lipoplexes that were heterogeneous in size and possessed undefined edges. This heterogeneity is absent when SLNs containing DNA are formed by microfluidics, which yields a monodisperse population of lipoplexes (Kulkarni et al, 2017).

In comparison with SLNs, liposomes have a characteristic aqueous core which results in larger than average complex sizes and higher loading capacity (Ghasemiyeh and Mohammadi-Samani, 2018). Depending on the method of preparation and composition, liposomes can have a single phospholipid bilayer or multiple bilayers arranged into concentric or non-concentric spheres, denoted as unilamellar, multilamellar, and multivesicular vesicles (Figure 3: Veera et al, 2022).

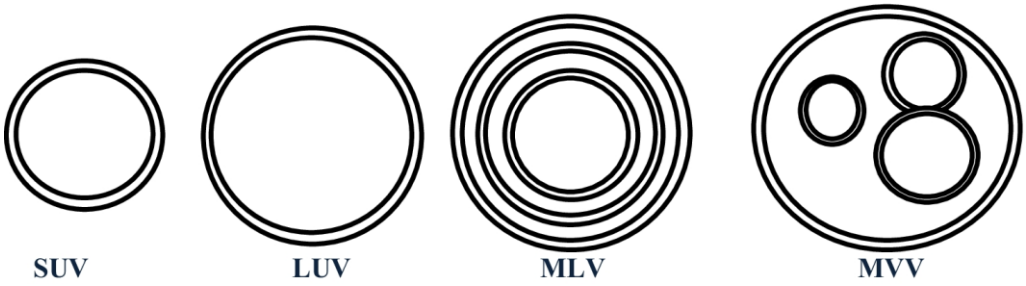

Figure 3. Liposomal structures, taken from Veera et al (2022). SUV = small unilamellar vesicles. LUV = large unilamellar vesicles. MLV = multilamellar vesicles. MVV = multivesicular vesicles.

The extensive modifiability and high DNA loading capacity of liposomes make them particularly attractive. Cationic liposomes have been successfully used in a variety of studies delivering plasmid DNA for cancer therapeutics (Liu et al, 2020; Luiz et al, 2022) or as self-adjuvanting prophylactic vaccines for a variety of infectious diseases (Tretiakova and Vodovozova, 2022) with a wide range of lipids possessing nuanced benefits in their design.

1.7 Cationic liposome formulations for DNA delivery

As of 2022, all FDA-approved lipid nanoparticle formulations contain four lipids: an ionisable cationic lipid, a neutral helper lipid, cholesterol, and a polyethylene glycol (PEG)-lipid conjugate (Albertsen et al, 2022). These lipids fulfil important roles in forming stable complexes with nucleic acids as well as affecting delivery *in vivo*, and preparation method can be determinative of the resulting structure (Cullis and Hope, 2017). These systems are primarily solid core structures but the function of each lipid can also be taken as a guide for liposomal bilayer composition.

To design liposomes capable of forming a stable complex with DNA, cationic lipids must be included. Positively charged amines on the cationic lipid interact with the negatively charged phosphate DNA backbone; this is measured and kept consistent by combing liposomes and DNA at molar nitrogen: phosphate (NP) ratios. The characteristics and composition of cationic lipids can be controlled to modulate the overall charge of the liposome, which has a resultant effect on how much DNA can be condensed into a single liposome (Caracciolo and Amenitsch, 2012). Two well-

established cationic lipids are 1,2-dioleoyl-3-trimethylammonium-propane (DOTAP) and 3β-[N-(N',N'-dimethylaminoethane)-carbamoyl] (DC-chol). Both lipids are monovalent, having only a single charged amine group. Ciani et al (2007) used circular dichroism to characterise liposomes composed of either lipid combined with the helper lipid 1,2-dioleoyl-sn-glycero-3-phosphoethanolamine (DOPE). The integrity of the liposomal bilayer structure was strongly preserved while the right handed helical structure of DNA was progressively lost after complexation, indicating that DNA wraps itself around the liposome structure. Using x-ray diffraction, Radler et al (1997) observed that as DNA content increased, the positive charge of DOTAP/DOPE liposomes decreased until an overall charge inversion was seen at the isoneutrality point, or the point at which the negative charge of DNA saturates the positive charge of the liposome. An overall cationic charge was deemed to be essential in ensuring colloidal stability and size monodispersity, because the positively charged complexes repelled each other in suspension but nearly neutral complexes were subject to fusion. The benefits of an overall cationic charge relate not only to the formation and stability of the DNA-liposome complexes, but also to their behaviour in biological environments. Henriksen-Lacey et al (2010) observed that cationic liposomes loaded with whole antigen remained at the site of injection and released antigen in a depot effect, while neutral liposomes easily released antigen into circulation and was associated with poorer immune responses. Cationic DNA-liposome complexes were also found to be more easily taken up by cells *in vitro*, with the endosomal pathway determined largely by complex size. In DC-Cholesterol-based lipoplexes, vesicles less than 300 nm in diameter were taken up by predominantly clathrin-mediated endocytosis in HEK293T cells while vesicles larger than 500 nm were taken up by predominantly clathrin-mediated endocytosis (Yang et al, 2013). Transfection success was concluded to be based on endocytosis vesicle escape.

More recently, variations in cationic lipid have been investigated for DNA delivery such as ionisable lipids, which are neutrally charged at physiological pH, and multivalent cationic lipids which possess more than

one protonatable amine group. The amphiphilicity of ionisable lipids is considered to be their strongest advantage; the neutral charge at administration makes the complex safer and better tolerated while retaining its capacity to destabilise the endosomal membrane when acidification induces a positive charge on the complex (Sun and Lu, 2023). The exact structures of ionisable lipids may strongly affect outcome *in vivo*; Algarni et al (2022) observed differential organ-specific gene expression dependent on ionisable lipid structure, with head group pKa and lipid tail structure potentially affecting strength of expression. As vaccine formulations they are strongly immunogenic and have been used in the COVID-19 BNT162b2 vaccine developed by Pfizer/BioNTech (Polack et al, 2020) and the mRNA-1273 vaccine developed by Moderna (Jackson et al, 2020; Baden et al, 2020). However, the exact structure of these lipids remains proprietary. Other ionisable lipids have been explored for use in an intratumourally administered subcutaneous cancer vaccine (Qin et al, 2024) and a variety of both infectious and cancer vaccine targets administered intradermally by needle free jet injection (Sonoda et al, 2023) with various degrees of success. Conversely, Gomez-Aguado et al (2020) observed that the permanently cationic DOTAP alone outperformed a combination of DOTAP and the ionisable lipid (1,2-dioleoyl-3-dimethylammonium propane) (DODAP). The importance of the relationship between structure and function is especially reflected when Zou et al (2022) formulated four ionisable lipids and found that liposomes formed with the multivalent lipid induced the highest expression of green fluorescent protein in A549 cells and effectively inhibited tumour growth when used to deliver an antitumour siRNA.

Permanently multivalent cationic lipids have also been explored as means to improve complexation with pDNA due to their potential to moderate membrane charge density, or the average charge per unit area of the membrane (Ahmad et al, 2005). By synthesising a library of mono-, bi-, tri-, and pentavalent cationic lipids which differed only in head group composition, Ahmad et al (2005) showed that membrane charge density increased as lipid charges increased and was strongly predictive of

transfection efficiency in mouse fibroblasts. Cationic lipids with a higher number of positive charges could also form lower proportions of the membrane composition without DNA complexation decreasing. Joseph et al (2006) compared liposomal formulations composed of different monovalent lipids and a novel trivalent lipid ceramide carbamoyl-spermine (CCS) in their ability to deliver an influenza subunit vaccine and elicit systemic immune responses. While the monovalent lipids elicited local and systemic responses, the multivalent CCS-containing liposomes elicited equivalent or superior responses to the commercial vaccine co-administered with cholera toxin as an adjuvant. Multivalent lipids were also found to load larger DNA molecules more efficiently when over 9,000 base pairs with stronger effects *in vitro* compared to lipofectamine 3000 (Sousa et al, 2022). The inclusion of multivalent lipids may also mirror the action of a self-assembly phenomenon where free multivalent cations in solution have been observed to interact with both DNA molecules and phospholipids in neutral or anionic liposome formulations (Tresset et al, 2007). Polyamines such as putrescine, spermidine, and spermine are naturally occurring bioactive polycations that have been observed to bind to nucleic acids and directly interact with multiple components and phases of an immune response (Proietti et al, 2020). Therefore, valency of cationic lipid may provide an important and potentially impactful variable in designing liposomes for DNA delivery to dendritic cells.

Helper lipids including neutral phospholipids and cholesterol form the next two parts of the classical four-part lipid nanoparticle formulation. Cholesterol is essential for maintaining lipid membranes with homogeneous lipid distributions and it is a strong modulator of membrane fluidity and mechanical strength (Redondo-Morata et al, 2012), particularly when forming between 35 and 50 mol% of the total lipid composition. Briuglia et al (2015) studied the effect of controlling cholesterol in a range of formulations on both long term stability and drug release, finding that the optimum composition was 30 mol% cholesterol. Cholesterol-based cationic lipids combine the roles of the cationic lipid with the structural benefits of cholesterol, including DC-Cholesterol and a variety of other modified

cholesterols (Ju et al, 2016). The lipid GL67 combines a cholesterol base and the polyamine spermine, forming a trivalent cationic lipid that has been found to induce strong anti-tumoural immune responses in a mouse model (Siders et al, 2002).

Neutral helper phospholipids form an equally essential part of the liposome formulation; selection of lipids with a conical shape at a carefully selected proportion of the overall liposome membrane have been found to significantly improve endosomal escape *in vitro* (Kolasinac et al, 2018). Endosomal maturation into lysosomes is a major bottleneck in preventing effective delivery of nonviral gene complexes, and formulations that have included fusogenic neutral helper lipids alongside cationic lipids have historically seen better DNA-encoded protein expression outcomes (Degors et al, 2019; Varga et al, 2005; Hatakeyama et al, 2009; Zheng et al, 2023). The conical shape of these lipids imposes a negative curvature on the bilayer and can induce a transition to non-bilayer phases (Zhigaltsev and Cullis, 2023; Lonez et al, 2010). This transition negatively affects stability of the liposome but is highly conducive to endosomal escape, since it also disrupts the endosomal membrane structure, and its effects on liposome stability can be ameliorated by including cylindrical lipids and/or cholesterol. In particular, the fusogenic helper lipid DOPE has been well characterised in its augmentative effect on transfection both *in vitro* and *in vivo* (Du et al, 2014; Caracciolo and Caminiti, 2005; Munoz-Ubeda et al, 2010).

The final component of the four-part formulation described above is a PEGylated lipid; this is primarily to increase colloidal stability and increase circulation time as well as reduce toxicity, although this has been shown to negatively impact immune responses when PEGylated liposomes were compared to non-PEGylated liposomes (Carstens et al, 2011). This is advantageous when delivered intravenously, where extremely rapid blood clearance needs to be avoided (Semple et al, 2005) or intramuscularly, where tissue degradation would otherwise be a significant problem (Zhao et al, 2021). However, intradermal administration of cationic liposomes benefits from their depot effect and increased circulation is not necessarily

needed when gene expression is impaired by inclusion of PEGylated lipids (Ho et al, 2018).

Some liposomal formulations have also included a functionalised lipid to encourage dendritic cell targeting and uptake through DC-specific endocytosis receptors. In particular, the mannose receptor is expressed on DCs and is involved in endocytic uptake as well as antigen internalisation for cross presentation (Schuette et al, 2016) and is therefore considered a potential target for DC delivery. Garu et al (2016) described a library of cationic lipids each containing a mannose-mimicking head chain and formulated liposomes with a 1:1 molar ratio of one of these lipids and dioleoylphosphatidylethanolamine (DOPE) to be complexed with DNA at a charge ratio of 4:1. The best performing lipid resulted in 20% of DCs transfected *in vitro*, and administration of the complex *in vivo* with DNA encoding for tumour antigens resulted in an almost complete tumour response. Liposomes described by Li et al (2013) included formulations composed of the cationic lipid DDAB, Cholesterol, and mannosylated cholesterol. Complexes were formed stepwise by complexation of DNA with protamine before addition of liposomes. Inclusion of the mannosylated cholesterol significantly increased cellular uptake while DC maturation was induced irrespective of mannose inclusion. Both of these papers alluded to mannose-dependent improvement in complex uptake but not expression. Expression of the mannose receptor on DCs also has the potential for negatively affecting an immune response due to mannose receptor interaction with CD45 on the T cell surface (Schuette et al, 2016). This upregulates expression of the inhibitory receptor CTLA-4 on the T cell surface and directly impairs its cytotoxic activity. Mannose receptors are also predominantly expressed on immature dendritic cells; activation of these receptors and downstream signalling pathways has been found to induce an anti-inflammatory immunosuppressive environment with the potential to induce antigen-specific immune tolerance (Chieppa et al, 2003). Functionalisation of dendritic cell ligands remains a promising strategy; another example is linolenic acid, a naturally occurring fatty acid that is metabolised into arachidonic acid and docosahexaenoic acid. All three

compounds have been found to be readily taken up by dendritic cells and induce dendritic cell maturation with knock-on effects on T cell activation and proliferation (Carlsson et al, 2015). Linolenic acid has been included in liposomal formulations previously and induced anti-tumour immune responses (Saad et al, 2023), but to date remains a novel strategy for liposomal DNA delivery to dendritic cells.

1.8 Thesis hypothesis

It was hypothesized that cationic liposomes are a suitable delivery vehicle for plasmid DNA vaccine delivery, and that multivalency of the cationic lipid in the liposome formulation may affect pDNA uptake and expression in dendritic cells. As DC-Cholesterol and DOPE are well characterised in their ability to deliver pDNA to a variety of cells *in vitro* and to initiate immune responses in certain *in vivo* models, it could be used as a starting point to evaluate in dendritic cells. As multivalent lipids have been demonstrated to improve uptake, expression, and immune activation, a multivalent cholesterol-based lipid may improve dendritic cell expression of GFP when used to deliver GFP pDNA.

1.9 Thesis aims and objectives

The aim of this project was to evaluate the effect of changing the valency of cationic lipid in liposome formulations on delivering pDNA to dendritic cells. An initial liposome formulation consisting of the monovalent cholesterol based lipid DC-Cholesterol and the helper lipid DOPE was characterised for physicochemical parameters including size, charge, encapsulation efficiency, and morphology. Expression of GFP was evaluated first in human embryonic kidney HEK293T, murine fibroblast NIH 3T3, and murine dendritic DC2.4 cell lines and cellular and humoural immune responses evaluated using a SARS-Cov-2 pDNA vaccine. The trivalent cholesterol-based lipid GL67 was then incorporated in a separate formulation with DOPE, characterised, and *in vitro* expression evaluated and compared with the previous formulation.

The project objectives were as follows:

- Characterise the physicochemical properties of liposomes composed of different ratios of DC-Cholesterol and DOPE, combined with GFP pDNA at different nitrogen: phosphate ratios (Chapter 3)
- Deliver pDNA using DC-Cholesterol/DOPE liposomes, evaluating *in vitro* GFP expression in three cell lines and *in vivo* immune responses to a SARS-Cov-2 pDNA vaccine (Chapter 4)
- Characterise physicochemical properties of, and evaluate *in vitro* expression of GFP induced by: DC-Cholesterol/DOPE/linolenic acid, GL67/DOPE, or GL67/DOPE/linolenic acid liposomes at different nitrogen: phosphate ratios (Chapter 5)

Chapter 2: Materials and Methods

2.1 Materials

Table 1. Materials and equipment, and the supplier

Materials and equipment	Supplier
Chloroform >99%	Sigma Aldrich
3β-[N-(N′,N′-dimethylaminoethane)-carbamoyl]cholesterol hydrochloride (DC-cholesterol)	Sigma Aldrich
Phosphate buffered saline (PBS) tablets	Sigma Aldrich
Chloroquine diphosphate	Sigma Aldrich
N4-Cholesteryl-Spermine HCl salt (GL67)	Avanti Polar Lipids
1,1'-Dioctadecyl-3,3,3',3'-Tetramethylindodicarbocyanine, 4-Chlorobenzenesulfonate Salt (DiD) solid	Avanti Polar Lipids
Linolenic acid (LA)	Sigma Aldrich
1,2-dioleoyl-sn-glycero-3-phosphoethanolamine (DOPE)	Avanti Polar Lipids
Zombie Violet™ Fixable Viability Kit	Biolegend, UK
GFP pDNA (pcDNA3-Clover)	Addgene #40259
Agarose powder	Sigma Aldrich, UK
Tris-acetate-EDTA (TAE) buffer 20x	Thermo-Fisher, UK
Luria Bertani (LB) broth powder	Sigma Aldrich, UK
LB agar powder	Sigma Aldrich, UK
Plasmid miniprep kit	Qiagen, UK
Plasmid midiprep kit	Qiagen, UK
1kb DNA ladder	Sigma Aldrich, UK
Ethidium bromide	Sigma Aldrich, UK
Hank's balanced salt solution (HBSS) media	Sigma Aldrich, UK
Roswell Park Memorial Institute 1640 medium (RPMI 1640)	Sigma Aldrich, UK
Dulbecco's modified Eagle's Medium (DMEM)	Sigma Aldrich, UK
foetal bovine serum (FBS)	Sigma Aldrich, UK
L-glutamine	Sigma Aldrich, UK
non-essential amino acids	Sigma Aldrich, UK
4-(2-hydroxyethyl)-1-piperazineethanesulfonic acid (HEPES) buffer solution 1 M	Sigma Aldrich, UK
2-mercaptoethanol >99%	Sigma Aldrich, UK

trypsin Ethylenediaminetetraacetic acid (EDTA) solution >99.7%	Sigma Aldrich, UK
dimethyl sulfoxide sterile filtered >99.7% (DMSO)	Sigma Aldrich, UK
isopropyl alcohol >99.7%	Sigma Aldrich, UK
paraformaldehyde 4%	Sigma Aldrich, UK
Lipofectamine 2000 transfection reagent	Thermo-Fisher, UK
Prestoblue viability reagent	Invitrogen, UK
Ampicillin sodium salt	Sigma Aldrich, UK
Filter syringe cap, 0.22 μm	Sigma Aldrich, UK
(3,3′ -dioctadecyloxacarbocyanine, perchlorate) (DiO)	Invitrogen, UK
(DiIC18(3); 1,1′-dioctadecyl-3,3,3′,3′-tetramethylindocarbocyanine) (DiI)	Invitrogen, UK
COVID-19 SN17 plasmid DNA	Scancell, UK

2.2 Plasmid DNA isolation and quantification

2.2.1 Isolation of GFP-expressing plasmid DNA from transformed E. Coli

Ampicillin stock (100 mg/ml) was made by dissolving ampicillin in DI water and sterilising by 0.22 μm filter syringe cap and storing at -20°C in 100 μl aliquots until use. LB agar plates were prepared by adding 4 g LB agar in 100 ml DI water in a 250 ml capacity bottle and microwaving until fully dissolved. The bottle cap was loosely taped in place and autoclaved before storing at 4°C until use. Prior to use, LB agar was microwaved until melted and left to cool slightly. Ampicillin stock was added to a final concentration of 100 μg/ml and approximately 20 ml agar was poured into each of five petri dishes and left to cool before storing wrapped in parafilm at 4°C upside down until use within one week. LB broth was prepared in 1 L glass bottles. 20 g broth powder was added to 760 ml DI water, loosely capped and autoclaved. Before use, LB broth was warmed to 37°C and ampicillin added to a final concentration of 100 μg/ml.

GFP-expressing transformed E. Coli resistant to ampicillin were taken from an agar stab and streaked on an agar plate containing ampicillin before

incubating at 37°C overnight. A single colony was taken using a sterile inoculating loop and inoculated into a 50 ml Falcon tube containing 10 ml LB broth with ampicillin and incubated for 6-8 h. Optical density of turbid broths were tested by diluting 500 µl bacteria with 500 µl fresh LB broth and measuring using a spectrophotometer. Broths with optical densities between 0.4 and 0.6 were centrifuged at 13000 rpm for 10 minutes, supernatants discarded, and pellets frozen at -20°C until needed.

To isolate plasmid DNA, the Qiagen spin miniprep kit was used according to the instructions. Frozen pellets were defrosted and each pellet resuspended in 250 µl buffer p1 before transferring to a 1.5 ml capacity microcentrifuge tube. 250 µl buffer p2 was added and mixed by inverting the tube 4-6 times until the solution became clear, no longer than five minutes. 350 µl buffer N3 was added and mixed by inverting the tube 4-6 times. Precipitates were removed by centrifuging at 17,900 g for 10 minutes and 800 µl supernatant added to the spin column by pipette. Columns were centrifuged briefly for 30 to 60 seconds and flow through discarded. Columns were washed by adding 750 µl buffer PE, centrifuging briefly and discarding flow-through. Columns were centrifuged for 1 minute to remove residual wash buffer and transferred to a clean 1.5 ml microcentrifuge tube. DNA was eluted by adding 50 µl sterile RNAse and DNAse-free water to the centre of the spin column, letting stand for 1 minute, and centrifuging for 1 minute.

Concentration of extracted DNA measured using the Nanodrop and purity confirmed by an absorbance value >1.8 at 260/280 nm. Plasmid size was confirmed by gel electrophoresis (see section 2.2.2). Expression of GFP was confirmed by sequencing through the SourceBioscience postal sequencing service. For ongoing plasmid use, pDNA was sent to Genewiz, UK for gigaprep expansion and stored in 1 mg/ml aliquots of 100 µl at -20°C until needed.

2.2.2 Confirmation of isolated plasmid DNA size by gel electrophoresis

Agarose gel was made by dissolving 1 g agarose in 100 ml 1X TAE buffer in the microwave in 30 second bursts until fully dissolved. Ethidium bromide

(20 µl of 2.5 mg/ml stock) was added and poured into a gel mould while still warm, popping any bubbles with a pipette tip. A 10-well comb was inserted and the gel left to cool for one hour. Prior to use, the comb was removed and placed in the agarose gel tray before submerged in 1X TAE buffer. Per well, 10 µl plasmid DNA mixture containing 8 µl plasmid DNA and 2 µl loading dye was loaded next to 5 µl of 1kb DNA ladder and the gel was run for 45 minutes at 120 V before imaging.

2.3 Liposome-DNA complex preparation and characterisation

2.3.1 Formation of cationic liposomes by thin film method

3β-[N-(N′,N′-dimethylaminoethane)-carbamoyl]cholesterol hydrochloride (DC-Chol, 537.26 g/mol), N4-Cholesteryl-Spermine HCl salt (GL67, 724.37 g/mol), 1,1'-Dioctadecyl-3,3,3',3'-Tetramethylindodicarbocyanine,4-Chlorobenzenesulfonate Salt (DiD, 959.91 g/mol) solid, linolenic acid (LA, 278.43 g/mol) and 1,2-dioleoyl-sn-glycero-3-phosphoethanolamine (DOPE, 744.03 g/mol) stock solutions were prepared at 1 mg/ml in chloroform and combined in round-bottom flasks at given molar ratios (Table X). Chloroform was evaporated in a rotary evaporator at 1 mbar of pressure, 40°C water bath and -10°C condenser. To ensure full evaporation of the solvent, dried thin films were subsequently placed under nitrogen for a minimum of 30 minutes per film. Films were then hydrated by the addition of 1 ml DI water filtered through 0.22 um filter warmed to 37°C to a final lipid concentration of 1 mM. Films were sonicated in 5-minute intervals until fully hydrated. Liposome suspensions were then extruded through Whatman polycarbonate filters with pore sizes of 0.2 µm using a hand extruder (Avanti Polar) and kept up to one week at 4°C.

Chapter 3 Formulations			
DC-Chol (mol%)	DOPE (mol%)	DiD (mol%)	
25	74.98	0.02	
30	69.98	0.02	
35	64.98	0.02	
40	59.98	0.02	
50	49.98	0.02	
Chapter 5 Formulations			
DC-Chol (mol%)	DOPE (mol%)	LA (mol%)	DiD (mol%)
32	47.98	20	0.02
GL67 (mol%)	DOPE (mol%)	LA (mol%)	DiD (mol%)
40	59.98		0.02
32	47.98	20	0.02

Table 2. Liposome formulations by molar percentage of total 1 mM lipid concentration. One formulation was used in chapter 4 for *in vitro* and *in vivo* studies, consisting of 40 mol% DC-Cholesterol as characterised in chapter 3.

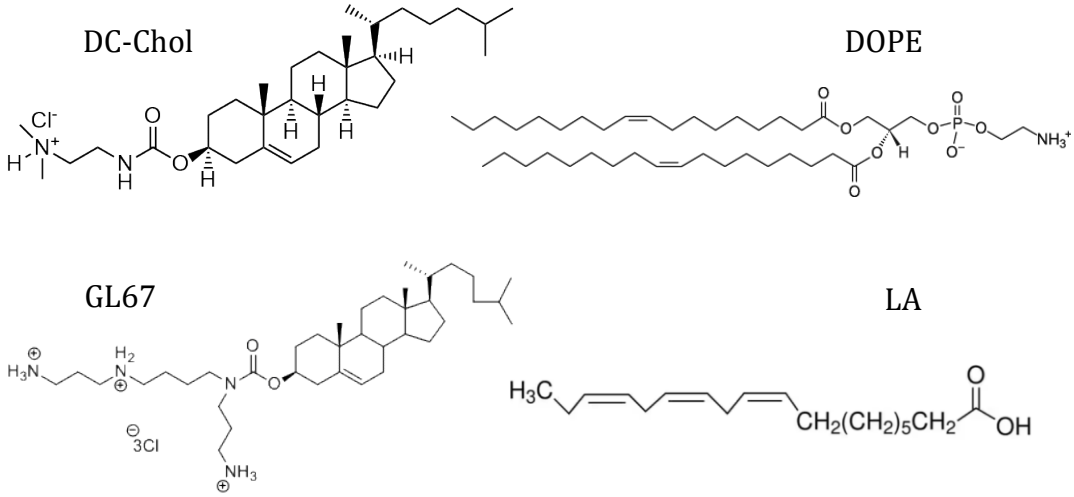

Figure 4. Chemical structures of liposomal lipids used in formulations detailed in section 2.3.1. Taken from Avanti Polar Lipids (DC-Chol, DOPE, GL67) and Sigma Aldrich (LA).

2.3.2 Formation of liposome-DNA complexes

Liposome-DNA complexes were made by combining relevant quantities of 1 mg/ml GFP pDNA stock to 100 µl 1mM liposome suspensions and incubating for 30 minutes at room temperature. DNA and liposome combinations were determined by nitrogen to phosphate ratios (NP ratios), where 2 moles Nitrogen per mole of DC-Chol and 1 mole of Phosphate per base (average mass 330 g/mol). NP ratios used include NP 3, 6, 9, and 12.

2.3.3 Characterisation of liposomes using dynamic light scattering and zeta potential measurements

The mean hydrodynamic diameter of liposomes was measured by dynamic light scattering (DLS) using the Malvern Zetasizer Nano ZS. Measurements represent a mean of 3 runs from one experiment, measured at 25°C and a fixed scattering angle of 173°. Zeta potential was measured using Malvern Zetasizer Nano ZS at 25°C and reported values are the mean of three runs from one experiment. Liposome suspensions were diluted to 0.1mM liposomes in 10mM NaCl and solution specifications were set to a medium viscosity of 0.8872 mPa and a medium refractive index of 1.540. Particle characteristics were set to measure phospholipids.

2.3.4 Gel electrophoresis and retardation assay

1% agarose gels were made by dissolving 1 g agarose powder in 100 ml TAE buffer in a microwave in 45 second intervals until clear. When cool to the touch, 20 µl of 2.5 mg/ml ethidium bromide (EtBr) was added and the gel poured into gel electrophoresis mould with 10-well combs inserted. When set, combs were removed and gels were submerged in TAE buffer. Wells were loaded with a 1-10kb DNA ladder, positive DNA-only control, and 30 µl liposome complexes prepared as in section 2.3.2. Gels were run at 130 mV for 45 minutes and imaged in a UV transilluminator.

2.3.5 Calculation of encapsulation efficiency by densitometry

Encapsulation efficiency in chapter 5 was determined by gel retardation as described in section 2.3.4. ImageJ V1.5 software was used for densitometry

to determine the intensity of the DNA band detected in the body of the gel. Band intensity found in each experimental condition was compared to the control band which contained a known quantity of pDNA (2 μg). Encapsulation efficiency was expressed as the percentage of DNA in the sample stably condensed by cationic liposome and calculated as in equation 1.

$$\left(1 - \frac{DNA\ in\ band}{DNA\ in\ sample}\right) x100 = Percentage\ DNA\ encapsulated$$

Equation 1

2.3.6 Ethidium bromide displacement assay

1.6 µl EtBr was diluted in 800 µl deionized water for EtBr-only control. 100 µl DNA at 1 mg/ml was mixed with 20 µl EtBr to make DNA/EtBr stock at 0.833 mg/ml DNA. In a black flat bottomed 96-well plate, 200 µl EtBr control was added to each of three wells. Relevant quantities of liposomes for each formulation and NP ratio were added to wells, supplied with 2.4 µl DNA/EtBr stock, and topped up to 200 µl total volume with water. For DNA control, 2.4 µl DNA/EtBr was added to 197.6 µl water. All samples were done in triplicate. Complexes were incubated at room temperature for 30 minutes and fluorescence read using the TECAN fluorescent plate reader at 560 nm excitation and 605 nm emission wavelengths.

2.3.7 Fluorescence resonance energy transfer (FRET) studies

FRET studies were carried out by Fady Mina and Abdullah Aljasser during Fady Mina's first year research project in collaboration with Freya Leech and Abdullah Aljasser. FRET was carried out to investigate liposome membrane fusion (Figure 5).

Dually labelled liposomes with DiO and DiI were prepared as described in section 2.3.1 with 33 µl of each DiO and DiI at 1mM added into the chloroform prior to evaporation. Plasmid DNA was added to a 1:1 mixture of dually labelled cationic liposomes and unlabelled cationic liposomes to achieve the relevant NP ratios. A fraction from this mixture without pDNA was used as a control. Samples were placed in a 96 well black flat bottomed plate and filtered DI water was added to reach a total sample volume of 200 µl. The lipoplexes were left to stabilise at room temperature in the dark for 30 minutes. For separate labelling, the same procedure was followed with one alteration: DiO-labelled liposomes and DiI-labelled liposomes were combined in a 1:1 mixture and pDNA added to investigate pDNA-initiated liposome fusion. Samples were excited at a wavelength of 460 nm and emission measured as follows: fluorescence of acceptor fluorophore (*Fa*) was measured at 566 nm and fluorescence of donor fluorophore (*Fd*) was

measured at 506 nm and FRET efficiency calculated as in equation 2. Experimental design and expected outcomes are detailed in Figure 5.

$$FRET\ efficiency\ (FRET\ E) = \frac{Fa}{Fd + Fa} \qquad \text{Equation 2}$$

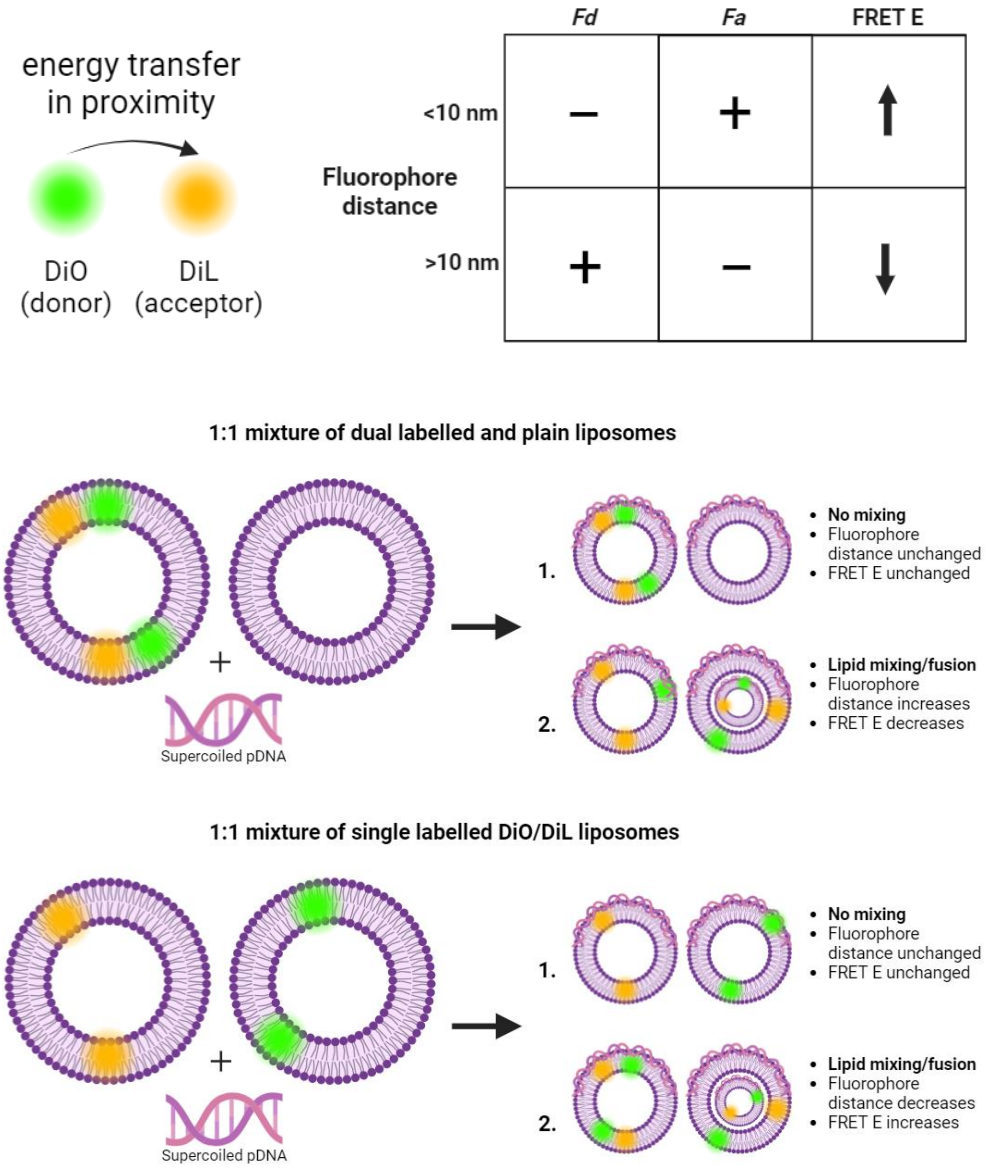

Figure 5. Experimental design of FRET studies. Lipid fusion and mixing is represented by changes in FRET efficiency when labelled and unlabelled liposomes are combined with pDNA.

2.3.8 Cryogenic Transmission Electron Microscopy (cryoTEM): sample preparation and imaging

Liposomes and liposome-DNA complexes at NP 3 and NP 9 were prepared as described in sections 2.3.1 and 2.3.2 at a total lipid concentration of 1 mM. 3 ul liposomes were pipetted onto carbon grids and rapidly frozen in liquid ethane using the Gatan Cryoplunge 3. Samples were imaged by staff at the nanoscale and microscale research centre (nmRC) on the JEM JEOL-2100 electron microscope.

2.4 Cell culture and treatments/transfection

2.4.1 Maintenance of DC2.4 murine dendritic cell line

The murine dendritic cell line DC2.4 was cultured in RPMI-1640 media and used between passages 3 and 10. Media were supplemented with Foetal Bovine Serum (10% v/v), L-glutamine (1% v/v), non essential amino acids (1% v/v), and HEPES buffer to a final concentration of 10 mM. Prior to use, 50 ml media were aliquoted and 2.7 µl of 2-mercaptoethanol added. Aliquots were used within 48 h of preparation due to instability of 2-mercaptoethanol in serum. Cells were incubated at 37°C and 5% CO_2. Cells were incubated in T75 cell culture flasks until 80-90% confluent before passaging. This was done by aspirating media, washing adherent cells in approximately 10 ml warmed PBS, and scraping cells under PBS before pouring into a 15 ml falcon tube and centrifuging at 180 G for five minutes. Media was aspirated and the cell pellet resuspended in 5 ml fresh media, 0.8 ml of which was transferred to a new flask and supplied with a further 10ml fresh media. Cells were passaged every 3-4 days.

2.4.2 Maintenance of NIH 3T3 murine fibroblast and HEK293T human embryonic kidney cell lines

The murine fibroblast cell line NIH 3T3 was used between passages 28 and 50. The human embryonic cell line HEK293T was used between passages 12 and 58. Both cell lines were cultured in DMEM media supplemented with Foetal Bovine Serum (10% v/v) and L-glutamine (1% v/v). Cells were incubated at 37˚C and 5% CO_2. Cells were incubated in T75 cell culture flasks until 80-90% confluent before passaging. This was done by aspirating media, washing adherent cells in approximately 10 ml warmed PBS, and incubating cells with 3ml Trypsin EDTA for five minutes at 37oC before diluting with 6 ml media and centrifuging at 180 G for five minutes. Media was aspirated and the cell pellet resuspended in 5 ml fresh media, 250 ul of which was transferred to a new flask and supplied with a further 10ml fresh media. Cells were passaged every 3-4 days.

2.4.3 Preservation of cells

Cryopreservation of cells was done by expanding cells in up to six T75 cell culture flasks to 80-90% confluence. Cells were washed and detached from the flasks as described above, with each cell pellet resuspended in 1 ml expansion media containing 10% dimethyl sulfoxide (DMSO) (v/v) and transferred to 1.5 ml capacity cryovial. Cryovials were immediately transferred to a Mr Frosty container filled with isopropyl alcohol and frozen at -80°C overnight before transferring to liquid nitrogen storage.

Cryopreserved cells were revived by rapidly defrosting the cryovials in a 37°C water bath and diluting immediately in 9 ml warmed expansion media in a 15 ml falcon tube. Cells were washed by centrifuging at 180 G for five minutes and resuspended in 10 ml expansion media before transferring to a T75 cell culture flask and incubating overnight at 37°C 5% CO_2. The next day, cells were counted and passaged as above.

2.4.4 Cell transfection with green fluorescent protein (GFP)-encoding plasmid

Cells were plated in 24-well cell culture plates at $1x10^5$ cells per well. After plating, cells were incubated overnight at 37 °C and 5% CO_2 to ensure adherence. Lipofectamine/DNA complexes were prepared in serum-free HBSS media at DNA: lipofectamine ratio of 1 µg: 4 µl. Lipofectamine/DNA complexes were made by preparing 500 ul HBSS containing 10 ug DNA and 500 µl HBSS containing 40 µl lipofectamine before adding the DNA mix to the lipofectamine mix and incubating for 5 minutes at room temperature. DNA alone was diluted 10 µg DNA in 1ml HBSS for the control. Media, DNA, and lipofectamine complexes (100 µl each well containing 1 ug DNA) were added to the cells in triplicate and incubated at 37°C, 5% CO_2 for 4 hours before washing and supplying with expansion medium and incubating for a further 24 hours.

2.4.5 Endosomal uptake assay by chloroquine diphosphate

Cells were plated in 24-well cell culture plates at $1x10^5$ cells per well. After plating, cells were incubated overnight at 37 °C and 5% CO_2 to ensure adherence. Chloroquine diphosphate was diluted in HBSS to 50 μM for the DC2.4 cell line and 100 μM for the HEK293T and NIH 3T3 cell lines according to data from chloroquine diphosphate toxicity obtained following the prestoblue assay as described in section 2.4.7. Cells were washed and supplied with 500 μl per well of HBSS containing the relevant concentration of chloroquine diphosphate or HBSS alone. The transfection protocol was followed as described in section 2.4.4, adding the treatments to cells with and without chloroquine diphosphate. Cells were prepared and assayed for flow cytometry as described in section 2.4.6.

2.4.6 Flow cytometry

At the end of the transfection studies, cells were washed with PBS and detached with trypsin as described previously. Contents of each well were transferred to a clear round bottom plate before centrifuging at 180 G for five minutes and supernatants discarded. Zombie Violet viability dye staining solution was prepared by adding 10 μl dye to 4990 μl HBSS media; 100 μl of the dye solution was added to each well, mixing gently by pipette, and incubated for 45 minutes at room temperature (approximately 25°C) wrapped in aluminium foil to protect from light. Cells were centrifuged at 180 G for five minutes, washing in 200 μl HBSS per well twice. To fix the cells, 200 μl paraformaldehyde (4% in PBS) was added to each well and incubated again for 20 minutes at room temperature before washing and resuspending in 200 μl HBSS per well. Samples were run on a Miltenyi MACSQuant Analyzer 12 flow cytometer.

2.4.7 Cellular toxicity of chloroquine diphosphate

Cellular toxicity to chloroquine diphosphate was performed by Prestoblue assay. A solution of 1.6 mM chloroquine diphosphate in HBSS was prepared and serially diluted one in two to obtain nine total concentrations including 1.6 mM, 800 μM, 400 μM, 200 μM, 100 μM, 50 μM, 25 μM, 12.5 μM, and 6.25

μM. DC2.4, NIH 3T3, and HEK293T cells were seeded at $1x10^5$ cells/well in complete media in black 96-well cell culture plates and incubated overnight at 37°C and 5% CO_2 to allow for adherence. Media were aspirated and chloroquine solutions added to triplicate wells and incubated for 4 h at 37°C and 5% CO_2 with 1% Triton X-100 in PBS as a positive cell death control and complete media as a negative control. Cells were washed and Prestoblue reagent diluted 1/10 in HBSS; 100 μl diluted Prestoblue was added to each well and incubated for one hour before reading at 560/600 nm.

2.5 Characterising immune responses *in vivo*

2.5.1 Liposome-DNA complex preparation for *in vivo* use

Liposomes composed of 40 mol% DC-Cholesterol and 60 mol% DOPE were prepared by thin film method as described in section 2.3.1 to a final lipid concentration of 20 mM. DNA encoding for SARS-Cov-19 spike (S) and nucleoprotein (N) antigens was used, referred to henceforth as SN17. DNA was diluted such that 200 μl contained 80 μg SN17 DNA in 2X PBS. Liposomes were diluted in nuclease free water and combined with the diluted SN17 DNA in equal volumes to obtain liposome-DNA complexes at NP 3 and NP 9 containing 10 μg DNA per 50 μl dose.

2.5.2 Murine *in vivo* study husbandry and maintenance

The murine immunisation study was carried out under a Home Office approved project licence (PC45ABD5B) held by Scancell, UK. Animal experiments were co-ordinated by Peter Symonds. Female Balb/C (Charles Rivers) mice were maintained in the animal unit at Nottingham Trent University according to home office guidelines and the project licence. Environmental conditions were maintained within 20 to 24°C ambient temperature and 40 to 70% humidity, with twelve hours of continuous artificial light per 24 h period and at least 15 air changes per hour. Animals were housed in groups of up to three in Techniplast Sealsafe Plus cages and furnished with Corn Cob bedding, sizzle-nest (Datesand Ltd., Cheshire, UK) and play tunnels. Animals were provided with Rodent 2018 Teklad Global Certified Diet (Envigo Laboratories U.K. Ltd., Oxon, UK) and tap water ad

libitum. Animals were provided with environmental enrichment items including wooden chew blocks and cardboard fun tunnels (Datesand Ltd., Cheshire, UK). The diet, water, bedding, and enrichment items were considered to not contain any contaminants that could reasonably be expected to affect the purpose or integrity of the study.

2.5.3 Mouse immunisations, observations, and sacrifice

Animal immunisations were carried out under a Home Office approved project licence (PC45ABD5B) by the team at at Scancell, UK. Mice were maintained in the animal unit at Nottingham Trent University according to home office guidelines and the project licence. Female Balb/C (Charles Rivers) mice were used and immunised with SN17. All mice in Group A received 1 DNA bullet via gene gun on days 1, 8, and 15, prepared by Peter Symonds and containing 5 ug DNA. Three mice in group B received a single 50 µl intradermal injection containing 10 µg SN17 pDNA with cationic liposomes at NP 3 on days 1, 8, and 15. Three mice in group C received a single 50 µl intradermal injection containing 10 µg SN17 pDNA with cationic liposomes at NP 9 on days 1, 8, and 15. Doses were selected in line with the standard protocol used by Scancell, UK.

Morbidity/mortality inspections were carried out twice daily, early and late during the working period with the exception of weekends and university closure dates where they were carried out once per day. Individual clinical observations and individual body weights were performed immediately before dosing on days 1, 8, and 15. Mice were sacrificed on day 19 of the study by cervical dislocation. Blood was harvested immediately after sacrifice through a cut in the neck of the mouse. Spleens were removed and used immediately after sacrifice.

2.5.4 Quantification of interferon gamma-producing splenocytes by ELISpot

ELISpot assay was performed ex vivo with respect to the peptides: Spike Receptor Binding Domain (RBD) 505-524, S protein, N protein, RBD peptide pool, and N peptide pool. All peptides were stored as lyophilised powder at

-80 prior to reconstitution at 1 mg/ml in solution containing 20% DMSO v/v and 80% PBS v/v.

Splenocytes harvested from mice from each group were treated and assayed independently. *Ex vivo* ELISpot assays were done using murine IFNγ capture and detection reagents according to the manufacturer's instructions (Mabtech AB, Nacka Strand, Sweden). Capture antibodies (10 μg/ml) were coated onto wells of 96-well Immobilin-P plate and triplicate wells were seeded with $5x10^5$ splenocytes in complete media (RPMI 10% FCS, 1% HEPES buffer, 1% glutamine, 1% penicillin/streptomycin) plus 2-mercaptoethanol. Synthetic peptides were used at a final concentration of 5 μg/ml in complete media plus 2-mercaptoethanol and added to these wells. Peptide pools and whole proteins (as detailed above) were used at a final concentration of 1 μg/ml.

Following incubation, captured antibody was detected by a biotinylated anti-IFNγ antibody (1/1000) and development with a streptavidin alkaline phosphatase (1/1000) and chromogenic substrate. Spots were analysed and counted using an automated plate reader (CTL Europe GmbH, Aalen, Germany). A total of 9 individuals were assayed.

2.5.5 Quantification of serum antibodies against S and N covid antigens by ELISA

Blood was collected from mice and allowed to clot for at least 30 minutes at room temperature. Sera were collected by centrifuging coagulated blood at 1000 g for 10 minutes and supernatant aspirated into a clean tube. Naïve mouse serum samples were used as a control. Aliquots of 25 μl were prepared and stored at -20°C for future assays if required. Sera were serially diluted 1/10 in 2% BSA-PBS and incubated for one hour at room temperature (RT) in coated S1 protein (GenScript Z03501), N protein (GenScript Z034880 and RBD proteins (Sino Biological 40592 V08H85 and V08H90), Nunc Immuno plate F96 MaxiSorp ELISA plates, all at 200 ng/well and then blocked with casein. Following three PBS washes, S1 and RBD antibody binding was detected using a 3-step approach consisting of Goat-

anti-mouse IgG, Fc biotin (Sigma B7401, 1:2000, 1 hour RT) followed by Streptavidin-HRPO conjugate (Invitrogen S911, 1:1500, 1 hour RT) and finally TMB core plus reagent (Bio-Rad BUF062C) for development. N antibody binding was detected using a 2-step approach where Goat pAb to mouse IgG (HRP) (Abcam ab20043, 1:5000, 1 hour RT) was used after the serum incubation step, followed by the development described above. In both instances, once sufficiently developed, the reaction was stopped using 1M H_2SO_4 and the plates were read at 450nm wavelength on a plate reader.

2.6 Role of temperature on the formation of DNA-liposome complexes

Liposomes composed of GL67:DOPE were prepared using the thin film method as described in section 2.3.2 and dessicated under nitrogen. Variation in laboratory ambient temperatures was observed during the formation of liposome-DNA complexes in chapter 5. Liposomes and DNA aliquots were incubated at 4°C, 18°C, or 37°C for 30 minutes. Liposome-DNA complexes at NP 3, 6, 9, and 12 were formed as described in section 2.3.2 and incubated at their given temperatures for a further 30 minutes. Size was measured by dynamic light scattering.

2.7 Statistical analysis

All data are displayed as mean ± standard deviation. Normal distribution was tested by the Shapiro-Wilk test. Student's t-tests were performed to compare means of two groups. One way analysis of variance (ANOVA) with post hoc Tukey's test was performed for comparisons of three or more group means. P-values of <0.05 were considered statistically significant; *$p<0.05$, **$p<0.01$, ***$p<0.001$, ****$p<0.0001$. Statistical analysis was carried out using Graphpad Prism version 10.

Chapter 3: Characterisation of a model liposome formulation (DC-Cholesterol/DOPE) capable of condensing DNA into a stable complex

3.1 Introduction

Delivery of DNA-liposome complexes relies on the careful control of their physicochemical properties to prepare for a variety of biological interactions. DC-Cholesterol, a cholesterol-derived cationic lipid, is well characterised in combination with DOPE, a fusogenic helper lipid, and the focus of this chapter will be on the characterisation of this formulation with a model GFP plasmid.

3.1.1 Methods of liposome preparation

Liposome formation has been historically carried out by a variety of methods. Yang et al (2012) examined the effect of formulating DC-Chol/DOPE liposomes using different preparation methods at mass ratios of 1:2, 1:1, and 3:2 and charge ratios of cationic lipid to DNA of 1, 2, and 4. Preparation of liposomes by thin film, reverse phase evaporation, or ethanol injection did not change morphology as measured by cryogenic transmission electron microscopy, all yielding spherical particles with integrated bilayers. Size was also not statistically different, forming liposomes 200 nm in diameter or lower. However, the thin film method yielded the most stable complexes with the highest zeta potential, resisting aggregation for up to two months. The researchers concluded that the thin film method was the most appropriate method for liposome formation.

In contrast, a study by Maitani et al (2007) compared DC-Cholesterol/DOPE liposomes formed by ethanol injection and thin film method, concluding that ethanol injection-prepared liposomes led to increased GFP expression in HeLa cells. However, this was less significant when DOPE formed a larger proportion of total lipid content and the authors theorised that the ethanol injection method was more effective at homogeneously distributing DOPE when present in lower proportions. This chapter will therefore investigate

a range of formulations where DC-Cholesterol consists of up to 50 mol% of the total lipid content.

3.1.2 DNA-liposome complex formation

Interaction between cationic liposomes and DNA is driven by electrostatic interactions between the positively charged cationic lipid and negatively charged phosphate backbone on DNA (Rodriguez-Pulido et al, 2008). In a study investigating the compaction of DNA by cationic liposomes, Rodriguez-Pulido et al (2008) formed liposomes out of a 1:1 ratio of DC-Cholesterol and DOPE, and combined them with calf thymus DNA (CT-DNA) at NP ratios of approximately 1, 2, 3, 4, 6, 8, and 10. Size and zeta potential were measured and complexes evaluated by cryogenic transmission electron microscopy and ethidium bromide displacement. The researchers plotted zeta potential as a function of NP ratio to identify the isoneutrality ratio (noted as L/D), or the ratio at which the negative charges of the DNA and positive charges of the cationic lipid result in a complex with a neutral overall charge (Figure 1). They discovered that with increasing NP ratio, the overall charge of the complex increased sigmoidally, reaching a plateau near the charge of the liposomes without DNA (Figure 6).

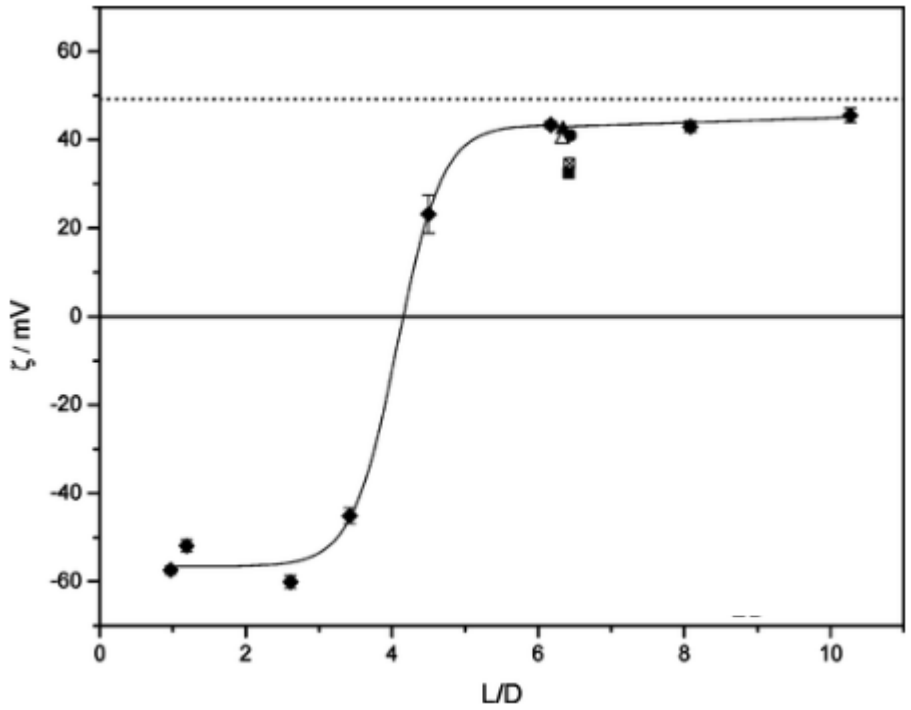

Figure 6. Taken from Rodrigues-Pulido et al (2008). Values of zeta potential (ζ, mV) of 1:1 DC-Chol/DOPE liposomes formed with calf thymus DNA in 40 mM HEPES buffer. Solid line: sigmoidal fit of zeta potential against lipid:DNA (L/D) mass ratio.

Optimised encapsulation efficiency of pDNA was found when the formulation contained DC-Chol and DOPE at a ratio of 0.89:1 and NP ratio of 3.8 using Box Behnken design, a statistical experimental design to yield response surface insights (Yang et al, 2012). However, optimal encapsulation efficiency may not correlate with optimal transfection efficiency; Maitani et al (2007) combined DC-Cholesterol and DOPE at ratios of 1:2, 1:1, and 3:2 at NP ratios of 1 to 11, finding that the charge ratio of liposome to DNA in the complex affected luciferase activity differently depending on DC-Cholesterol:DOPE ratio. Without DOPE, the optimum charge ratio of liposomes to DNA for luciferase activity was 7:1, but formulations of DC-Chol:DOPE at 3:2 and 1:2 had an optimum charge ratio of 2:1, decreasing slightly as charge ratio increased. Strongest expression across all formulations was observed in liposomes composed of DC-Chol:DOPE at a ratio of 1:2. This indicates that both content of DC-Cholesterol as a proportion of total lipid content and liposome:DNA ratio affects transfection outcome.

3.2 Chapter Aims and Objectives

3.2.1. Hypothesis

- Liposomes composed of DC-Cholesterol and DOPE formed by thin film method are small, monodisperse, and positively charged, and efficiently condense DNA into a stable complex.

3.2.2. Aims

- To optimise the formulation method of liposome using DC-Cholesterol and DOPE as model lipids.
- To investigate complexation between DNA and cationic liposomes.
- To evaluate mechanism of complexation between DNA and cationic liposomes.

3.2.3. Objectives

- Formulate liposomes at a range of cationic lipid compositions using the thin film method and measure size and polydispersity
- Add DNA to liposomes during thin film hydration or after extrusion to optimise complexation method
- Measure complexation efficiency using gel electrophoresis and ethidium bromide displacement
- Assess structure of DNA-liposome complexes by cryogenic transmission electron microscopy
- Investigate mechanism of DNA-liposome complexation by fluorescence resonance energy transfer

3.4 Results

3.4.1 Empty liposomes by filter size

Liposomes were initially formulated by thin film method as described in section 2.3.1 with a range of formulations consisting of 25, 30, 35, 40, and 50 mol% DC-Cholesterol, with the aim to obtaining small, monodisperse liposomes with an overall positive charge. Liposomes were extruded by hand through membranes with pore sizes of 400, 200, or 100 nm. Size was measured by dynamic light scattering and monodispersity judged to be 0.2 or below on the polydispersity index (Figure 7).

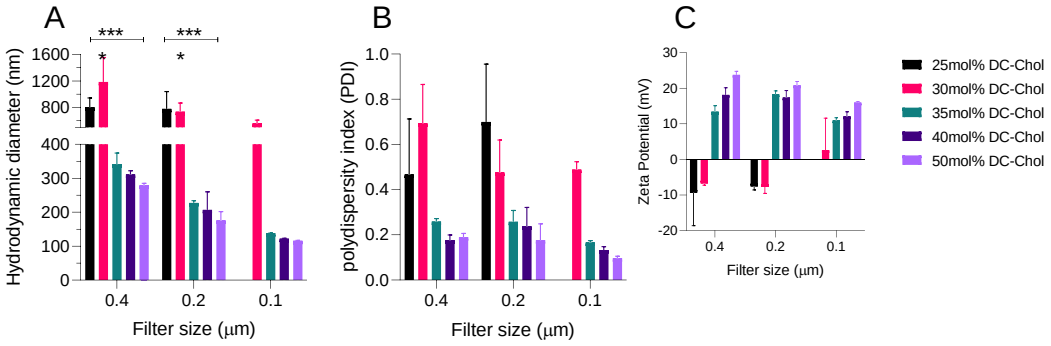

Figure 7. Physicochemical characterisation of cationic liposomes according to molar ratio of DC-Chol:DOPE. A) hydrodynamic diameter of liposomes and B) polydispersity index measured by dynamic light scattering, and C) zeta potential measured by electrophoretic mobility. Bars represent mean ± one standard deviation, one batch each filter size with 9 repeats for filter sizes 0.4 and 0.2 μm, three repeats for filter size 0.1 μm. ****p<0.0001; one-way ANOVA.

For each formulation, a slight decrease in particle size was observed as membrane pore size decreased. Extrusion through any pore size resulted in liposomes greater than 600 nm with a negative zeta potential for formulations containing 25 mol% or 30 mol% DC-Cholesterol. Formulations containing 35 mol%, 40 mol%, or 50 mol% DC-Cholesterol were monodisperse and positively charged across membrane pore sizes, increasing in charge with DC-Cholesterol content.

When liposomes were extruded through 400 nm pore size membranes, a reduction in liposome size was observed as DC-cholesterol content increased. This was also noticeable when extrusion was through 200 nm

pore size membranes, albeit to a lesser extent, and least of all through 100 nm. Formulations containing 35 mol%, 40 mol%, or 50 mol% DC-Cholesterol were taken forward due to the predictability in particle size and low polydispersity, extruded through 100 nm membranes for the consistency.

3.4.2 Hydration of liposome thin films with DNA

Formation of liposome-DNA complexes was first explored by hydrating lipid thin films with DI water. Thin films were first hydrated by water alone, either by vortex for 20 minutes (Figure 2A), shaking water bath for 24 hours (Figure 2B), or sonication for one minute (Figure 2C). Thin films were not hydrated by the water bath; water was still clear and there were visible lipid deposits on the bottom of the glass. Vortexing hydrated thin films moderately well, showing few lipid aggregates in solution. Sonication hydrated thin films into cloudy suspensions with no aggregates, but is not suitable for DNA due to shear stress.

Vortexing was selected for further study in hydrating thin films with a DNA solution at NP 3. Vortexing for 23 minutes and 45 seconds yielded a homogenous suspension (Figure 2D) but visible aggregation was observed within minutes in the flask (Figure 2E) and in the extruder, preventing further extrusion (Figure 2F-G). Furthermore, vortexing for that duration presents potential for shear stress and associated damage to DNA. Therefore, sonication was chosen as the hydration method going forwards; to avoid excessive shear stress, DNA was added to liposomes after hydration as described in section 2.3.2.

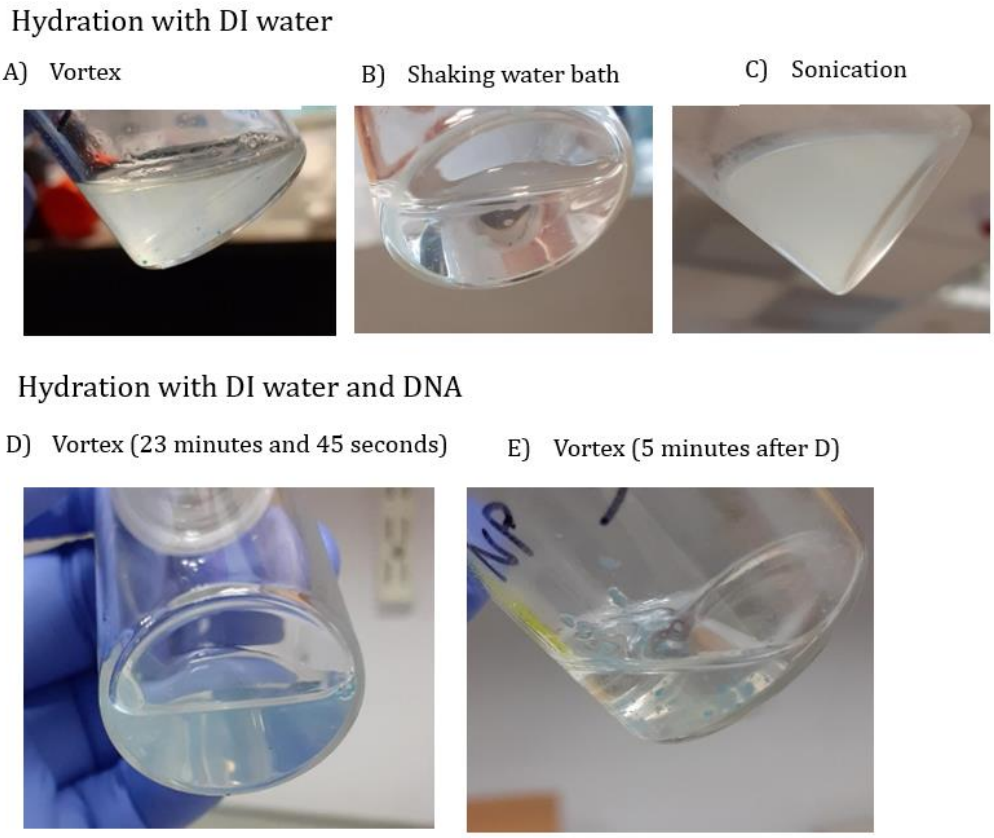

Figure 8. Attempted encapsulation of DNA during hydration of lipid thin films. A-C represent hydration methods of thin films without DNA with DI water. A) thin film was vortexed for 20 minutes. B) thin film was placed in a water bath at 37°C for 24 hours and shaken continuously at 100 rpm. C) thin film was sonicated for one minute. D-E represent hydration of thin film with water containing DNA; D) immediately after vortexing for 23 minutes and 45 seconds, E) five minutes after stopping the vortex.

3.4.3 Characterisation of complexes made by combining DNA and liposomes in suspension

To understand the effect of adding DNA to cationic liposome preparations, liposomes extruded through a polycarbonate membrane of 0.1 um with DC-Cholesterol content at or above 35 mol% were incubated with DNA at NP ratios of 3, 6, 9, and 12 as described in section 2.3.2. NP ratios were calculated by molar ratio of nitrogen groups (N) on DC-Cholesterol to phosphate groups (P) on DNA backbone where DNA is assumed to have a molecular weight of 660 g/mol. NP 3 can be understood as 3 nitrogen groups to 1 phosphate group.

Particle size and charge were measured as described in section 2.3.3 (Table 3). Addition of DNA to liposomes was observed to lead to increase in particle size regardless of formulation or ratio. For formulations with 40mol% or 50mol% DC-Cholesterol, addition of pDNA at NP3 increased particle size the most. A decrease in polydispersity upon the addition of pDNA was observed regardless of ratio for all formulations. Addition of DNA led to a decrease in particle charge for 40mol% DC-Cholesterol when pDNA was added at NP3.

	Empty	NP 3	NP 6	NP 9	NP 12	
Size (nm)						***p***
35mol% DC-Chol	82 ± 4	105 ± 2	99 ± 1	92 ± 2	89 ± 1	****
40mol% DC-Chol	119 ± 5	240 ± 7	159 ± 4	140 ± 3	141 ± 5	****
50mol% DC-Chol	120 ± 1	218 ± 7	148 ± 1	140 ± 2	140 ± 5	****
PDI						
35mol% DC-Chol	0.382 ± 0.005	0.158 ± 0.004	0.160 ± 0.011	0.196 ± 0.020	0.215 ± 0.012	****
40mol% DC-Chol	0.213 ± 0.011	0.060 ± 0.016	0.120 ± 0.003	0.114 ± 0.014	0.113 ± 0.017	****
50mol% DC-Chol	0.217 ± 0.020	0.068 ± 0.032	0.114 ± 0.007	0.134 ± 0.014	0.158 ± 0.021	****
Charge (mV)						
35mol% DC-Chol	25.7 ± 1.5	33.6 ± 2.5	40.3 ± 0.53	40.3 ± 2.6	37.4 ± 3.7	ns
40mol% DC-Chol	42.3 ± 3.0	8.4 ± 2.0	35.9 ± 2.3	39.8 ± 1.2	43.2 ± 0.2	****
50mol% DC-Chol	42.7 ± 1.6	40.7 ± 2.4	40.0 ± 3.05	42.7 ± 0.8	40.9 ± 2.8	ns

Table 3. Hydrodynamic size, polydispersity index, and zeta potential of liposome-DNA complexes. Liposomes formulated with different molar ratios of DC-Cholesterol:DOPE were combined with plasmid DNA encoding GFP (GFP pDNA) at different nitrogen: phosphate (NP) ratios. Data for hydrodynamic diameter and polydispersity index indicate mean of nine repeats ± one standard deviation. Data for zeta potential indicate mean of three repeats ± one standard deviation. Differences in group means were analysed by one-way ANOVA; ****p<0.0001, ns=not significant.

3.4.4 DNA encapsulation efficiency by gel retardation

To investigate whether any DNA remained free in solution after complexation with liposomes, liposome-DNA complexes were run through 1% agarose gels containing ethidium bromide as described in section 2.3.4 (Figure 9). DNA detected within the gel is visible under ultraviolet light due to ethidium bromide intercalation; if DNA is uncomplexed, it should travel within the gel and be visible as a band the same distance as the free DNA control.

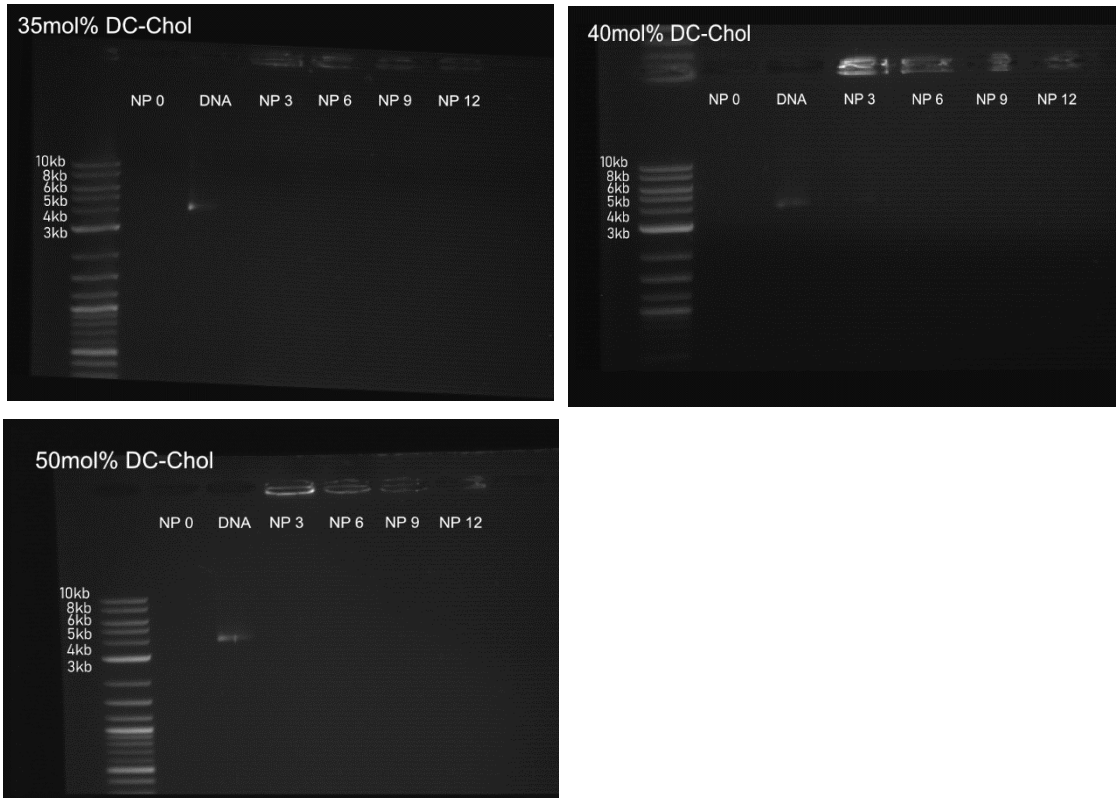

Figure 9. Gel retardation of liposome-DNA complexes. Liposomes composed of DC-Cholesterol and DOPE at A) 35mol% DC-Chol, B) 40mol% DC-Chol, and C) 50mol% DC-Chol were combined with GFP pDNA at NP ratios and loaded into 1% agarose gels to visualise unbound DNA.

Gel retardation relies on free DNA having the ability to travel within the body of the agarose gel when a 120 V current is applied; no bands were observed in liposome conditions, indicating that 100% of the DNA was successfully condensed in all NP ratios. Densitometry was carried out in ImageJ and used to confirm that in all formulations, DNA was detectable within the body of the gel for the control DNA band but not in liposomal conditions at any NP ratio.

3.4.5 DNA encapsulation efficiency by ethidium bromide displacement

Quantification of DNA complexation by cationic liposomes was investigated by ethidium bromide displacement as described in section 2.3.6. Before complexation, DNA was stained with ethidium bromide and fluorescence measured to investigate the degree to which conformational changes undergone in DNA during complexation to liposomes displaced the ethidium bromide. Reduction in fluorescence intensity was taken as indication of successful complexation (Figure 10).

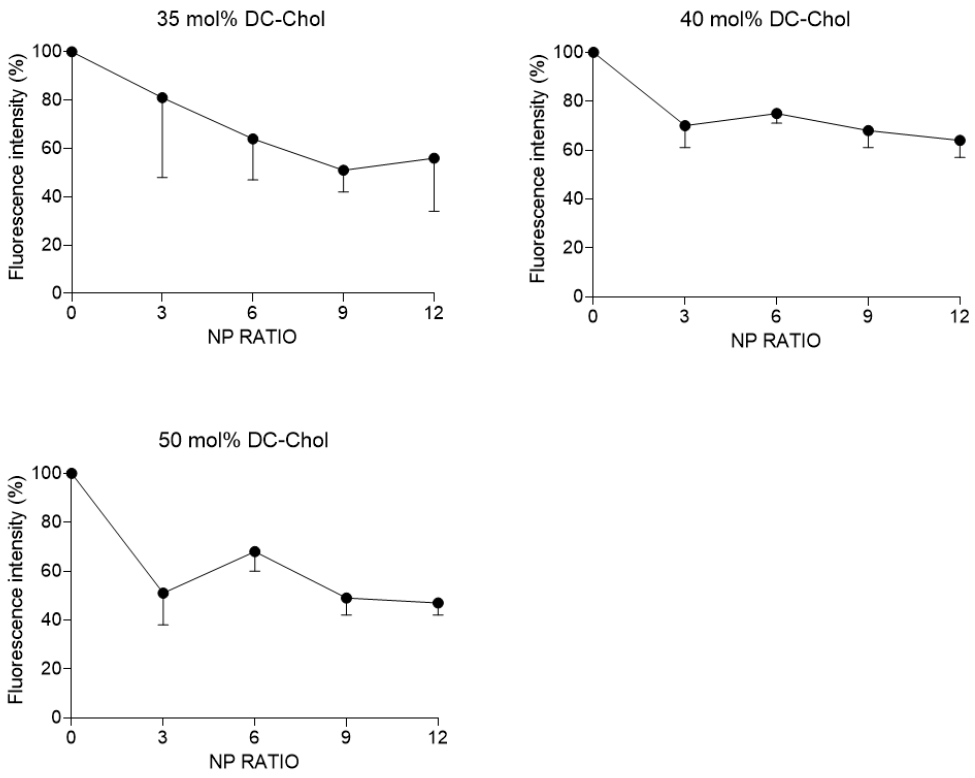

Figure 10. Ethidium bromide displacement of cationic liposomes prepared at a range of DC-Chol:DOPE liposomes and NP ratios. Data represent mean ± one standard deviation (N=4 measurements of single batch).

At NP 12, a 50% reduction in fluorescence was observed across formulations. Liposomes with 50 mol% DC-Cholesterol showed the greatest displacement at lower NP ratios compared to formulations with lower DC-Cholesterol content.

Ethidium bromide displacement is variable by formulation, resulting in a reduction in ethidium bromide fluorescence from 20-50%.

3.4.6 Cryogenic transmission electron microscopy (cryoTEM) of DNA-liposome complexes

Structural analysis of liposome-DNA complexes was done by cryoTEM in collaboration with the nmRC at the University of Nottingham (section 2.3.8). A uniform population of single layered liposomes was observed in A. In B and C, addition of DNA yields "doughnut" shapes of multi-layered liposomes with darker, grainy space between layers suggested to be DNA.

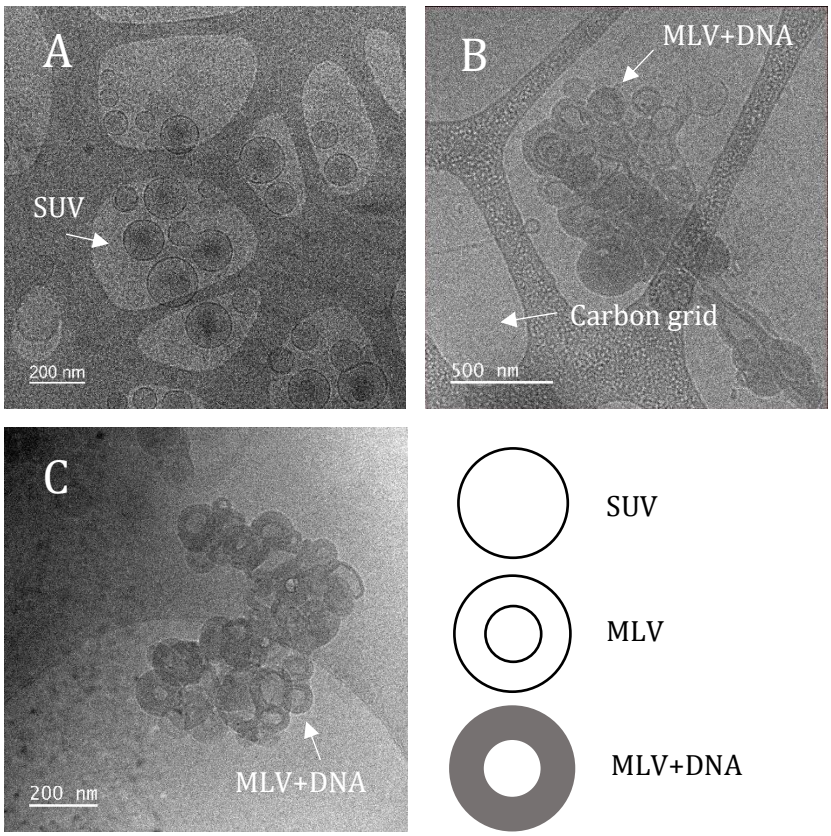

Figure 11. Cryogenic transmission electron microscopy images of liposomes prepared with 40 mol% DC-Cholesterol. A) liposomes without DNA, B) liposomes with DNA at NP 3, and C) liposomes with DNA at NP 9. Structures observed are indicated by arrows and referenced in the diagram.

To compliment dye exclusion studies and investigate further the effect of the addition of DNA to liposomes on the structure of the resulting complex, cryogenic transmission electron microscopy (cryo-TEM) was used to image the complexes (Figure 11). Due to the aqueous core, flash freezing in liquid ethane provided a more accurate representation of the complex structure than traditional dessication methods. Imaging of liposomes prior to the addition of DNA showed a uniform population of unilamellar liposomes. After the addition of DNA, multilamellar structures were observed with dark, grainy space between layers suggestive of DNA.

3.4.7 Liposome membrane fusion as a mechanism for DNA-liposome complexation

To investigate the mechanism of liposome-DNA complex formation as observed by cryoTEM images in section 3.4.6, liposome membrane fusion was measured by fluorescence resonance energy transfer (FRET). FRET data was collected by Fady Mina during a project rotation at the beginning of his PhD under the supervision of the author of this thesis as described in section 2.3.7 (Figure 12).

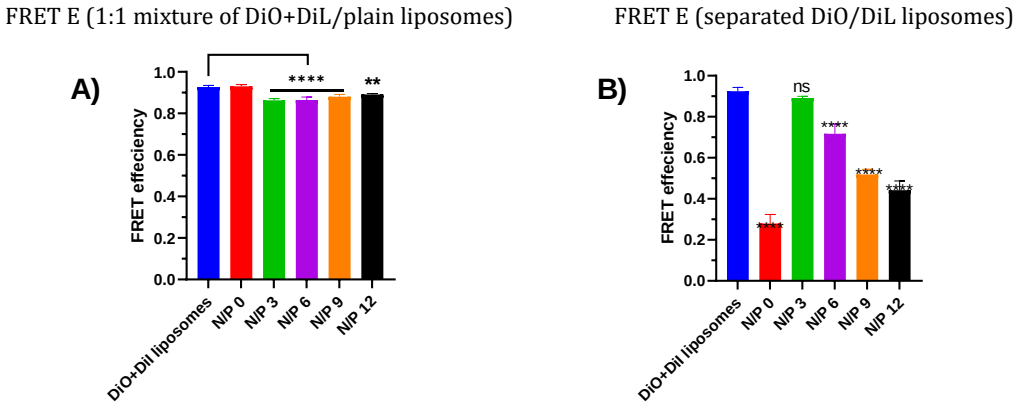

Figure 12. FRET efficiency (FRET E) by two different approaches of DC-Chol:DOPE lipoplexes with different N/P ratios. A) FRET E of lipoplexes composed from a 1:1 mixture of dually labelled DiO+DiI liposomes and unlabelled liposomes in presence of different N/P ratios. B) FRET E of lipoplexes composed from a 1:1 mixture of DiO and DiI labelled liposomes in presence of different N/P ratios. Results are displayed as mean ± S.D. with n=3; ****= P<0.0001 in comparison against all groups; **=P<0.01 in comparison against control group, ns=not significant compared to control groups.

The first experiment (Figure 12A) involves the incubation of liposomes dually labelled with DiO and Dil with liposomes containing no fluorophores. A reduction in fluorescence indicates dilution of the dyes and fusion of the liposomal membranes, which was observed when DNA was added regardless of NP ratio.

In the second experiment (Figure 12B), two populations of liposomes were prepared with only one of each fluorophore. When combined and DNA added, an increase in fluorescence (FRET E) was observed, indicating liposomal membrane fusion by DiO and DiL proximity. When DNA was added at NP 3, fluorescence equalled the positive control of dually labelled

DiO+Dil liposomes with a gradual lessening of the effect as less DNA was added at higher NP ratios.

3.5 Discussion

Cationic liposomes present the capacity to condense negatively charged DNA into small, monodisperse, positively charged stable complexes. These complexes are attractive vehicles for vaccination purposes due to their nontoxicity and modifiability. In this study we have used a well-characterised liposome formulation shown in the literature to be capable of condensing DNA into stable complexes (Rodriguez-Pulido et al, 2008; Maitani et al, 2007; Munoz-Ubeda et al, 2010) and initiating an antigen-specific immune response (Perrie et al, 2003). In this chapter, the key aims were to formulate liposomes containing DC-Cholesterol and DOPE and condense them with DNA to obtain and characterise small monodisperse cationic complexes in preparation for cellular delivery studies in chapter 4.

First, liposomes were formulated with DC-Chol and DOPE at different molar ratios. Small, monodisperse suspensions of liposomes were observed when DC-Cholesterol exceeded 35 mol% of total lipid content. Cholesterol is known to increase rigidity and permeability of liposome membranes (Kaddah et al, 2018). Redondo-Morata et al (2012) investigated the local properties of lipid bilayers in liposomes in a range of compositions of cholesterol forming up to 50 mol% using temperature-controlled atomic force microscopy. At 30 mol% or below, hydration was observed to yield heterogeneous populations of cholesterol-rich and cholesterol-poor liposomes. In the system described in this chapter, this would result in a heterogeneous population of liposomes with one population formed of primarily DC-Cholesterol and one formed of primarily DOPE. This may account for the increase in particle size, since an excess of DOPE in liposomal formulations has been linked to aggregation (Maitani et al, 2007). Redondo-Morata et al (2012) also noted that in compositions containing 40 mol% and 50 mol% cholesterol, liposome bilayers were homogeneous. Although some heterogeneity was observed in formulations between 30 mol% and 40 mol%, it was to a lower extent than observed in formulations

containing less than 30 mol%; it was suggested that the two populations of cholesterol-rich and cholesterol-poor liposomes were no longer in equilibrium and instead were able to enrich each other. For these reasons, formulations containing above 35 mol% DC-Cholesterol were proceeded with to examine capability of condensing DNA.

DNA was first added to liposomes during hydration, in the interest of encapsulating DNA within the liposome core. Significant aggregation was observed and presented a risk of shear stress to DNA integrity by the length of time on vortex. This led to the conclusion that complex formation should be pursued by adding DNA after liposome hydration and extrusion. When liposomes were hydrated without DNA by sonication and extruded, and DNA added to liposomes in suspension, small stable monodisperse complexes were obtained.

Efficiency of DNA-liposome complexation was obtained by agarose gel retardation (Figure 3), ethidium bromide displacement (Figure 4), and cryogenic transmission electron microscopy (Figure 6). At first glance, the ethidium bromide displacement assay indicated only a moderate displacement of ethidium bromide at NP ratios of 9 and 12 and statistically insignificant displacement at NP 3 and 6, suggesting that the DNA is not bound tightly enough to the liposome to displace the ethidium bromide from where it intercalates between base pairs. This is in contrast to the agarose gels, which did not show detectable free DNA. However, Cryo-TEM showed multilamellar lipid structures with a dark, grainy layer between membranes suggestive of DNA. Previous literature has observed similar (Sternberg, Cevc papers). It is possible that DNA entrapment between liposome bilayers also entrapped ethidium bromide, preventing disassociation and decrease in signal.

The mechanism of complex formation was investigated by FRET studies carried out by Fady Mina. FRET relies on the use of two or more fluorophores that can yield a stronger or distinct fluorescence spectra when in proximity with each other. When combined in the same suspension and DNA added, fusion of the membranes was observed by an increase in FRET

E due to the proximity of dyes recombining. When DNA was added at NP 3, fluorescence equalled the positive control of dually labelled DiO+Dil liposomes with a gradual lessening of the effect as less DNA was added at higher NP ratios. Fusion was therefore observed with the addition of DNA in proportion to the amount added; lower NP ratios with higher concentration of DNA caused a greater degree of fusion. It has been reported in the literature that DNA can initiate dynamic fusion of liposomal and biological membranes (Li et al, 2023) by structural reconfiguration, resulting in geminally bound liposomes with distinct loading compartments, or fully fused liposomes with mixed containments as observed in the cryoTEM images in this chapter. Using a FRET labelling system, Paez-Perez et al (2022) observed that addition of DNA to liposomes resulted in tendril-like DNA-based fusogenic nanostructures which were capable of overcoming repulsive electrostatic and steric forces between liposomes and destabilising membranes for lipid molecules to be exchanged between layers. This fusion mechanism was rapid, resulting in reorganisation of liposome membranes that yielded a population of stable complexes. This fusogenicity has promising implications for cellular uptake, and in chapter 4 will be investigated alongside induced GFP expression by liposome-DNA complexes composed of liposomes with 40 mol% DC-Cholesterol.

3.6 Conclusions

DC-Cholesterol and DOPE yield small monodisperse liposomes when DC-Cholesterol exceeds 35 mol% of total lipid composition. Complexes were best formed when DNA was added after liposomes were hydrated and extruded, and complexed 100% of DNA added at NP ratios 3, 6, 9, and 12. Cryo-TEM showed multilamellar structures, potentially due to restructuring of membranes and trapping of DNA between layers. This may account for additional trapping of ethidium bromide in the displacement assay and only moderate displacement, and is supported by FRET data indicating membrane fusion.

Chapter 4: Evaluation of encoded protein expression by DNA-liposome complexes formulated with DC-Cholesterol and DOPE

4.1. Introduction

As discussed in Chapter 1, elicitation of immune responses *in vivo* is dependent on the presentation of antigen by antigen presenting cells (APC). The intradermal microenvironment contains such APCs as dendritic cells, Langerhans cells, and fibroblasts (Drabick et al, 2001). Dendritic cells and their subtypes have been extensively researched as drivers of T cell response, and dermal fibroblasts have been found to influence the activation and maturation of dermal dendritic cells (Montes-Gomez et al, 2020). Investigation of the transfection efficiency of DC-Cholesterol and DOPE liposomes in cell lines representative of these cell types provides an opportunity to model the liposomes efficacy when administered intradermally *in vivo* (Garu et al, 2016).

4.1.1. DC-Chol DOPE and cell line selection

DC-Cholesterol/DOPE liposomes have been used to deliver plasmid DNA to a range of cell lines including the human breast cancer cell line SK-BR3 (Zhang et al, 2010), the human embryonic kidney cell line derivative HEK293T (Yang et al, 2013; Choi et al, 2001), and the murine fibroblast cell line NIH 3T3 (Choi et al, 2001).

A study by Inoh et al (2017) detailed the formation of liposomes using a cationic cholesterol lipid, cholesteryl-3β-carboxyamido ethylene-N-hydroxyethylamine (OH-Chol), and DOPE. By complexing these liposomes with a plasmid DNA encoding luciferin, they evaluated transfection efficiency in bone marrow derived dendritic cells using the luciferase assay. A correlation was found between lipoplex size and gene transfection efficiency, as well as with the predominant endocytosis pathway; lipoplexes with an average diameter of less than 275nm were taken up by caveolae-mediated endocytosis which is largely deemed non-degradative. This study highlighted that liposomes composed of DOPE and a cationic cholesterol

lipid structurally similar to DC-Cholesterol (Figure 1) are capable of efficiently transfecting dendritic cells.

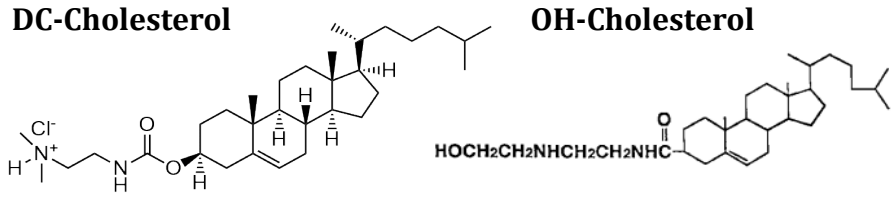

Figure 13. DC-Cholesterol structure taken from Avanti Polar Lipids, US. OH-Cholesterol structure taken from Okayama et al (1997).

Comparison of DC-Chol/DOPE lipoplex transfection efficiency in HEK293 and NIH 3T3 cells reported low toxicity of the liposomes and cell-dependent transfection efficiency (Choi et al, 2001). Using a plasmid encoding for beta Gal and quantifying its production by beta galactosidase assay, HEK293 showed activity approximately 40% of the positive control polyethyleneimine but significantly higher cell survival while NIH 3T3 showed low transfection. For the purpose of this chapter, the transfection efficiency of DC-Cholesterol/DOPE liposomes will be investigated in HEK293T cells, a variant of HEK293 containing an SV40 cassette to improve transfection (Yang et al, 2013) as a well-established transfection model, NIH 3T3 cells as a stromal fibroblast model, and a murine dendritic cell line DC2.4 (Perche et al, 2010) as the dendritic cell model. These cell lines were chosen to represent dermal dendritic cells to investigate direct immune cell uptake of lipoplexes (DC2.4), bystander fibroblast cells to assess bystander cell uptake of lipoplexes (NIH 3T3), and uptake of lipoplexes in a well-characterised early screening transfection model (HEK293T).

4.1.2. Methods for *in vitro* investigations of transfection efficiency

The evaluation of transfection efficiency in cells has been done by quantification of protein expression using enzymatic assays such as luciferase (Drabick et al, 2001) or beta galactosidase (Choi et al, 2001), or fluorescent marker expression such as GFP (Garu et al, 2016). Both systems have advantages and disadvantages. Enzymatic assays quantify protein expression accurately, quickly, and cheaply. However, this quantifies total

expression over a given cell population without providing information on how many cells express the encoded proteins, and cell toxicity assays must be carried out separately. Conversely, evaluating GFP by flow cytometry offers the opportunity to determine the population of cells expressing GFP and correlate with cell survival, as well as measure fluorescence intensity as an indirect indicator of levels of expression. For the cell population data, a pGFP DNA will be used in this chapter.

4.1.3. Methods for *in vivo* investigations of vaccine delivery

In vivo investigations of immune responses to a vaccine formulation are designed to measure antigen-specific responses including cell-mediated pathways such as proinflammatory cytokine production and humoural pathways such as antibody production. Both are initiated by T cells, which rely on the presentation of antigens by APCs (Clausen and Stoitzner, 2015); in the dermal compartment, dendritic cells continually sample the microenvironment for foreign or "dangerous" antigens before trafficking to local lymph nodes to present to naïve T cells. Immature dendritic cells can have a deleterious or tolerogenic effect on T cells reactive to the antigen, while sufficiently activated mature dendritic cells initiate T cell responses, which can include both B cell activation for antibody production and systemic T cell expansion for cell-mediated responses. Measurement of these responses differs depending on both route of administration and the antigen being delivered. Dermal vaccination has potential benefits for both therapeutic and prophylactic vaccines, and investigation methodology differs slightly between the two.

A study conducted by Layek et al (2015) examined immune responses initiated by an intradermally delivered polymeric hepatitis B DNA vaccine. Female balb/c mice were immunised intradermally with a second dose two weeks after the first. Antibody response in sera was evaluated by enzyme linked immunosorbent assay (ELISA), which consists of coating a 96-well plate with a detection antibody before incubating with serum and detecting antibody present by an enzymatic colour change. Cellular immune responses were evaluated by isolating splenocytes and stimulating with

hepatitis B antigen. Proinflammatory cytokine production was then measured again by ELISA, and cell proliferation was measured by MTT assay. Alternatively, cell-mediated immune responses can be measured by chromium release assay and the ex vivo ELISpot (Pudney et al, 2010). Chromium release assay measures the release of sodium chromate by splenocytes in response to cell death induced by incubation with antigen. The ex vivo ELISpot combines the steps followed in the study by Layek et al (2015), where splenocytes are incubated in a 96-well plate, stimulated with the target antigen, and interferon gamma production is measured by counting visible colorimetric spots. Pudney et al (2010) immunised mice with the melanoma antigen TRP2 and carried out a tumour challenge study by immunising mice with melanoma cells and measuring tumour growth with and without additional TRP2 vaccination. However, this chapter will model immune reactions using a SARS-Cov-2 model plasmid provided by Scancell, UK and evaluate antibody response by ELISA and splenocyte response by ELISpot in accordance with their preexisting protocols.

4.2. Hypothesis, Aims, and Objectives

4.2.1. Hypothesis

- Liposomes composed of DC-Cholesterol and DOPE effectively deliver DNA to fibroblasts and dendritic cells.

4.2.2. Aims

- To control for cell confluency and lipofectamine content in the transfection protocol
- To evaluate the cellular uptake of DC-Cholesterol and DOPE liposomes in the HEK293T, NIH 3T3, and DC2.4 cell lines
- To investigate the expression of GFP *in vitro* when GFP pDNA is delivered by DC-Cholesterol and DOPE liposomes
- To investigate murine antigen-specific humoural and cell-mediated immune responses *in vivo* when a model SARS-Cov-2 pDNA is delivered intradermally by DC-Cholesterol and DOPE liposomes

4.2.3. Objectives

- Determine the effect of cell confluency and lipofectamine concentration on GFP expression in RAW cells
- Assess uptake of GFP pDNA-liposome complexes in HEK293T, NIH 3T3, and DC2.4 cells by flow cytometry
- Measure GFP expression in HEK293T, NIH 3T3, and DC2.4 cells when GFP pDNA is delivered by DC-Cholesterol/DOPE liposomes
- Assess the extent of *in vitro* endosomal trapping by measuring expression of GFP with and without a chloroquine diphosphate pretreatment of cells
- Measure murine serum anti-nucleoprotein and anti-spike protein antibodies after immunisations with DC-Cholesterol and DOPE liposomes delivering a model SARS-Cov-2 pDNA
- Measure interferon gamma production by splenocytes in response to SARS-Cov-2 nucleoprotein and spike protein antigens after immunisations with DC-Cholesterol and DOPE liposomes delivering a model SARS-Cov-2 pDNA

4.4 Results

4.4.1 Influence of cell confluency and lipofectamine concentration on GFP expression and cell viability

Initial transfection by lipofectamine 2000 was carried out in DC2.4 cells to control for cell seeding density and lipofectamine concentration due to its use as a positive control in subsequent transfections. Cells were seeded at either $1x10^5$ or $2x10^5$ cells per well in a 24-well cell culture plate and transfected with GFP pDNA at a ratio of 1 μg pDNA to 1.5 μl lipofectamine reagent, or 1 μg pDNA to 3 μl lipofectamine reagent. GFP expression was imaged by fluorescence microscopy in the EVOS fl microscope at 48 and 72 h post transfection (Figure 14).

When cells were plated at $1x10^5$ cells per well, stronger GFP expression was observed in cells transfected using 3 μl lipofectamine per 1 μg pDNA. Viability of cells measured by live/dead stain as described in section 2.4.6 did not appear to be reduced with the higher lipofectamine concentration. GFP expression remained stable up to 72 h. When cells were plated at $2x10^5$ cells per well, stronger GFP expression was also observed in cells transfected by the higher lipofectamine concentration. However, GFP expression decreased at 72 h compared to 48 h. Cell viability also decreased at 72 h and was lower overall compared to cells plated at a lower density. Experimentally going forward, cells were plated at $1x10^5$ cells per well and transfected using 3 μl lipofectamine per 1 μg DNA.

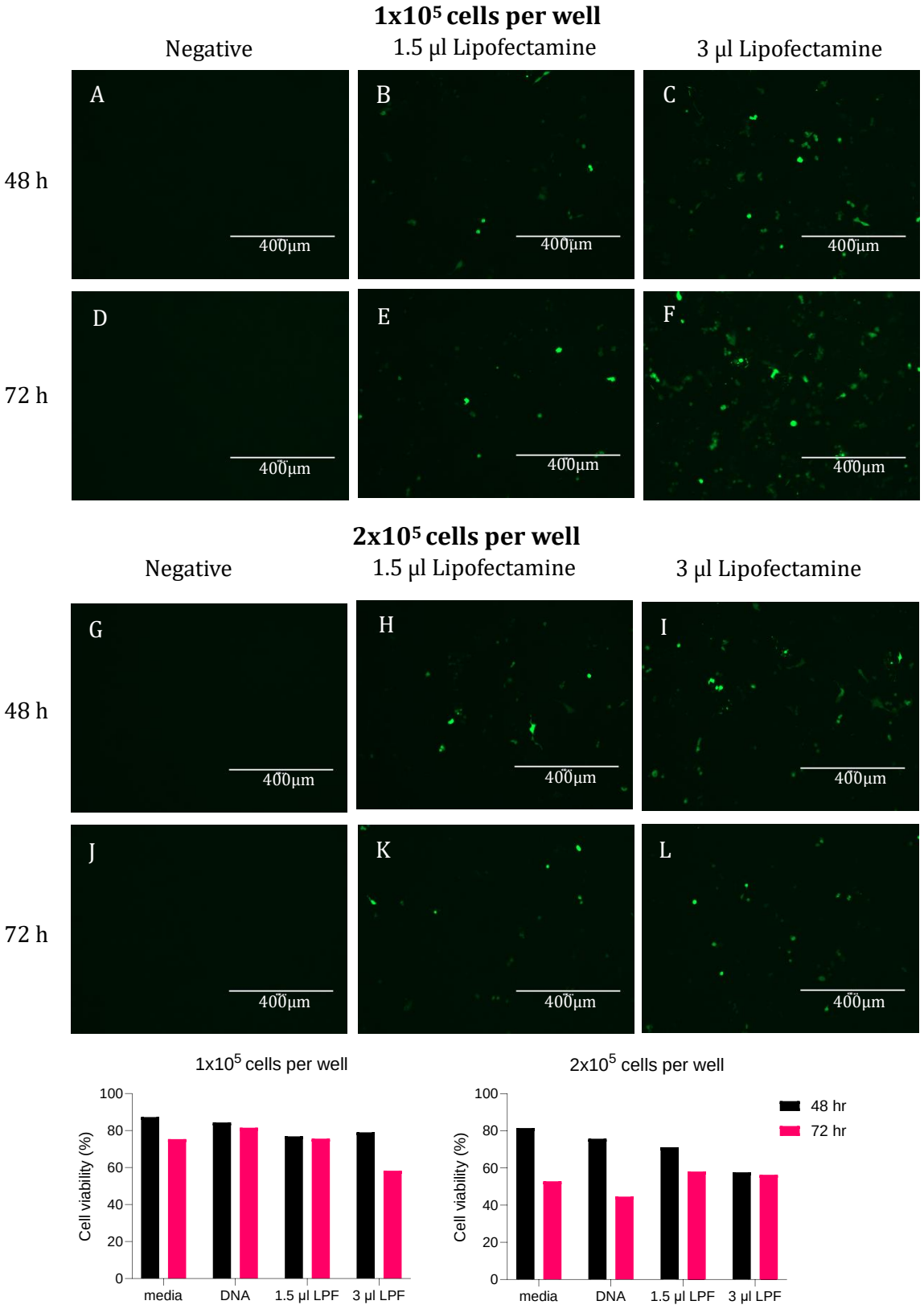

Figure 14. GFP expression and cell viability of DC2.4 cells when lipofectamine and cell plating densities are controlled. DC2.4 cells were plated in 24-well plates at $1x10^5$ (A-F) or $2x10^5$ (G-L) cells per well and incubated for 2 h with 1 µg DNA per well. DNA was delivered by lipofectamine 2000 at a ratio of either 1.5 µl or 3 µl lipofectamine per 1 µg DNA. Cells were imaged at 48 and 72 h to detect GFP expression, and flow cytometry was used to determine cell viability by live/dead stain.

4.4.2 Cellular uptake of DNA-liposome complexes by cell line

Liposomal uptake was investigated to establish the degree of internalisation in three cell lines, chosen to represent a classical transfection model (HEK293T), murine fibroblasts (NIH 3T3) and murine dendritic cell (DC2.4). Transfection was carried out as described in section 2.4.4, with cells prepared for flow cytometry as described in section 2.4.6. Data from flow cytometry were gated on live cells, determined by live/dead zombie stain, and DiD-associated fluorescence quantified by logarithmic shift in comparison to a negative cell population. Strong fluorescence was observed in all three cell lines, indicating effective (greater than 90% positive) uptake in live cells regardless of NP ratio or cell line (Figure 15).

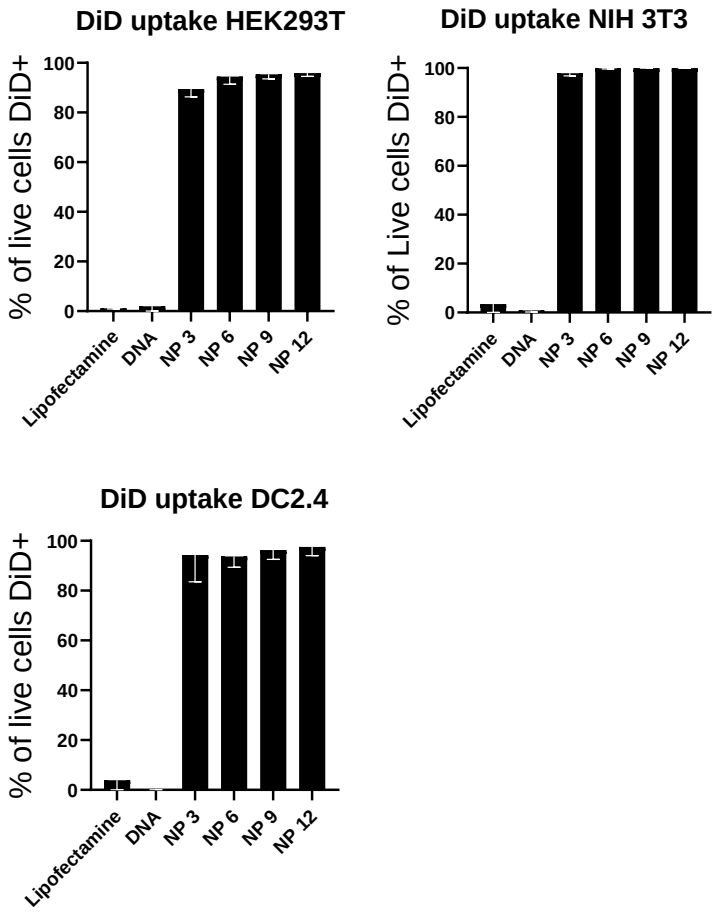

Figure 15. Uptake of DiD-labelled liposome complexes composed of DC-Chol:DOPE (43:57) and GFP pDNA at different NP ratios. Bars represent percentage of live cells positive for DiD-associated fluorescence in HEK293T (left), NIH 3T3 (middle) and DC2.4 (right) cell lines. Viability was greater than 75% across all conditions. Bars represent mean ± one standard deviation (n=6 across two experiments).

4.4.3 GFP expression by cell line

The capacity of DC-Chol/DOPE liposomes to induce GFP expression in the chosen cell lines was investigated by transfection and flow cytometry. Transfection efficiency and GFP expression was seen to be dependent on cell line more than NP ratio; while a slight increase in expression was observed with increase in NP ratio for DC2.4 and NIH 3T3 cells, the opposite was true for HEK293T cells. However, the strongest expression was observed in HEK293T cells, with moderate expression observed in NIH 3T3 cells, and low expression observed in DC2.4 cells (Figure 16).

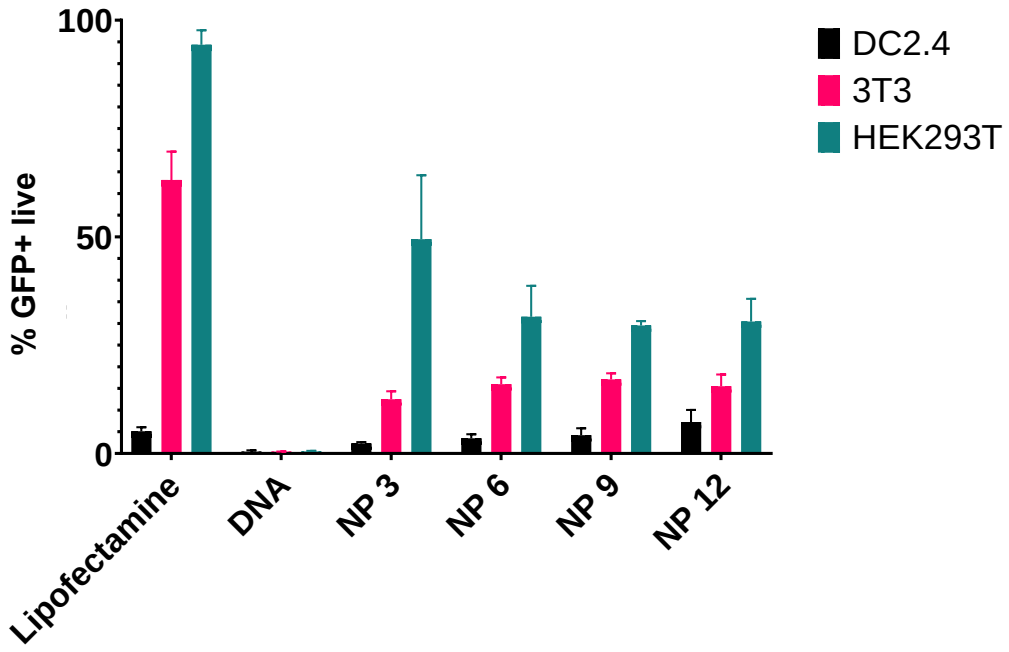

Figure 16. Expression of GFP when delivered by DC-Chol:DOPE liposomes analysed by flow cytometry. Bars represent percentage of live cells that show GFP-associated fluorescence. N=3, n=3 per cell line.

4.4.4 Chloroquine toxicity by cell line

To investigate potential endosomal entrapment of liposomes as a mechanism for limiting GFP expression, each of the three cell lines (NIH 3T3, DC2.4, and HEK293T) was treated with a logarithmic curve of the endosome disruptor chloroquine disphosphate as described in section 2.4.7 (Figure 17).

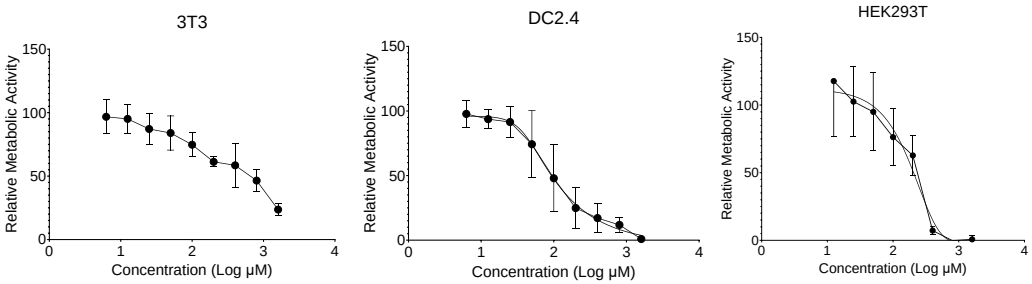

Figure 17. Chloroquine toxicity on NIH 3T3, DC2.4, and HEK293T cell lines by prestoblue assay. Cells were incubated with a range of chloroquine concentrations for 4 h and prestoblue used to determine cell viability. Data represent mean ± one standard deviation (N=12 across 3 experiments each) with nonlinear regression.

DC2.4 cells were more sensitive to chloroquine diphosphate than NIH 3T3 or HEK293T cells, with nonlinear regression showing a steeper curve. Concentrations were chosen below IC50 for each cell line for subsequent chloroquine diphosphate studies; 50 μM for DC2.4 and 100 μM for NIH 3T3 and HEK293T.

4.4.5 GFP expression with endosomal disruption by cell line

Transfection was repeated with a 30 minute pretreatment with chloroquine diphosphate to prevent endosome acidification as described in section 2.4.5; an increase in transfection efficiency with chloroquine pretreatment would indicate that endosomal entrapment of liposome complexes is occurring as a mechanism of GFP expression limitation.

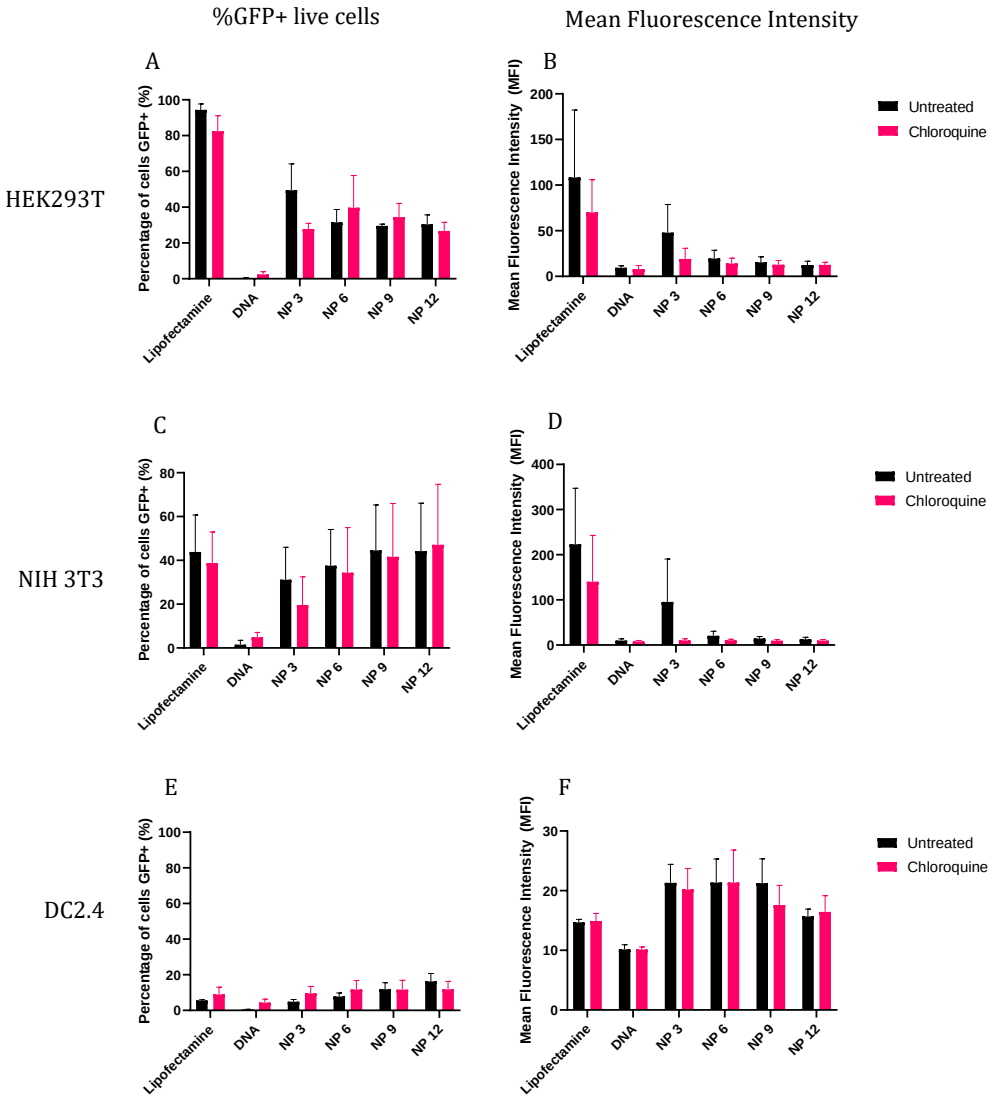

Figure 18. Flow cytometry of HEK293T, NIH 3T3, and DC2.4 cells by DC-Chol:DOPE liposomes with and without chloroquine. Graphs show percentage of live cells expressing GFP (A, C, and E) and mean fluorescence intensity of the GFP-expressing cell population (B, D, and F) with and without chloroquine. Bars represent mean ± one standard deviation (N=6, two experiments). A one-way ANOVA with post hoc Tukey's test was carried out to compare expression in each condition between untreated and chloroquine-treated cells. Differences were nonsignificant.

Across cell lines and NP ratios, no statistically significant difference in GFP expression was observed with or without chloroquine as determined by one-way ANOVA with individual comparisons.

4.4.6 Murine serum antibody response to a SARS-Cov-2 DNA vaccine

A pilot animal study (described in sections 2.5.1-2.5.3) was carried out to investigate whether uptake and expression of encoded antigens in fibroblast or other dermal bystander cells is sufficient to mount an immune response to intradermally administered liposome-DNA complexes. Serum antibody response to pDNA encoding SARS-Cov-2 spike and nucleocapsid proteins was investigated by ELISA as described in section 2.5.5 (Figure 19).

A) Anti-Nuclear protein (N) antibody

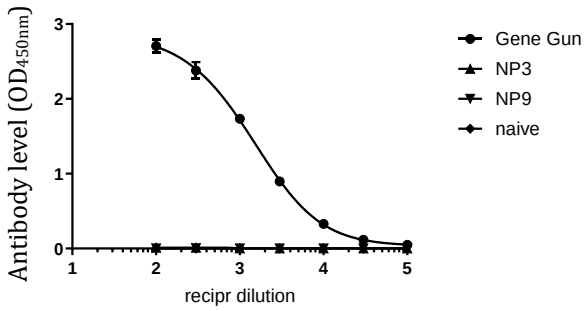

B) Anti-Spike protein (S1) antibody

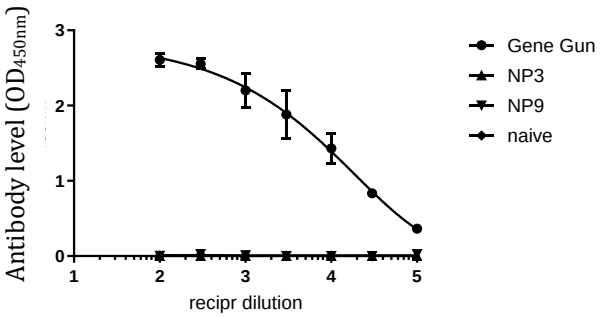

Figure 19. Murine serum antibody response to DNA-liposome complexes at NP 3 and NP 9. Curves represent concentration of anti-COVID antibody in murine sera in a serial dilution of 1/10 for A) Nuclear protein and B) Spike 1 protein, N=3 mice per group.

DNA was delivered by intradermal administration of liposomes at NP 3 or NP 9 and compared to DNA delivered by gene gun. Immune response is represented by increase in optical density at 450 nm; reciprocal dilution of serum shows a decreasing sigmoidal curve. This is observed in the gene gun control condition for both antigens (Figure 7), however there is no response observed when DNA is delivered by the liposomal formulations.

4.4.7 Murine splenocyte response to a SARS-Cov-2 DNA vaccine

Splenocyte response to SARS-Cov-2 spike and nucleocapsid proteins was investigated by ELISpot as described in section 2.5.4 and response indicated by spots per million splenocytes. Cell stimuli included lipopolysaccharide (LPS), a gram-negative bacterial membrane component that induces a nonspecific immune response, as well as whole N and S1 protein, digested protein peptide pools for N protein and the receptor binding domain (RBD) for the S1 protein, and a specific immunogenic peptide sequence for the S1 RBD. LPS initiated strong cellular response across all groups (Figure 8).

A) Murine splenocyte responses to SN17 pDNA delivered by gene gun

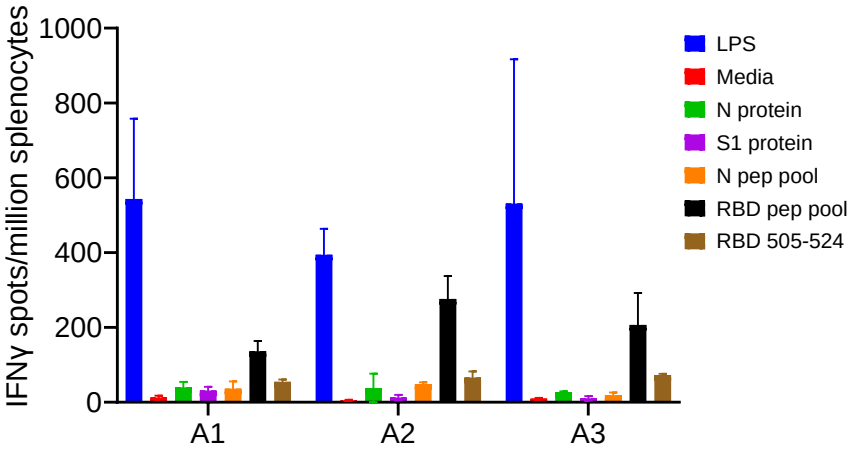

B) Murine splenocyte responses to SN17 pDNA delivered by DC-Chol/DOPE liposomes at NP 3

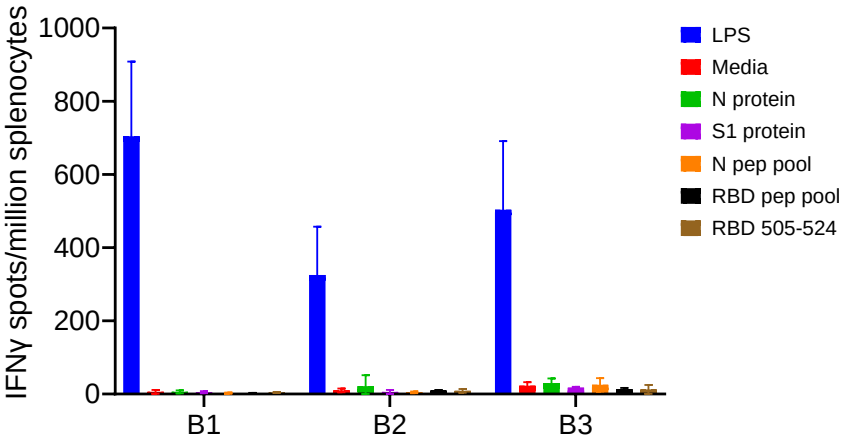

Figure 20. Splenocyte response to DNA-liposome complexes at NP 3. Bars represent number of IFNγ spots per million splenocytes in response to given stimuli for A) 3x mice immunised with gene gun and B) 3x mice immunised with DNA-liposome complexes combined with SN17 pDNA at NP 3. N=3 mice per group.

DNA delivered by gene gun (Group A, Figure 8) showed antigen-specific response across stimuli but was strongest in response to the S1 RBD peptide pool. DNA delivered by liposome did not show any antigen-specific response.

4.5 Discussion

Dendritic cells are key instigators of antigen-specific immune responses and present an ideal target for vaccine delivery. A major limitation of traditionally effective immunogenic delivery systems is their toxicity; liposomes composed of DC-Cholesterol and DOPE are well characterised and established as a system that can deliver DNA to a range of cell lines including SK-BR3 (Zhang et al, 2010), HEK293T (Yang et al, 2013; Choi et al, 2001), and NIH 3T3 (Choi et al, 2001) with low toxicity. However, they have not been investigated regarding their capacity for DNA delivery to dendritic cells. In this chapter, we aimed to investigate whether liposomes can deliver to dermally relevant cells and initiate an immune response to antigens encoded in DNA.

The murine dendritic cell line DC2.4 was used alongside the murine fibroblast cell line NIH 3T3 and the human embryonic kidney cell line HEK293T to establish a panel of cell lines designed to investigate transfection efficiency in the context of both classical *in vitro* screening (HEK293T) and the dermal immune landscape (NIH 3T3 and DC2.4). Expression of GFP revealed that transfection efficiency is cell line dependent, with HEK293Ts displaying transfection rates of 30-50%, NIH 3T3s displaying transfection rates of 10-20%, and DC2.4s displaying transfection rates of 2-7%. In a study comparing transfection efficiency using the beta galactosidase assay in HEK293 and NIH 3T3 cells, Choi et al (2001) found that DC-Cholesterol/DOPE liposomes induced expression twice as strongly as lipofectin in HEK293T cells but NIH 3T3 cells were refractory to both conditions. The protocol used in this study mimics the protocol used by Choi et al (2001) very closely; liposome-DNA complexes were formed for 30 minutes before incubating on cells plated at 1x10^5 cells per well in a 24 well plate for 4 h. The main differences were that, in this chapter, cells were incubated with only 1 μg DNA per well rather than 2 μg, and results measured at 24 h rather than 48 h. In this study, we established that lipofectamine 2000 induced stronger expression than any NP ratio of liposome:DNA complex in HEK293Ts, however this can be

explained by the improved action of lipofectamine 2000 compared to lipofectin. Expression in NIH 3T3s were higher in this study; Choi et al (2001) also associated significant toxicity in NIH 3T3 cells which could be explained as a limiting factor of transfection. Decreasing DNA content per well during transfection to 1 μg would likely decrease associated toxicity, potentially accounting for the better expression.

Efficient uptake with limited gene expression indicates that the limiting factor is in the processing of the DNA; commonly, this is thought to involve endosomal degradation of DNA prior to its escape into the cytoplasm where it is can cross the nuclear membrane for transcription. Chloroquine diphosphate prevents the acidification of the endosome when used to pretreat cell lines and has been used in previous literature to investigate endosomal escape by therapeutics. A study by Maitani et al (2007) evaluated DC-Chol/DOPE liposome transfection of a luciferase plasmid in HeLa cells. The effect of chloroquine diphosphate on luciferase activity was dependent on the molar ratio of DC-Chol to DOPE in formulation, finding that chloroquine diphosphate reduced luciferase activity in liposomes with a ratio of DC-Chol:DOPE of 1:2, but in formulations with a lower lipid fraction of DOPE (1:0 and 3:2), chloroquine made no difference. The conclusion drawn from this was that a higher content of DOPE led to endosomal escape, while formulations with a predominant content of DC-Cholesterol did not. In this study, chloroquine diphosphate did not significantly alter GFP expression, but this could be explained by either a lack of endosomal escape or lack of endosomal uptake. Chloroquine toxicity indicated that DC2.4 cells were more sensitive to chloroquine diphosphate than HEK293Ts or NIH 3T3s. For endosomal assays, the concentration below IC50 was selected; for DC2.4 cells, this was 50 uM and for HEK293T and NIH 3T3 cells, this was 100 uM.

Despite the low transfection in DC2.4 cells, we showed that transfection in NIH 3T3 cells is moderate. We proceeded with a pilot animal study to investigate the capacity of this formulation to initiate an immune response through bystander cells when delivered intradermally. Effective immune

responses occur through antigen specific responses by both cell-mediated and humoural pathways, characterised by splenocyte response and serum antibody response respectively. Assayed by ELISA, no antibody response was observed to either the encoded N or S1 SARS-Cov-2 protein when delivered by DC-Cholesterol: DOPE liposomes. Similarly, no splenocyte response was observed by ELISpot. The main limitation of this study is that splenocyte and antibody responses are systemic ones, and responses local to the site of administration were not measured. There is a chance that localised immune responses were initiated, which would need further study by measurement of cell phenotypes and inflammatory markers in the dermis or local lymph nodes and/or titration of pDNA encoding for bioluminescence markers for biodistribution (Roth et al, 2022).

Effectiveness of DC-Cholesterol/DOPE liposomes in eliciting antigen specific immune responses has previously been found to be dependent on site of administration. Perrie et al (2003) described the immunisation of female B57 mice with DC-Chol/DOPE liposomes delivering plasmid DNA encoding for a hepatitis B antigen. Two subcutaneous doses 28 days apart resulted in systemic antigen-specific immune responses. In contrast, a study by Joseph et al (2006) found that two intranasal doses of DC-Chol/DOPE liposomes delivering a plasmid encoding for the hemagglutinin antigen seven days apart elicited only a low, local antibody response in the lung. The effect of site of delivery on immune responses to a given vaccine formulation has been examined at some length; a systematic review by Schnyder et al (2021) compared intradermal, intramuscular, and subcutaneous vaccinations. Although in some instances intradermal delivery was observed to induce better immune responses when compared to the equivalent dose subcutaneously or intramuscularly, intradermal vaccination was also observed to be more susceptible to local immune responses without systemic immune participation. A comparison of intranasal and intradermal delivery of a nanoparticle OVA DNA vaccine observed higher antibody titers via the intradermal route (Bal et al, 2012). Immune responses measured in this chapter are systemic ones, consisting of serum antibody response and splenocyte response. It can be suggested

that this is due to immune responses being either absent or restricted to local responses at the site of delivery, but local immune responses were not tested. Regardless, future formulations will need to increase immunogenicity in order for systemic immune responses to be observed.

4.6 Conclusions

DC-Cholesterol and DOPE were formulated and characterised in the previous chapter to establish a stable, monodisperse population of DNA-liposome complexes. When delivered to DC2.4, NIH 3T3, and HEK293T cells, efficient uptake was observed across cell lines regardless of NP ratio. Expression of GFP was cell line dependent, with low expression in DC2.4 cells, moderate expression in NIH 3T3s, and moderate to high expression in HEK293T cells. Expression was unchanged by chloroquine pretreatment, indicating that endosomal degradation of complexes is unlikely to be the limiting factor in low expression. A pilot animal study showed no significant immune response to the N or S1 SARS-Cov-2 antigens.

DC-Cholesterol and DOPE alone are unable to initiate an immune response, either by direct dendritic cell expression or indirect cross presentation by bystander cells. Liposomes will be reformulated to attempt improvement of transfection in DC2.4 cells as an indication of immunogenicity; multivalency of the cationic lipid will be investigated by replacing DC-Cholesterol with the commercial lipid GL67, and linolenic acid will be included as a model adjuvant.

Chapter 5: Reformulation of liposomes for DNA delivery

5.1. Introduction

Results in chapter 3 established that liposomes prepared with DC-Cholesterol efficiently condenses GFP pDNA with NP-ratio-dependent membrane fusion. However, results in chapter 4 show that this formulation yielded low expression of GFP in DC2.4 cells and failed to mount an immune response when administered intradermally in a pilot murine vaccination study. Previous research has indicated that formation of cationic liposomes with multivalent cationic lipids results in higher surface charge density of the liposome, better interactions between cationic lipid and negatively charged DNA or cell membranes, and consequently improved transfection (Sousa et al, 2022). The high positive charge density is also regarded as a factor that allows for decrease of cationic lipid content in formulations in order to reduce toxicity while maintaining transfection efficiency.

Previous research detailing successful transfections of dendritic cell lines has involved additional immunostimulation alongside DNA-carrier complexes (Kornuta et al 2021; Heller et al, 2017) or been associated with significant cytotoxicity (Palumbo et al, 2012). However, antigen specific immune responses have been observed in studies when *in vitro* studies showed as little as 15-20% of DCs were transfected (Chen et al, 2013, Moku et al 2021, and Garu et al, 2016). Increasing the percentage of GFP positive live dendritic cells is likely to be associated with increased strength and specificity of immune responses elicited by *in vivo* delivery, and will be the focus of this chapter.

5.1.1. Multivalent lipids

A study investigating membrane charge density by synthesising bi-, tri- and pentavalent multivalent lipids found that transfection efficiency follows a bell shaped curve when plotted as a function of membrane charge density (Figure 1; Ahmad et al, 2005). A lower fraction of cationic lipid in overall liposome composition was associated with low transfection but as fraction increased, so did transfection efficiency, reaching an optimal peak before

levelling off and decreasing again. This was attributed to few or poor interactions between complexes and negatively charged cell membranes when membrane charge density is low, and inability for DNA release once in the cytoplasm when membrane charge density is high. The peak of the bell curve was observed to shift to favour lower molar percentage compositions as valency increased, suggesting there is an optimal charge density for both DNA binding and transfection. However, cell toxicity was not explored. Increasing charge density and overall positive charge of branched polyphosphoramidates, polymeric pDNA carriers, was found to increase transfection efficiency in HeLa, HEK293, and HepG2 cell lines (Ren et al, 2010). In response to Ahmad et al (2005), Caracciolo et al (2008) found an optimal charge density for transfection about one order of magnitude lower than Ahmad et al had reported and suggested that the discrepancy is due to structural changes in the cationic liposome upon interaction with anionic lipids. However, they showed that transfection efficiency does not correlate with structural phase changes of the liposomes, nor their rate of DNA release.

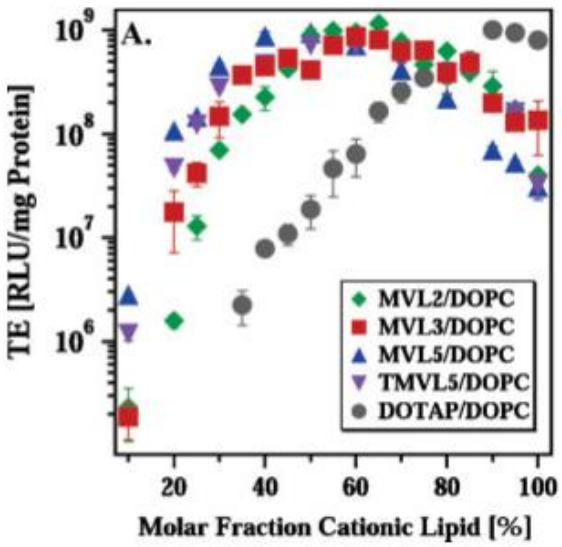

Figure 21. Taken from Ahmad et al (2005). Transfection efficiency in relative light units (RLU) per mg total cellular protein plotted as a function of mol% DOPC for DNA complexes prepared with bivalent (green diamonds), trivalent(red squares), and two pentavalent (blue triangles and purple inverted triangles) lipids as well as the control monovalent lipid DOTAP (gray circles).

Joseph et al (2006) compared ten liposomal formulations delivered intranasally and intramuscularly. Liposomal formulations containing

monovalent cationic lipids varied in efficacy; liposomes containing DC-Cholesterol did not efficiently initiate immune responses, but liposomes containing DMTAP or DOTAP initiated low level immune responses. The liposome formulation containing the multivalent cationic lipid CCS consistently initiated the highest immune response. Neither intradermal delivery nor the role of dendritic cells was explored, rendering direct comparisons to this project impossible. However, the acknowledgement was made that a single i.m. injection of cationic liposomes elicited comparable systemic and splenic responses to two i.n. administrations. Lung antibody titers were much higher after i.n. administrations, suggesting local effects of delivery. Multivalent lipids have been shown to initiate strong, reliable immune responses when compared to their monovalent counterparts, and this comparison will be investigated in dendritic cells in this chapter.

5.1.2. Spermine as a multivalent lipid

Spermine has been used in a variety of polycationic DNA delivery systems including the polysaccharide spermine-dextran (Chen et al, 2013) and lipids ceramide-carbamoyl-spermine (CCS) (Joseph et al, 2006), L-shaped spermine derivatives (Thongbamrer et al, 2022), and GL67 (Siders et al, 2002) all used in liposome systems. Spermine-dextran was used to deliver plasmid encoding the melanoma antigen gp100 to dendritic cells ex-vivo, which were then injected intradermally and significant tumour shrinkage observed in a mouse model (Chen et al, 2013). Joseph et al (2006) examined a range of liposome formulations delivering subunit influenza antigens, evaluating humoral and cellular responses in mice and rabbits. Neutral and anionic liposomes elicited low immune responses compared to select monovalent lipids, which induced broad local and systemic immune responses. The formulation including the multivalent spermine-based CCS induced superior immune responses to the commercial influenza vaccine when delivered intranodally. Intravenous delivery of a liposomal formulation consisting of GL67 and DOPE at a 1:3 molar ratio yielded strong antitumour effects in a mouse model (Siders et al, 2002).

5.1.3. Linolenic acid and metabolites

Linolenic acid has been shown to have strong immune modulating effects, albeit driving anti-inflammatory states as examined in a psoriatic skin model (Morin et al, 2022) and *in vitro* monocyte model (Rodway et al, 2023), as well as reducing severe Covid-19 symptoms such as cytokine storms (Cianciosi et al, 2023). Morin et al (2022) developed an *in vitro* skin model by culturing psoriatic human fibroblasts in two plates until they formed an extracellular matrix. Human T cells were cultured on one plate and keratinocytes on the second plate for seven days before the sheet containing keratinocytes was seeded on the other. Treatment of these models with linolenic acid was observed to reduce the expression of CD45 in the tissue, a key T cell marker, and reduce the expression of proinflammatory cytokines including tumour necrosis factor alpha and interferon gamma, concluding that T cell mobility and activation were both suppressed. However, Rodway et al (2023) observed gene expression in the human monocyte cell line THP-1 after treatment with alpha-linolenic acid; a selection of genes associated with chemotaxis, cell motility, and extravasation were upregulated, and membrane fluidity and integrity was found to be affected. Production of the anti inflammatory cytokine interferon beta was also measured, which was unaffected by the treatment. A meta-analysis (Ciancosi et al, 2023) examined linolenic acid when administered in a variety of *in vitro* models as well as orally, intramuscularly, and intravenously *in vivo*, including murine, bovine, and human models. All found an overall systemic anti-inflammatory effect marked by decreases in proinflammatory cytokines such as interleukin 6 and tumour necrosis factor alpha, chemokines such as interleukin 8, and reactive oxygen species. Downstream metabolites of linolenic acid including arachidonic acid and docosahexaenoic acid have been found to have differential effects on the immune system (Carlsson et al, 2015). This study found that dendritic cells readily take up these fatty acids and increase cell maturity, prostaglandin expression, and costimulatory receptor expression. When cocultured with T cells, T cell proliferation was reduced in response to a model OVA antigen; however, this suppression was not observed with linolenic acid.

Liposomal linolenic acid has been used in antiinfectives against heliobacter pylori (Thamphiwatana et al, 2014; Wang et al, 2022) and viruses including Covid-19 and respiratory syncytial virus (RSV) (McGill et al, 2023). Thamphiwatana et al (2014) formed liposomes containing egg phosphatidylcholine, cholesterol, and linolenic acid at a weight ratio of 6:1:3 by thin film method and hand extruding through a 100 nm filter. The liposomes were observed to have a hydrodynamic diameter of 105.7 ± 0.3 nm, a polydispersity index of 0.18 ± 0.01, and a surface zeta potential of -54.9 ± 1 mV. When delivered orally in mice infected with helicobacter pylori, the liposomes significantly reduced bacterial counts which was attributed to its exceptional fusogenic properties. Wang et al (2022) confirmed this by exploring content leakage in scanning electron microscopy, finding that liposomal linolenic acid destroyed the outer membrane and ultrastructure of helicobacter pylori. Intranasal administration of the same formulation of liposomes encapsulating acetate in a murine *in vivo* study (McGill et al, 2023) found they augmented antiviral effects against SARS-Cov-2. They attributed this to a dual mechanism of binding directly to SARS-Cov-2 viral particles and augmenting macrophage-mediated antiviral pathways including expression of free fatty acid receptors 2 and 4. Another liposome formulation consisting of lecithin, cholesterol, and gamma-linolenic acid formed by ethanol injection was developed into a thermoreversible liposomal gel loaded with an undisclosed chemotherapeutic agent (Saad et al, 2023). This formulation was observed to sustain drug release over 120 hours when the gel was injected intratumourally, and was associated with tumour regression and systemic nontoxicity. To date, liposomal formulations including linolenic acid have not been examined with respect to pDNA delivery in dendritic cells, but the enhanced uptake and biocompatibility detailed in these formulations suggest it is worth exploring in this chapter.

5.1.4. Evaluation of transfection and activation threshold of DCs

Few papers have investigated the correlation between *in vitro* dendritic cell transfection and capacity for immune response initiation. Chen et al (2013)

investigated expression of GFP delivered by plasmid DNA complexed to spermine-dextran in dendritic cells and determined that 16% of dendritic cells successfully transfected was sufficient to initiate an antitumour response. Garu et al (2016) transfected 20% of dendritic cells with liposomes composed of a 1:1 ratio of mannose-derived cationic lipid and DOPE and observed significant antitumour response. Layek et al (2015) observed antibody responses when 25% of dendritic cells were transfected with phenylalanine and mannose grafted dual functionalised chitosan. Moku et al (2021) transfected only 15% of dendritic cells with lipid nanoparticles containing the cationic lipid DSG and still initiated immune responses. However, transfecting up to 45% of dendritic cells using polyethyleneimine was accompanied by cytotoxicity too high for immune studies (Palumbo et al, 2012).

5.2. Hypothesis, Aims, and Objectives

5.2.1. Hypothesis:

- Reformulating cationic liposomes with a multivalent cholesterol-based cationic lipid with or without linolenic acid will increase expression of GFP across cell lines.

5.2.2. Aims:

- To reformulate liposomes and characterise liposome-GFP pDNA complexes to obtain cationic complexes less than 200nm in diameter that stably condense GFP pDNA
- To determine whether reformulated liposomes efficiently transfect cell lines *in vitro*

5.2.3. Objectives:

- Reformulate liposomes and form liposome-DNA complexes according to the preparation protocol optimised in chapter 3 and characterise the particle size and charge.
- Assess complexation of reformulated liposomes using gel retardation. Use densitometry to calculate encapsulation efficiency and compare amounts of free DNA between NP ratios and formulations.
- Screen reformulated liposomes for uptake and expression of GFP in DC2.4 cells by flow cytometry.
- Investigate transfection of the formulation resulting in highest uptake and GFP expression in DC2.4, NIH 3T3, and HEK293T cells by flow cytometry.

5.4. Results

5.4.1. Dynamic light scattering and zeta potential of reformulated liposomes

Liposomes were reformulated, exchanging DC-Cholesterol for GL67 in an equivalent ratio to DOPE. Particle size and polydispersity was measured by dynamic light scattering and charge was measured by electrophoretic mobility. GL67/DOPE liposomes without DNA were slightly smaller than DC-Chol/DOPE liposomes with a slightly higher positive charge and polydispersity index. When DNA was added, both formulations were observed to increase in particle size and PDI with increasing NP ratio, except for NP 3 which had a negative particle charge as described in chapter 3.

Additional formulations were made with linolenic acid forming 20 mol% of the total formulation, maintaining the ratio between cationic lipid and DOPE. DC-Chol/DOPE/linolenic acid liposomes were slightly larger than DC-Chol/DOPE liposomes with a lower positive charge. Addition of DNA at any NP ratio resulted in a negative charge (Table 4). GL67/DOPE/LA liposomes were slightly smaller than GL67/DOPE liposomes with a lower positive charge. Addition of DNA resulted in an increasing positive charge with increasing NP ratio. For lipid structures of GL67 and linolenic acid, see section 2.3.1.

Only liposome formulations containing GL67 will be taken forward into gel retardation studies due to the overall negative charge on DNA-liposome complexes for the DC-Chol/DOPE/LA formulation which would result in visible bands in agarose gel retardation studies regardless of DNA binding. DC-Chol/DOPE/LA liposomes, GL67/DOPE liposomes, and GL67/DOPE/LA liposomes will be screened for initial uptake and transfection studies in DC2.4 cells.

Size (nm)	**Empty**	**NP 3**	**NP 6**	**NP 9**	**NP 12**	***p***
DC-Chol/DOPE (chapter 3)	119 ± 5	240 ± 7	159 ± 4	140 ± 3	141 ± 5	****
DC-Chol/DOPE/LA	179 ± 3	179 ± 2	230 ± 2	228 ± 6	231 ± 9	****
GL67/DOPE	93 ± 1	196 ± 4	177 ± 2	183 ± 4	171 ± 4	****
GL67/DOPE/LA	82 ± 1	173 ± 2	157 ± 2	158 ± 2	154 ± 2	****
PDI						
DC-Chol/DOPE (chapter 3)	0.213 ± 0.011	0.060 ± 0.016	0.120 ± 0.003	0.114 ± 0.014	0.113 ± 0.017	****
DC-Chol/DOPE/LA	0.162 ± 0.026	0.181 ± 0.014	0.251 ± 0.031	0.238 ± 0.021	0.219 ± 0.013	**
GL67/DOPE	0.208 ± 0.007	0.242 ± 0.013	0.238 ± 0.003	0.313 ± 0.010	0.301 ± 0.032	****
GL67/DOPE/LA	0.208 ± 0.008	0.169 ± 0.013	0.229 ± 0.014	0.234 ± 0.021	0.269 ± 0.023	****
Charge (mV)						
DC-Chol/DOPE (chapter 3)	42.3 ± 3.0	8.4 ± 2.0	35.9 ± 2.3	39.8 ± 1.2	43.2 ± 0.2	****
DC-Chol/DOPE/LA	54.3 ± 8.7	-32.8 ± 3.5	-29.2 ± 0.6	-28.1 ± 0.4	-28.4 ± 1.2	****
GL67/DOPE	77.9 ± 6.7	-32.3 ± 0.8	73.7 ± 1.8	75.0 ± 1.3	71.6 ± 0.7	****
GL67/DOPE/LA	66.0 ± 1.0	59.9 ± 0.4	71.6 ± 1.4	73.4 ± 0.8	74.0 ± 1.9	****

Table 4. Hydrodynamic size, polydispersity index, and zeta potential of liposome-DNA complexes. Liposomes formulated with DC-Cholesterol:DOPE (43:57 molar ratio), DC-Cholesterol:DOPE:linolenic acid (34:46:20 molar ratio), GL67:DOPE (43:57 molar ratio), or GL67:DOPE:linolenic acid (34:46:20 molar ratio) were combined with plasmid DNA encoding GFP pDNA at different nitrogen: phosphate (NP) ratios. Data for hydrodynamic diameter and polydispersity index indicate mean of three repeats (n=3) ± one standard deviation. Data for zeta potential indicate mean of three repeats (n=3) ± one standard deviation. Differences between group means were measured by one-way ANOVA; **p<0.01, ****p<0.0001.

5.4.2. Encapsulation efficiency by gel retardation

Encapsulation efficiency of DNA after complexation was investigated by agarose gel retardation and free DNA quantified by densitometry. Uncomplexed DNA is observable as a band in the body of the gel and densitometry used to calculate encapsulation efficiency (section 2.3.5).

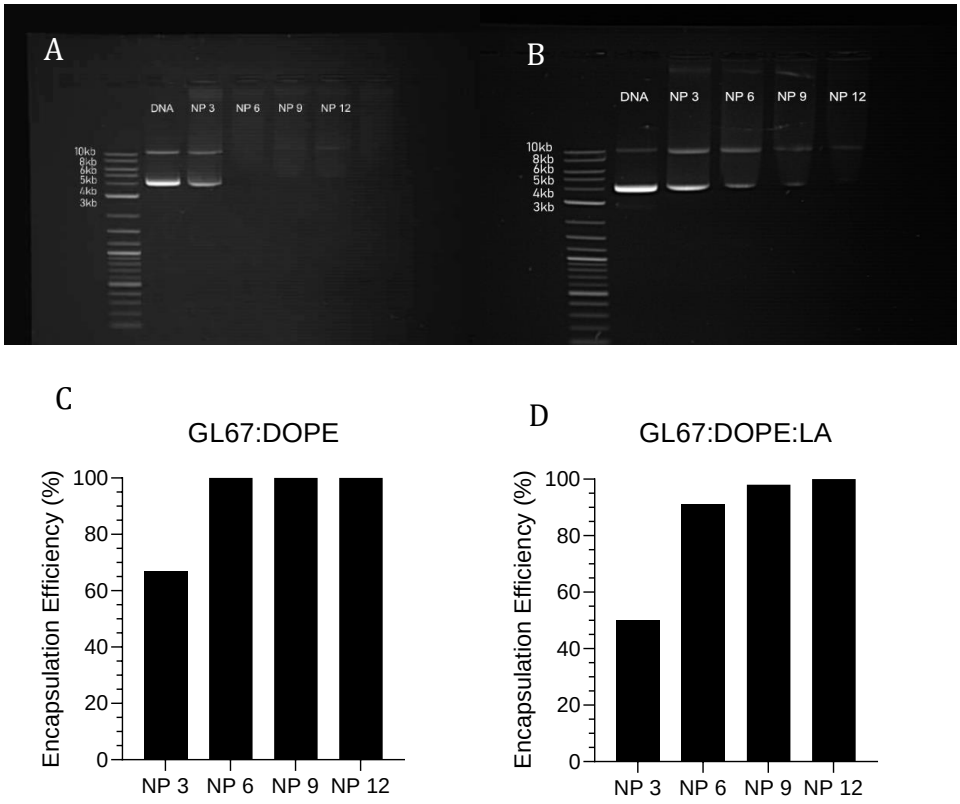

Figure 22. Gel retardation of liposome-DNA complexes. Liposomes composed of GL67 and DOPE (43:57 molar ratio) or GL67:DOPE:linolenic acid (34:46:20 molar ratio) were combined with GFP pDNA at NP ratios and loaded into 1% agarose gels to visualise unbound DNA. Images represent agarose gel retardation of A) GL67/DOPE and B) GL67/DOPE/LA. Bars represent encapsulation efficiency of C) GL67/DOPE and D) GL67/DOPE/LA.

For GL67/DOPE, only NP 3 resulted in a detectable band with an optical intensity of 34% of the control DNA band (Figure 22). For GL67/DOPE/LA, encapsulation efficiency appeared to be NP ratio dependent. The band at NP 3 showed an optical intensity of 50% of the control, which decreased with NP ratio increase. The band at NP 6 showed an optical intensity of 9% of the control, reducing to 2% at NP 9, and no detectable free DNA at NP 12. Both formulations were taken forward into screening uptake studies in DC2.4 cells.

5.4.3. Cellular uptake of reformulated liposomes

Cellular uptake of reformulated liposomes was investigated by including the lipophilic fluorophore DiD in liposomal membranes before forming DNA-liposome complexes and incubating with DC2.4 cells. Live cells were gated by live/dead stain and single cells isolated before gating on cells that had not been incubated with liposomes (section 2.4.6).

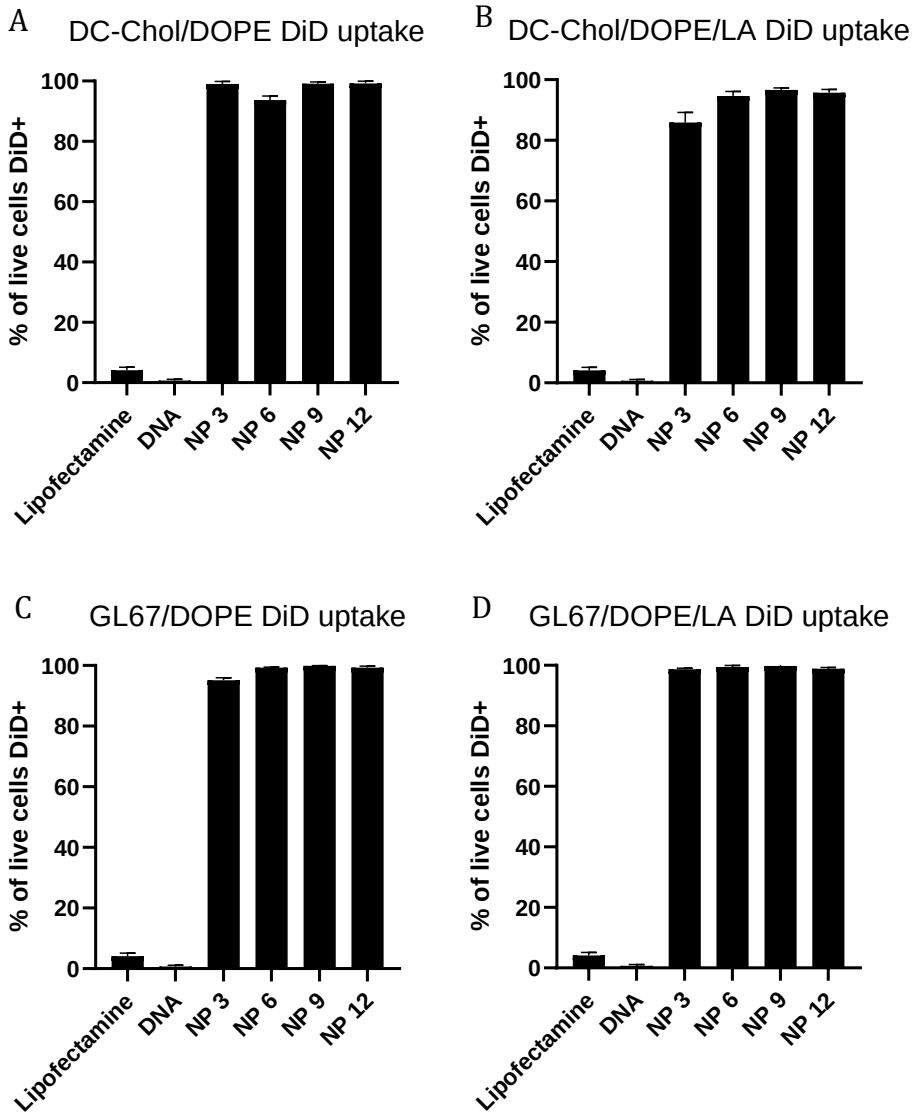

Figure 23. Liposome complex uptake by flow cytometry. DC2.4 cells were incubated with DiD-labelled liposomes formulated with A) DC-Cholesterol:DOPE (43:57 molar ratio), B) DC-Cholesterol:DOPE:linolenic acid (34:46:20 molar ratio), C) GL67:DOPE (43:57 molar ratio), or D) GL67:DOPE:linolenic acid (34:46:20 molar ratio) combined with GFP pDNA at different nitrogen: phosphate (NP) ratios. Bars represent percentage of live cells expressing DiD-associated fluorescence; mean of three repeats (n=3) ± one standard deviation.

The DC-Cholesterol/DOPE/LA formulation showed an NP ratio-dependent decrease in uptake when compared to DC-Cholesterol/DOPE. However, the population with the lowest uptake (NP 3) still showed uptake in more than 80% of live cells. Both formulations with GL67 showed close to 100% uptake across NP ratios and will be taken forward into transfection.

5.4.4 GFP expression in DC2.4 cells when delivered by reformulated liposomes

Three new formulations were screened for transfection efficiency as measured by percentage of live cells expressing GFP in DC2.4 cells. GFP expression compared with previous data from DC-Chol/DOPE liposomes as detailed in chapter 4 (Figure 24).

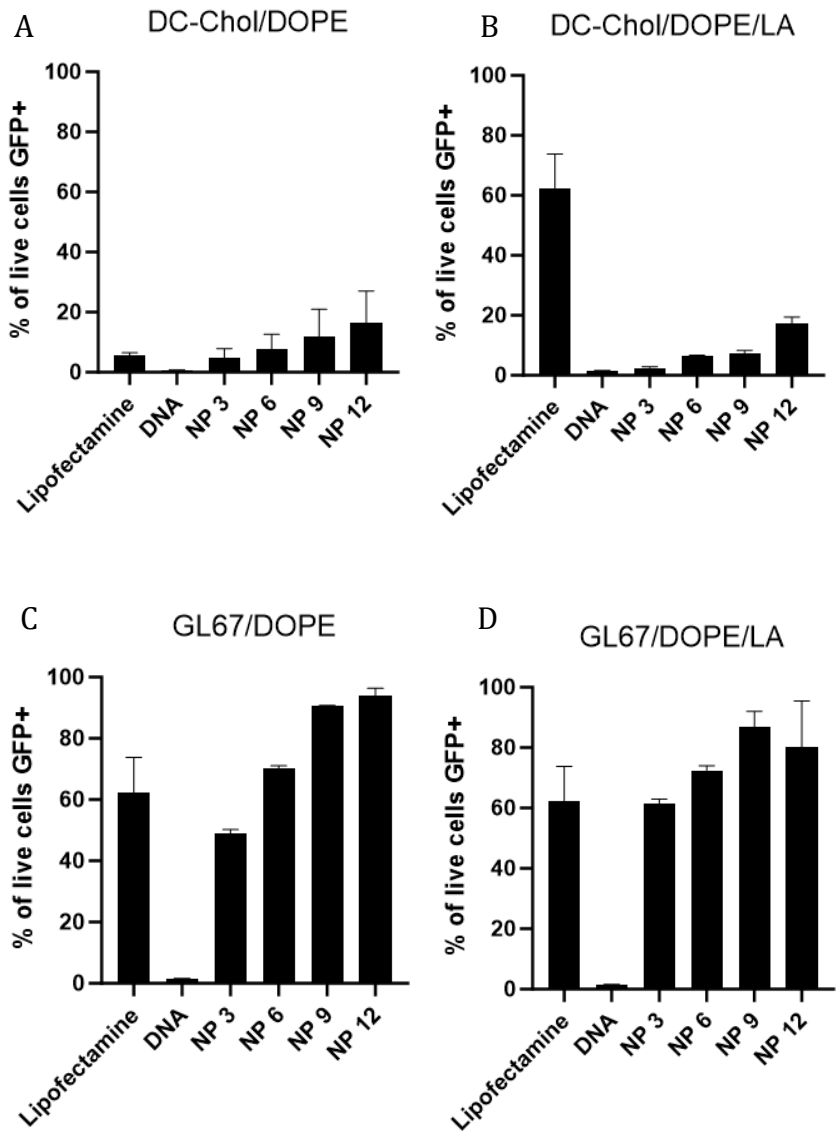

Figure 24. Transfection with liposome complexes by flow cytometry. DC2.4 cells were incubated with liposomes formulated with DC-Cholesterol:DOPE (43:57 molar ratio), DC-Cholesterol:DOPE:linolenic acid (34:46:20 molar ratio), GL67:DOPE (43:57 molar ratio), or GL67:DOPE:linolenic acid (34:46:20 molar ratio) combined with plasmid DNA encoding GFP pDNA at different nitrogen: phosphate (NP) ratios. Bars represent percentage of live cells expressing GFP; mean of three repeats ± one standard deviation.

Formulations containing GL67 showed an increase in the population of cells positive for GFP when compared to formulations containing DC-Cholesterol. Inclusion of linolenic acid in either formulation did not change transfection efficiency compared to formulations without linolenic acid. The GL67/DOPE formulation was taken forward into transfection and cell viability studies involving NIH 3T3 and HEK293T cells because it resulted in the highest percentage of cells positive for GFP.

5.4.5. GFP expression by cell line delivered by GL67/DOPE liposomes

5.4.5.1 In HEK293T cells

Liposomes formulated with GL67/DOPE were used to transfect HEK293T cells with GFP DNA to examine and compare transfection efficiency with the data described in chapter 4. Based on initial screening results, improved transfection was expected. High variability in both cell viability and expression was observed across biological repeats but not technical (Figure 25). The first biological repeat (repeat 1) showed the highest percentage of live cells expressing GFP and more than 80% of single cells alive at the time of fixation; for lipofectamine, approximately 75% of live cells were transfected. The weakest expression was observed in repeat 2, showing less than 20% of live cells expressing GFP. However, repeat 2 also showed the least percentage of single cells alive at the time of fixation.

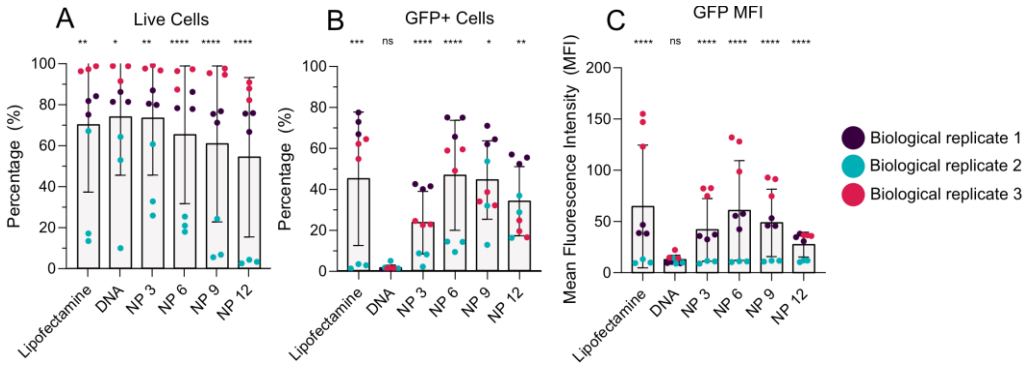

Figure 25. Cell viability and GFP expression in HEK293T cells after transfection with GL67/DOPE liposome-DNA complexes. Bars represent mean ± one standard deviation; dots represent individual technical repeats while colours indicate biological/experimental repeat. A) Percentage of single cells alive at time of fixation. B) Percentage of live cells expressing GFP. C) Mean fluorescence intensity of GFP positive populations. Three biological repeats (N=3) containing three technical repeats each (n=3). One-way ANOVA with a Tukey's post-test was carried out to determine statistical significance between biological replicates. * shows $p < 0.05$, ** shows $p < 0.01$, *** shows $p < 0.001$, **** shows $p < 0.0001$, and ns = not significant.

Each biological repeat showed similar percentage of live cells positive for GFP between lipofectamine and liposome-DNA complexes formed at NP6. GFP expression is also NP ratio dependent; each biological repeat showing

peak expression for NP 6 in both population and fluorescence intensity. Expression of GFP decreases as NP ratio decreases.

A one-way ANOVA was carried out to determine any statistically significant differences between biological replicates. Cells incubated in the presence of DNA alone were the only replicates with no statistical difference in GFP expression between groups. A tukey's post-hoc test revealed there were statistically significant differences in percentage of cells expressing GFP and MFI between all replicates for the lipofectamine, NP 3, and NP 6 conditions. However, no difference in percentage of cells expressing GFP was found between the second and third repeats. Likewise, no difference in MFI was found between the first and third repeats for MFI.

5.4.5.2 In NIH 3T3 cells

Liposomes formulated with GL67/DOPE were used to transfect NIH 3T3 cells with GFP DNA. Based on initial screening results, a larger population of live cells positive for GFP was expected compared to transfection with DC-Chol/DOPE liposomes but a smaller population compared to that observed in HEK293T cells with the same formulation. As in HEK293T cells, high variability in both cell viability and expression was observed across biological repeats but not technical (Figure 26).

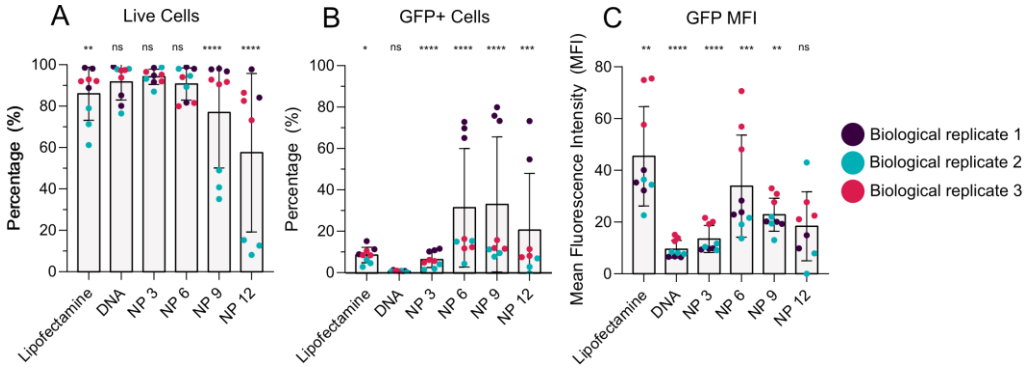

Figure 26. Cell viability and GFP expression in NIH 3T3 cells after transfection with GL67/DOPE liposome-DNA complexes. Bars represent mean ± one standard deviation; dots represent individual technical repeats while colours indicate biological/experimental repeat. A) Percentage of single cells alive at time of fixation. B) Percentage of live cells expressing GFP. C) Mean fluorescence intensity of GFP positive populations. Three biological repeats (N=3) containing three technical repeats each (n=3). One-way ANOVA with a Tukey's post-test was carried out to determine statistical significance between biological replicates. * shows $p < 0.05$, ** shows $p < 0.01$, *** shows $p < 0.001$, **** shows $p < 0.0001$, and ns = not significant.

Repeat 1 showed the highest percentage of live cells expressing GFP and more than 90% of single cells alive at the time of fixation. The weakest expression was observed in repeat 2, showing less than 20% of live cells expressing GFP. However, repeat 2 also showed the least percentage of single cells alive at the time of fixation. Repeat 3 showed good cell viability but low percentage of cells expressing GFP; however, this repeat showed the highest fluorescence intensity. As observed in HEK293T cells, liposome-

DNA complexes at NP 6 showed the highest transfection efficiency for each biological repeat.

A one-way ANOVA was carried out to determine any statistically significant differences between biological replicates. No difference in percentage GFP expression was observed between groups incubated with DNA, nor MFI between groups incubated with liposome-DNA complexes at NP 12. A Tukey's post-hoc test revealed that MFI between the first and second repeats were not significant for all conditions except NP 12. Percentage of cells expressing GFP was insignificant between second and third repeats for liposome-DNA complexes at NP 6, NP 9, and NP 12, and insignificant between first and second repeats for lipofectamine.

5.4.5.2 In DC2.4 cells

Liposomes formulated with GL67/DOPE were used to transfect DC2.4 cells with GFP DNA. Based on initial screening results, improved transfection was expected compared to transfection with DC-Chol/DOPE liposomes but the lowest expression in the three cell lines examined. As in both HEK293T and NIH 3T3 cells, high variability was observed across biological repeats but not technical (Figure 27).

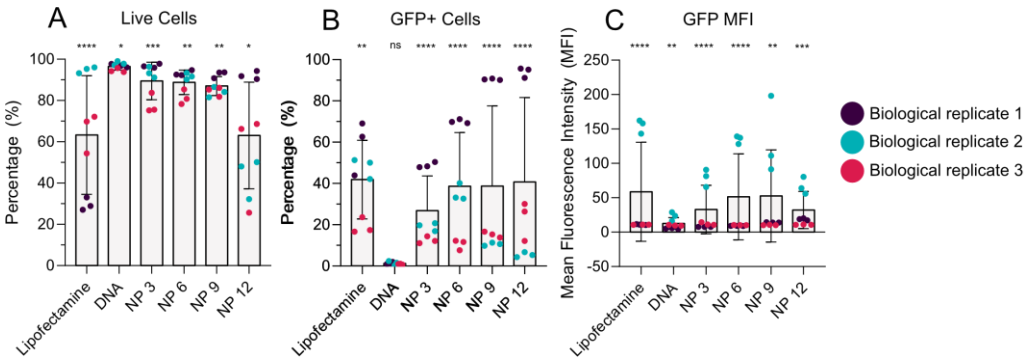

Figure 27. Cell viability and GFP expression in DC2.4 cells after transfection with GL67/DOPE liposome-DNA complexes. Bars represent mean ± one standard deviation; dots represent individual technical repeats while colours indicate biological/experimental repeat. A) Percentage of single cells alive at time of fixation. B) Percentage of live cells expressing GFP. C) Mean fluorescence intensity of GFP positive populations. Three biological repeats (N=3) containing three technical repeats each (n=3). One-way ANOVA with a Tukey's post-test was carried out to determine statistical significance between biological replicates. * shows $p < 0.05$, ** shows $p < 0.01$, *** shows $p < 0.001$, **** shows $p < 0.0001$, and ns = not significant.

Repeat 1 showed the highest percentage of live cells expressing GFP and more than 90% of single cells alive at the time of fixation in all conditions except lipofectamine, which showed that approximately 30% of single cells were alive. The weakest expression was observed in repeat 3, showing less than 30% of live cells expressing GFP and the lowest cell viability in liposomal conditions. Repeat 2 showed the high cell viability of over 80% in all conditions except for NP 12, with population expression of GFP and MFI in between that of repeats 1 and 3. The trend observed in HEK293T and NIH 3T3 cells of peak GFP expression occurring with complexes at NP 6 was observed in DC2.4 cells only in repeat 2. Repeats 1 and 3 instead showed a

linear increase in transfection efficiency with increasing NP ratios and low fluorescence intensity across conditions. High variation across repeats can be attributed to a variety of variables including liposomal batch variation; GL67/DOPE liposomes will be taken forward to investigate the effect of temperature on complexation between batches.

5.4.6. Formation of DNA-liposome complexes under variable temperatures

Batch variation may be a contributing factor to the variation observed in section 5.4.5 since one batch of liposomes was used per biological repeat; effect of temperature on DNA-liposome complexation was investigated due to temperature changes of the relevant components between 4°C storage, approximately 18°C room temperature, and 37°C warmed media as described in section 2.6 (Figure 28).

DNA, two batches of liposomes, and water were all brought to the indicated temperatures for 30 minutes before and 30 minutes after complexation, before diluting and measuring hydrodynamic size and polydispersity by Zetasizer. Although liposomes prior to complexation showed a hydrodynamic diameter 50 nm apart, complexation with DNA reduced this disparity by 30 nm or more. Temperature at complexation did not significantly affect the hydrodynamic size of the complexes for all NP ratios aside from NP 3, which showed increase in size at 4°C. However, differences in polydispersity were observed between batches; batch 1 had a low polydispersity index of around 0.2, but batch 2 had a slightly raised polydispersity index (up to 0.4).

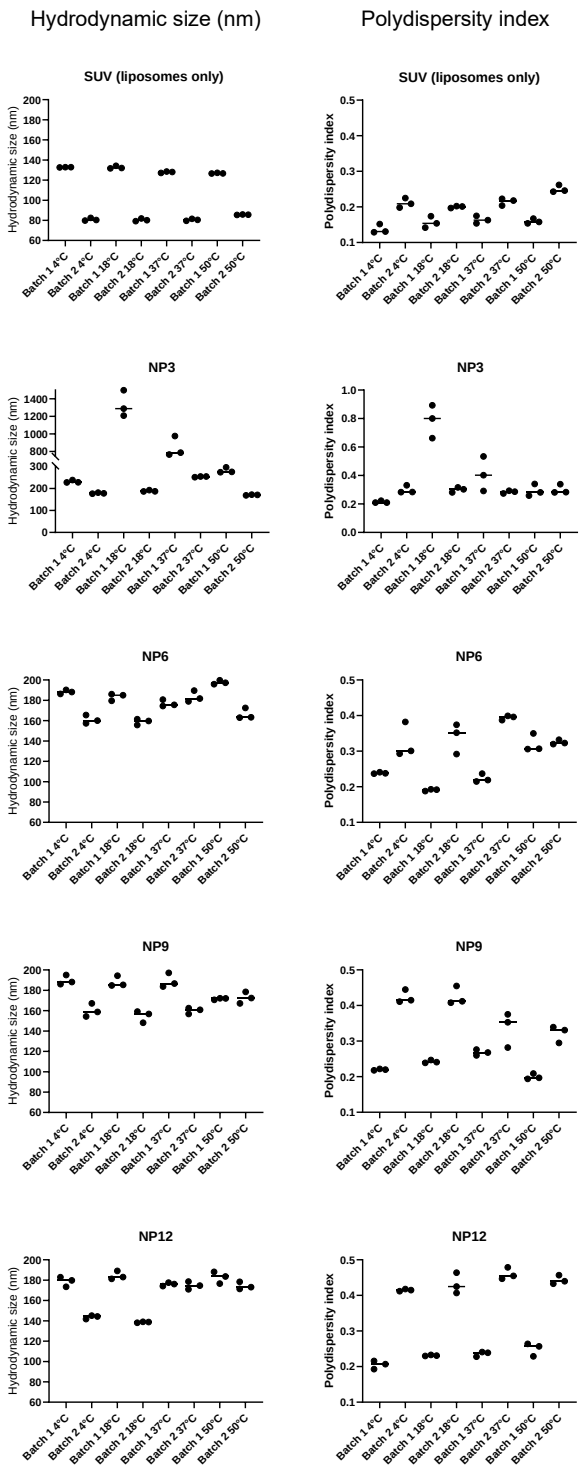

Figure 28. Investigation of batch variation by temperature at complexation. Two batches of GL67/DOPE liposomes were made using the same method and incubated at 4°C, 18°C, 37°C, or 50°C for thirty minutes prior to and after complexation.

5.5 Discussion

Chapter 3 focused on the formulation of a classic liposome system composed of DC-Cholesterol and DOPE, while chapter 4 established cell line dependent transfection efficiencies and the lack of capacity to elicit antigen-specific immune responses. In this chapter, we reformulated liposomes with a multivalent spermine-cholesterol cationic lipid and investigated the potential for the addition of linolenic acid to increase cellular uptake in dendritic cells. All new liposome formulations formed DNA complexes less than 250nm in diameter with low polydispersity. The formulation GL67:DOPE yielded the most stable condensation of DNA and was the most efficiently taken up by DC2.4 cells out of all new formulations. However, further biological repeats and transfection in NIH 3T3 and HEK293T cells showed significant variation in transfection efficiency alongside cell survival.

5.5.1 Characterisation of reformulated liposomes and DNA complexes

The cationic lipid DC-Cholesterol was exchanged for GL67, a trivalent cationic lipid, maintaining the preparation protocol optimised in chapter 4. Like DC-Cholesterol, GL67 has a cholesterol backbone; exchanging these lipids directly without altering the mol% of the cationic lipid prevents the need for adding cholesterol to maintain membrane rigidity while also allowing for comparison of charge valency. Linolenic acid was added to form 20 mol% of formulations composed of either DC-Chol/DOPE or GL67/DOPE, due to efficient uptake in dendritic cells (Carlsson et al, 2015).

Liposomes formulated with GL67 and DOPE showed a similar zeta potential after the addition of DNA at different NP ratios as liposomes formulated with DC-Cholesterol and DOPE; addition of DNA at NP ratios 6, 9, and 12 did not significantly decrease overall charge in comparison to empty liposomes. However, when DNA was added at NP 3, a charge inversion was observed and an overall negative charge due to saturation of the positive charges by DNA. Addition of linolenic acid into each formulation altered this pattern, yielding an overall negative charge with the addition of DNA to DC-

Chol/DOPE/LA liposomes and an overall positive charge to GL67/DOPE/LA regardless of NP ratio. An overall negative charge to DNA-liposome complexes made DC-Chol/DOPE/LA liposomes unsuitable for encapsulation efficiency studies by agarose gel, but comparison of the formulations containing GL67 with and without linolenic acid observed poorer encapsulation efficiencies when linolenic acid was incorporated into the formulation. This may be due to the effect on membrane structure of linolenic acid; its fusogenic or membrane destabilising properties were detailed in McGill et al (2023) where the liposomal nanoparticles were found to immediately break down in contact with viral particles during coculture, which was directly attributed to the inclusion of linolenic acid. Furthermore, in a micellar structure (Yang et al, 2023), inclusion of linolenic acid in the membrane yielded a low critical micelle concentration which refers to the concentration at which micelles begin to aggregate. Combined with the cryoTEM and FRET data from chapter 3, which indicated membrane fusion as a mechanism for complexation, it is possible that linolenic acid may negatively affect membrane stability of the complex overall.

5.5.2 Uptake

Uptake studies were conducted using the transfection protocol optimised in chapter 4. Initial uptake studies by the new formulations containing the label DiD indicated efficient uptake by all formulations in DC2.4 cells. Given that uptake was strong regardless of formulation, it is challenging to isolate specific variables that influence uptake. In chapter 3, efficient uptake was attributed to an overall positive charge and the inclusion of the fusogenic lipid DOPE (Maitani et al, 2007), although Caracciolo et al (2008) suggested that phase transitions in the membrane initiated by fusogenic lipid was not correlated with gene expression. Linolenic acid possesses membrane destabilising properties when included in liposomal formulations (McGill et al, 2023; Yang et al, 2023) which may positively influence uptake upon contact with cell membranes. Dendritic cells have also been observed to directly take up linolenic acid and its metabolites through receptor-

mediated uptake via peroxisome proliferator-activated receptor gamma (PPARγ) (Zapata-Gonzalez et al, 2008). Linolenic acid has also been observed to be taken up by receptor=mediated endocytosis in HepG2 cells (Cho et al, 2002) and other cells such as macrophages by G-protein coupled receptor 40 (Ohue-Kitano et al, 2018). Membrane charge density has also found to strongly influence uptake, which increases as membrane charge density and overall charge increases (Ahmad et al, 2005; Caracciolo et al, 2008; Ren et al, 2010).

5.5.3 Transfection

Initial screening of transfection efficiency in DC2.4 cells indicated strong expression of GFP when delivered by formulations including GL67. Spermine based nanoparticles have been found to elicit strong expression in dendritic cells; Markov et al (2012) formulated cholesterol-based spermine cationic lipids and included them in several formulations with DOPE. Liposomes were formed of a 1:1 ratio of cationic lipid and DOPE by thin film method before combining with pGFP DNA at NP ratios of 4, 6, 8, and 10. Using GFP expression in bone marrow derived murine DC cells, between 20% and 50% of cells were positive for GFP expression, increasing with NP ratio. This pattern is observable in the results detailed in section 5.4.5: liposomes formed of GL67 and DOPE yielded between 50% and 90% of live cells positive for GFP. This is markedly higher than Markov et al (2012) details, but this could be explained by either cationic lipid differences or flow cytometry gating strategy. In this chapter, we gated on live cells while Markov et al (2012) gated on single cells. Although they did not report cell viability, it is possible that the cells they gated on contained dead or dying cells that this chapter's gating strategy would have removed from analysis. Chen et al (2013) prepared the polysaccharide spermine-dextran (SD) and complexed with pGFP DNA at a mass ratio of 3:1 SD:DNA. Murine bone marrow derived dendritic cells were harvested and transfected using the same procedure as detailed in chapter 4, measuring GFP expression by visual count in fluorescence microscopy. Approximately 16% of cells were positive for GFP, with evidence of nuclear trafficking as

determined by confocal microscopy. Hence, expression of GFP in this chapter when plasmids were delivered by GL67/DOPE liposomes was higher than previously established in the literature. Inclusion of linolenic acid did not change GFP expression when included with either DC-Cholesterol or GL67. Previous work conjugating linolenic acid to PEI (Cheong et al, 2009) or other linear polymers and lipidic oligomers (Yi et al, 2014) found that inclusion of linolenic acid conferred benefit predominantly in terms of uptake, membrane traversal, or endosomal escape rather than improved expression. Given that DOPE was included in this chapter's liposomal formulation for that purpose, it is possible that DOPE and linolenic acid have a similar biochemical function. The slight decrease in GFP expression by GL67/DOPE/LA liposomes compared to GL67/DOPE is potentially due to the overall lower content of GL67 within the membrane when linolenic acid is included.

Transfections repeated with GL67 and DOPE observed strong expression linked to cell survival, with significant variation across biological replicates. This has not been observed in the literature; however, papers reporting repeatability have not reported both biological and technical repeats. Transfection between papers varies greatly, although few include both technical and biological repeats. Markov et al (2012) reported "three independent transfection repeats" in total with low variation, although this is unclear whether these repeats are technical ones done on the same day or biological. Cell passage numbers were not reported. Similarly, Chen et al (2013) reported six technical repeats, but no biological repeats and passage number was not reported. Xie et al (2019) reported three technical repeats, without biological repeats or reported passage numbers. Each of these papers reported vastly different populations positive for GFP as a percentage of total cells, ranging from 16% (Chen et al, 2013), to 50% (Markov et al, 2012), to 100% (Xie et al, 2019). Although these differences can be partially attributed to formulation of spermine-derived nanoparticles and type of cell line, it highlights other variations that are important to account for.

In a review of factors affecting transfection of eukaryotic cells *in vitro*, Fus-Kujawa et al (2021) discussed a range of factors applicable to the transfection in this chapter. In terms of transfection reagent, variation depends on consistency in DNA quantity, quality, ratio to cationic lipid, and incubation time. As detailed in chapter 3, these factors were controlled for by using the same batch of DNA produced by gigaprep and using the optimised protocol. One potential area for variation in formulation is in the temperature at which liposomes and DNA were complexed, due to fluctuating room temperatures in the laboratory and temperature changes between removal from storage at 4°C, to room temperature at approximately 18°C, to warmed cell media at 37°C. Investigation of liposome complex size as an indicator for batch variation revealed that there was approximately 50 nm difference between two batches prepared on different days, but this difference reduced when DNA was added. Complexation at different temperatures did not change the size of complex apart from NP3 at 37°C; given that complexation occurred in small volumes at room temperature, it is likely that the usual temperature of complexation yielded liposome-DNA complexes with reproducible characteristics.

Cell variations are common, where transfection efficiency in terms of uptake or processing pathways and protein production depend heavily on cell metabolism and growth (Fus-Kujawa et al, 2021). Transfection in this chapter is controlled for cell confluency (see chapter 4), ensuring that cells are transfected while in a growth phase and plentiful enough that loss of cell number due to toxicity does not prevent meaningful insights. Cell passage is also controlled, using DC2.4 cells of a passage lower than 10 as recommended by the supplier; NIH 3T3 and HEK293T cells were both used in passages lower than 30. High cell passages can exhibit traits of early cellular senescence, impacting gene expression, although stable transfection of the SV40 cassette can attenuate this effect (Cheng et al, 1989). By this rationale, HEK293T cells, which include SV40, would be resistant to cell passage-related variations in transfection. Regardless, variation is seen in this cell line alongside DC2.4 and NIH3T3 cells. It is possible that the cells experienced some kind of contaminant, given that

penicillin and streptomycin were excluded from cell media due to their effects on dendritic cell morphology (Lopez et al, 2015). However, cells were regularly checked for visible signs of contamination and the laboratory underwent regular monitoring for mycoplasma and endotoxins, which were negative.

It is therefore likely that the variation in transfection is due to a combination of variables including temperature, passage, liposomal batch variation, and toxicity of complex. All variables have been controlled to the best of the protocol's ability, and despite the likelihood that the GL67/DOPE formulation induces strong expression of GFP in live cells, it is unethical to test this formulation *in vivo* with this amount of variation and potential toxicity.

5.6 Conclusions

In chapter 4, liposomes composed of DC-Cholesterol and DOPE induced GFP expression strongly dependent on cell line and failed to initiate immune responses to SARS-Cov-2 spike and nucleocapsid proteins encoded by Scancell's SN17 plasmid. Liposomes were reformulated to include the multivalent cholesterol-based cationic lipid and/or the bilayer soluble fatty acid linolenic acid. When delivered to DC2.4 cells, efficient uptake was observed across cell lines regardless of NP ratio or formulation. Expression of GFP was highly variable across biological repeats but not technical repeats. The effect of temperature on DNA-liposome complexation was minimal and unlikely to account for the degree of variation observed. Variation is likely due to a combination of factors such as cell passage, liposome batch variation, environmental variation, and other unknown variables. Despite the variation, there remains a possibility of multivalent cationic lipid improvement on gene expression in dendritic cells. Further study on identification of these variables and expansion in valency and/or liposome membrane charge density is needed to conclusively state its effect on expression in dendritic cells.

Chapter 6: Discussion, Summary, and Future Directions

6.1 Discussion

DNA vaccines have demonstrated efficacy in initiating immune responses against a variety of encoded targets, having been licenced for veterinary use (Davis et al, 2001; Grosenbaugh et al, 2011) and more recently Covid-19 (Khobragade et al, 2022), the technology lending itself to rapid vaccine development which is essential given the high chance of future pandemics (Marani et al, 2021). The strength and duration of immune responses are strongly influenced by DNA vector, route of delivery, and involvement of innate immune cells such as dendritic cells. As of 2021, over two thirds of gene-based vaccine clinical trials used viral vectors (Sharma et al, 2021) but have issues with toxicity and possess risks such as oncogenesis, encouraging the development of nonviral alternatives. Cationic liposomes have demonstrated efficacy in condensing negatively charged plasmid DNA encoding for a wide range of vaccination targets, but formulation efforts have struggled with immunogenicity due to the dual influence of liposome formulation and antigen selection on vaccine efficacy (Joseph et al, 2006). An understanding of the liposome-related factors that influence successful uptake and gene expression, particularly in dendritic cells, could improve formulation strategies and expedite development.

Hence, the overarching aim of this project was to compare mono- and multivalent cationic liposome formulations to determine whether cationic valency or inclusion of linolenic acid may differentially affect dendritic cell gene expression. Liposomes composed of DC-Cholesterol/DOPE have been well characterised in the literature with conflicting reports on immunogenicity in vaccination studies. Perrie et al (2003) reported strong systemic immune responses to H1N1 influenza antigens encoded on pDNA and delivered by DC-Chol/DOPE liposomes. However, Joseph et al (2006) observed only local responses to influenza antigens encoded on pDNA and delivered by DC-Cholesterol based liposomes. Some papers have suggested that inclusion of multivalent cationic lipids and the resultant increase in liposomal membrane charge density improves both pDNA loading in the

liposome and transfection efficacy (Ahmad et al, 2005; Caracciolo et al, 2008), but multivalency of cationic lipid in dendritic cell-targeted liposomal formulations is novel to this thesis. Additionally, linolenic acid has been suggested to be suitable for liposomal inclusion and membrane destabilising properties (Thampiwatwana et al, 2014; McGill et al, 2023). It also is known to directly interact with several components of the immune system (Carlsson et al, 2015). However, linolenic acid as a component in the liposomal membrane for pDNA delivery to dendritic cells is a novel application of the fatty acid.

The thesis hypothesis was that modulation of the membrane charge density on cationic liposomes and/or the inclusion of linolenic acid would differentially impact gene expression in a panel of cell lines including DC2.4 cells, NIH 3T3 cells, and HEK293T cells. First, liposomes were formulated with DC-Cholesterol and DOPE at a range of molar ratios before combining with DNA at a range of NP ratios. Physicochemical properties and mechanism of liposomes-pDNA interactions were assessed. Next, the *in vitro* expression of GFP was measured in dendritic cells (DC2.4), murine fibroblasts (NIH 3T3), and a classical transfection model cell line (HEK293T). Liposomes composed of DC-Cholesterol/DOPE were then administered *in vivo* to measure splenocyte and serum antibody response to pDNA-encoded SARS-Cov-2 antigens. Next, liposomes were reformulated to consist of GL67/DOPE. Linolenic acid was included in separate formulations: DC-Cholesterol/DOPE/Linolenic acid and GL67/DOPE/Linolenic acid. *In vitro* uptake was measured in DC2.4 cells, and GFP expression measured in DC2.4, NIH 3T3, and HEK293T cells.

In Chapter 3, liposomes formulated of DC-Cholesterol and DOPE at a range of molar ratios (DC-Cholesterol at 25 mol%, 30 mol%, 35 mol%, 40 mol%, and 50 mol%) were formed by the thin film method (section 2.3.1). Plasmid DNA was initially added during hydration to explore novel variations on the classic method, but difficulties with aggregation prevented this from being taken forward and liposomes were thereafter hydrated in water alone and combined with pDNA after extrusion. When liposome-DNA complexes were

made by adding pDNA to hydrated and extruded liposomes, stable complexes were observed less than 200 nm in diameter. Zeta potential showed a positive charge in empty liposomes, a negative charge at NP 3, and a slightly increasing positive charge as NP ratio increased. This is consistent with data found in the literature, which suggests that the isoneutrality point for this formulation is around NP 4 (Rodruguez-Pulido et al, 2004).

DNA encapsulation efficiency was measured by gel retardation assay, which showed close to 100% encapsulation by virtue of no detectable DNA in the body of the gel. This method relies on ultraviolet imaging of pDNA stained by ethidium bromide trapped within the agarose gel matrix, and may suffer from lack of sensivity in low concentrations of pDNA. To verify this, an ethidium bromide displacement assay was carried out, which showed only partial displacement. The results of these two assays are conflicting; if close to 100% encapsulation efficiency is accurate, a greater degree of displacement would have been observed. This could be explained by the structures observed in cryogenic transmission electron microscopy, which showed a pDNA-initiated multilamellar structure, potentially with entrapped plasmids between layers as previously described by Huebner et al (1999). Molecules of ethidium bromide are brightly fluorescent when trapped between pDNA bases; displacement occurs during direct pDNA-lipid binding and some displacement may be prevented by trapping of pDNA between phospholipid membranes where it cannot escape (Nitsch et al, 2019).

The multilamellar structures observed in cryoTEM raised questions regarding the mechanism of MLV formation upon the addition of pDNA. Zhigaltsev and Cullis (2023) suggested that inducing osmotic or membrane stress on small unilamellar vesicles containing cone-shaped phospholipids can lead to bilamellar vesicle formation through lipid mixing and membrane fusion. Given that DOPE is a cone shaped lipid, it was suggested that the charge-based interactions between cationic lipids and anionic pDNA may induce MLV formation by this mechanism. Using FRET (described in section 2.3.7), membrane fusion and lipid mixing was investigated by two methods.

First, addition of pDNA to a 1:1 mixture of dually labelled and unlabelled liposomes system observed decrease in fluorescence. This could be due to dilution of fluorophores that remain in close proximity, or increase in distance between fluorophores; both suggest lipid mixing is taking place. Secondly, addition of pDNA to a mixed population of singly labelled liposomes observed increase in fluorescence, likely due to an increase in proximity between fluorophores. Both suggest fusion of liposome membranes. Liposome membrane fusogenicity is correlated with cellular uptake and transfection efficiency, possibly because of increased endosomal escape (Inoh et al, 2017).

Chapter 4 aimed to evaluate the efficacy of DC-Cholesterol/DOPE liposomes delivering GFP pDNA to DC2.4, NIH 3T3, and HEK293T cells. Uptake was strong across cell lines and NP ratios, which has been described previously and attributed to a combination of an overall positive liposome charge and inclusion of the strongly fusogenic lipid DOPE (Inoh et al, 2017). GFP expression was strongly dependent on cell line, showing the strongest expression in HEK293T cells, moderate expression in NIH 3T3 cells, and low expression in DC2.4 cells where less than 5% of cells expressed GFP despite high uptake. This is common in the literature, where dendritic cells are refractory to many novel transfection reagents (Awasthi et al, 2019), possibly due to altered environmental uptake pathways and additional antigen presentation pathways compared to a non-professional antigen presenting cell. However, treatment with chloroquine diphosphate revealed that lack of endosomal escape was unlikely to be the limiting factor in transfection efficiency. Transfection in fibroblasts has been shown to be able to initiate dendritic cell responses *in vivo* (Saalbach et al, 2007), so DC-Cholesterol/DOPE liposomes were taken forward into an *in vivo* study. However, no systemic immunity was observed. Liposomes composed of DC-Cholesterol and DOPE have had mixed reports of immunogenicity in the literature; Perrie et al (2003) reported systemic immunogenicity, while Joseph et al (2006) did not. The latter describes that immunogenicity of gene-based vaccines is thought to be a complex result of multiple influences including formulation, site of administration, and encoded antigen; both

papers use influenza antigens but deliver preparations through the subcutaneous and intranasal routes respectively. The lack of immune response observed in this murine study may involve a combination of factors including immunogenicity or efficacy of the pDNA-encoded COVID-19 antigen or site of administration. It is possible that immune responses occurred but were limited to the local site of injection; a repeat of the experiment using local tissue sampling for immunohistochemistry or fluorescent expression in biodistribution studies would identify this.

It was then hypothesised that increasing the percentage of DC2.4 cells positive for GFP would be predictive of better immune responses. This is not a high threshold, and immune responses *in vivo* have been observed in studies that reported *in vitro* percentages of dendritic cells expressing GFP of only 14% (Dhanoya et al, 2012) and 15% (Moku et al, 2021). Uptake was high across cell lines and linolenic acid did not change expression of GFP in DC2.4 cells in comparison to formulations without linolenic acid. This is possibly due to an overlap in function between linolenic acid and DOPE; both have fusogenic/membrane destabilising properties (McGill et al, 2023; Caracciolo and Caminiti, 2005). Further biological repeats in DC2.4, NIH 3T3, and HEK293T cells showed extremely high variation in both cell viability and GFP expression. Cell confluency was ruled out as a determining factor due to optimisation data in chapter 4, and ambient temperature variation was ruled out as a factor that may have affected complexation during experimentation. The variation was suggested to be due to a combination of potentially inextricable factors including but not limited to: liposome toxicity of GL67, liposome batch variation in terms of polydispersity, environmental cell culture factors, cell passage, and other unknown variables. It remains possible that multivalency and/or linolenic acid may improve transfection in dendritic cells and warrants further study.

6.2 Summary

In summary, the work completed in this thesis has demonstrated that multivalency of the cationic lipid in liposomal formulations delivering pDNA has the potential to influence encoded gene expression in dendritic cells.

DC-Cholesterol/DOPE, DC-Cholesterol/DOPE/linolenic acid, GL67/DOPE and GL67/DOPE/linolenic acid liposomes are stable, positively charged, and possess particle sizes less than 200 nm. Expression of GFP *in vitro* was cell dependent and for GL67/DOPE, highly variable. DC-Cholesterol/DOPE liposomes were insufficient in initiating systemic immune responses and it was suggested that improving dendritic cell transfection efficiency *in vitro* would be predictive of immune responses *in vivo*. Multivalency of cationic lipids and/or linolenic acid warrant further study in delivering pDNA to dendritic cells.

6.3 Future Directions

Areas for further optimisation and experimentation would address the variation seen in chapter 5. Variation in both cell viability and GFP expression were observed, while this variation was not observed in chapter 4. Previous research has correlated toxicity and transfection efficiency; therefore, there is rationale for testing the correlation between the cytotoxicity of GL67 and expression of GFP in the given cell lines. This would be done by expanding formulations to contain varying molar percentages of GL67 and carrying out a dose-toxicity curve to examine the toxicity of GL67 and its relation to total membrane composition. This may involve switching to a luciferase-encoding plasmid to correlate protein production with liposome formulation and its associated toxicity. Investigation into the specific cause of toxicity could also be carried out using autolysis or necrolysis dyes.

Furthermore, to fully interrogate the effect of valency on dendritic cell uptake, further lipids could be assembled with a cholesterol backbone and bivalent, quadrivalent, and pentavalent cationic head groups. Ahmad et al (2005) explored transfection in this way, mapping overall charge density and liposome complex charge on transfection efficiency. Modulation of their content could be mirrored with the aforementioned correlation between toxicity and transfection efficiency.

Furthermore, gene expression in dendritic cells does not always correlate with immunogenicity *in vivo*. The above formulations with controlled cationic lipid content and multivalency could interrogate DC activation and phenotype response to investigate whether multivalent lipids can sufficiently induce dendritic cell maturation. This would be carried out by flow cytometry, measuring expression of dendritic-cell specific maturation markers such as CD80 and CD86. This could then be paired with a mixed lymphocyte reaction, which measures antigen-specific T cell response to transfected dendritic cells.

References

Arta, B., Litzinger, D. C., Brown, J. M., Wala, I., Kaufman, S. A., Van, G. Y., Farrell, C. L., & Collins, D. (1996). Biological fate of cationic liposomes and their complex with oligonucleotide *in vivo*. Biochimica et Biophysica Acta, 1281, 139–149.

Ackerman, A. L., & Cresswell, P. (2003). Regulation of MHC Class I Transport in Human Dendritic Cells and the Dendritic-Like Cell Line KG-1. The Journal of Immunology, 170(8), 4178–4188. https://doi.org/10.4049/jimmunol.170.8.4178

Ahmad, A., Evans, H. M., Ewert, K., George, C. X., Samuel, C. E., & Safinya, C. R. (2005). New multivalent cationic lipids reveal bell curve for transfection efficiency versus membrane charge density: lipid–DNA complexes for gene delivery. The Journal of Gene Medicine, 7(6), 739–748. https://doi.org/10.1002/JGM.717

Alazzo, A., Lovato, T., Collins, H., Taresco, V., Stolnik, S., Soliman, M., Spriggs, K., & Alexander, C. (2018). Structural variations in hyperbranched polymers prepared via thermal polycondensation of lysine and histidine and their effects on DNA delivery. Journal of Interdisciplinary Nanomedicine, 3(2), 38–54. https://doi.org/10.1002/jin2.36

Algarni, A., Pilkington, E. H., Suys, E. J. A., Al-Wassiti, H., Pouton, C. W., & Truong, N. P. (2022). *In vivo* delivery of plasmid DNA by lipid nanoparticles: the influence of ionizable cationic lipids on organ-selective gene expression. Biomaterials Science, 10(11), 2940–2952. https://doi.org/10.1039/D2BM00168C

Audouy, S. A. L., de Leij, L. F. M. H., Hoekstra, D., & Molema, G. (2002). *In vivo* characteristics of cationic liposomes as delivery vectors for gene therapy. In Pharmaceutical Research (Vol. 19, Issue 11, pp. 1599–1605). https://doi.org/10.1023/A:1020989709019

Bal, S. M., Slütter, B., Verheul, R., Bouwstra, J. A., & Jiskoot, W. (2012). Adjuvanted, antigen loaded N-trimethyl chitosan nanoparticles for nasal and intradermal vaccination: Adjuvant- and site-dependent immunogenicity in mice. European Journal of Pharmaceutical Sciences, 45(4), 475–481. https://doi.org/10.1016/J.EJPS.2011.10.003

Balazs, D. A., & Godbey, WT. (2011). Liposomes for Use in Gene Delivery. Journal of Drug Delivery, 2011, 1–12. https://doi.org/10.1155/2011/326497

Behzadi, S., Serpooshan, V., Tao, W., Hamaly, M. A., Alkawareek, M. Y., Dreaden, E. C., Brown, D., Alkilany, A. M., Farokhzad, O. C., & Mahmoudi, M. (2017). Cellular uptake of nanoparticles: Journey inside the cell. In Chemical Society Reviews (Vol. 46, Issue 14, pp. 4218–4244). Royal Society of Chemistry. https://doi.org/10.1039/c6cs00636a

Bok, K., Sitar, S., Graham, B. S., & Mascola, J. R. (2021). Accelerated COVID-19 vaccine development: milestones, lessons, and prospects. Immunity, 54(8), 1636–1651. https://doi.org/10.1016/J.IMMUNI.2021.07.017

Briuglia, M. L., Rotella, C., McFarlane, A., & Lamprou, D. A. (2015). Influence of cholesterol on liposome stability and on *in vitro* drug release. Drug Delivery and Translational Research, 5(3), 231–242. https://doi.org/10.1007/s13346-015-0220-8

Brownlie, R., & Zamoyska, R. (2013, 4 25). T cell receptor signalling networks: Branched, diversified and bounded. Nature Reviews Immunology, 13(4), 257-269. Nature Publishing Group. https://doi.org/10.1038/nri3403

Byrne, K. T., & Vonderheide, R. H. (2016). CD40 Stimulation Obviates Innate Sensors and Drives T Cell Immunity in Cancer. Cell Reports, 15(12), 2719–2732. https://doi.org/10.1016/j.celrep.2016.05.058

Capriotti, A. L., Caracciolo, G., Cavaliere, C., Foglia, P., Pozzi, D., Samperi, R., & Laganà, A. (2012). Do plasma proteins distinguish between liposomes of varying charge density? https://doi.org/10.1016/j.jprot.2012.01.003

Caracciolo, G., & Amenitsch, H. (2012). Cationic liposome/DNA complexes: From structure to interactions with cellular membranes. In European Biophysics Journal (Vol. 41, Issue 10, pp. 815–829). https://doi.org/10.1007/s00249-012-0830-8

Caracciolo, G., Callipo, L., Candeloro, S., Sanctis, D., Cavaliere, C., Pozzi, D., & Laganà, A. (2009). Surface adsorption of protein corona controls the cell internalization mechanism of DC-Chol-DOPE/DNA lipoplexes in serum. https://doi.org/10.1016/j.bbamem.2009.11.007

Caracciolo, G., & Caminiti, R. (2005). Do DC-Chol/DOPE-DNA complexes really form an inverted hexagonal phase? https://doi.org/10.1016/j.cplett.2005.06.070

Caracciolo, G., Pozzi, D., Amenitsch, H., & Caminiti, R. (2005). Multicomponent cationic lipid-DNA complex formation: Role of lipid mixing. Langmuir, 21(25), 11582–11587. https://doi.org/10.1021/LA052077C/ASSET/IMAGES/LARGE/LA052077CF00007.JPEG

Caracciolo, G., Pozzi, D., Caminiti, R., Marchini, C., Montani, M., Amici, A., & Amenitsch, H. (n.d.). Enhanced Transfection Efficiency of Multicomponent Lipoplexes in the Regime of Optimal Membrane Charge Density. https://doi.org/10.1021/jp803077n

Carlsson, J. A., Wold, A. E., Sandberg, A. S., & Östman, S. M. (2015). The Polyunsaturated Fatty Acids Arachidonic Acid and Docosahexaenoic Acid Induce Mouse Dendritic Cells Maturation but Reduce T-Cell Responses *In Vitro*. PLOS ONE, 10(11), e0143741. https://doi.org/10.1371/JOURNAL.PONE.0143741

Carroll, S. L., Pasare, C., & Barton, G. M. (2024). Control of adaptive immunity by pattern recognition receptors. In Immunity (Vol. 57, Issue 4, pp. 632–648). Cell Press. https://doi.org/10.1016/j.immuni.2024.03.014

Carstens, M. G., Camps, M. G. M., Henriksen-Lacey, M., Franken, K., Ottenhoff, T. H. M., Perrie, Y., Bouwstra, J. A., Ossendorp, F., & Jiskoot, W. (2011). Effect of vesicle size on tissue localization and immunogenicity of liposomal DNA vaccines. Vaccine, 29(29–30), 4761–4770. https://doi.org/10.1016/j.vaccine.2011.04.081

Casper, J., Schenk, S. H., Parhizkar, E., Detampel, P., Dehshahri, A., & Huwyler, J. (2023). Polyethylenimine (PEI) in gene therapy: Current status and clinical applications. https://doi.org/10.1016/j.jconrel.2023.09.001

Caster, J. M., Callaghan, C., Seyedin, S. N., Henderson, K., Sun, B., & Wang, A. Z. (2019). Optimizing Advances in Nanoparticle Delivery for Cancer Immunotherapy. In Advanced Drug Delivery Reviews (Vol. 144, pp. 3–15). Elsevier B.V. https://doi.org/10.1016/j.addr.2019.07.009

Chakraborty, C., Bhattacharya, M., & Dhama, K. (2023). SARS-CoV-2 Vaccines, Vaccine Development Technologies, and Significant Efforts in Vaccine Development during the Pandemic: The Lessons Learned Might Help to Fight against the Next Pandemic. https://doi.org/10.3390/vaccines11030682

Chapman, R., van Diepen, M., Douglass, N., Hermanus, T., Moore, P. L., & Williamson, A. L. (2023). Needle-Free Devices and CpG-Adjuvanted DNA Improve Anti-HIV Antibody Responses of Both DNA and Modified Vaccinia Ankara-Vectored Candidate Vaccines. Vaccines, 11(2). https://doi.org/10.3390/vaccines11020376

Chen, K., Fan, N., Huang, H., Jiang, X., Qin, S., Xiao, W., Zheng, Q., Zhang, Y., Duan, X., Qin, Z., Liu, Y., Zeng, J., Wei, Y., & Song, X. (2022). mRNA Vaccines Against SARS-CoV-2 Variants Delivered by Lipid Nanoparticles Based on Novel Ionizable Lipids. Advanced Functional Materials, 32(39), 2204692. https://doi.org/10.1002/ADFM.202204692

Chen, X., Shaulov Kask, A., Crichton, M. L., Mcneilly, C., Yukiko, S., Dong, L., Marshak, J. O., Jarrahian, C., Fernando, G. J. P., Chen, D., Koelle, D. M., &

Kendall, M. A. F. (2010). Improved DNA vaccination by skin-targeted delivery using dry-coated densely-packed microprojection arrays. https://doi.org/10.1016/j.jconrel.2010.09.001

Chen, Y., Sun, J., Lu, Y., Tao, C., Huang, J., Zhang, H., Yu, Y., Zou, H., Gao, J., & Zhong, Y. (2013). Complexes containing cationic and anionic pH-sensitive liposomes: Comparative study of factors influencing plasmid DNA gene delivery to tumors. International Journal of Nanomedicine, 8, 1573–1593. https://doi.org/10.2147/IJN.S42800

Chen, Y. Z., Ruan, G. X., Yao, X. L., Li, L. M., Hu, Y., Tabata, Y., & Gao, J. Q. (2013). Co-transfection gene delivery of dendritic cells induced effective lymph node targeting and anti-tumor vaccination. Pharmaceutical Research, 30(6), 1502–1512. https://doi.org/10.1007/S11095-013-0985-8/METRICS

Cheng, C. Y., Ryan, R. F., Vo, T. P., & Hornsby', P. J. (1989). Cellular Senescence Involves Stochastic Processes Causing Loss of Expression of Differentiated Function Genes: Transfection with SV40 as a Means for Dissociating Effects of Senescence on Growth and on Differentiated Function Gene Expression. In Experimental Cell Research (Vol. 180).

Cheong, S. J., Lee, C. M., Kim, S. L., Jeong, H. J., Kim, E. M., Park, E. H., Kim, D. W., Lim, S. T., & Sohn, M. H. (2009). Superparamagnetic iron oxide nanoparticles-loaded chitosan-linoleic acid nanoparticles as an effective hepatocyte-targeted gene delivery system. International Journal of Pharmaceutics, 372(1–2), 169–176. https://doi.org/10.1016/J.IJPHARM.2009.01.009

Chesnoy, S., & Huang, L. (2000). Structure and function of lipid-DNA complexes for gene delivery. In Annual Review of Biophysics and Biomolecular Structure (Vol. 29, pp. 27–47). https://doi.org/10.1146/annurev.biophys.29.1.27

Chesnoy, S., & Huang, L. (2002). Enhanced Cutaneous Gene Delivery Following Intradermal Injection of Naked DNA in a High Ionic Strength Solution. MOLECULAR THERAPY, 5(1). https://doi.org/10.1006/mthe.2001.0511

Cho, H., Bhatti, F.-U.-R., Yoon, T. W., Hasty, K. A., Stuart, J. M., & Yi, A.-K. (2016). Non-invasive dual fluorescence *in vivo* imaging for detection of macrophage infiltration and matrix metalloproteinase (MMP) activity in inflammatory arthritic joints. Biomedical Optics Express, 7(5), 1842. https://doi.org/10.1364/boe.7.001842

Cianciosi, D., Diaz, Y. A., Gaddi, A. V., Capello, F., Savo, M. T., Palí Casanova, R. del J., Martínez Espinosa, J. C., Pascual Barrera, A. E., Navarro-Hortal, M. D., Tian, L., Bai, W., Giampieri, F., & Battino, M. (2024). Can alpha-linolenic acid be a modulator of “cytokine storm,” oxidative stress and immune response in SARS-CoV-2 infection? Food Frontiers, 5(1), 73–93. https://doi.org/10.1002/FFT2.319

Ciani, L., Casini, A., Gabbiani, C., Ristori, S., Messori, L., & Martini, G. (2007). DOTAP/DOPE and DC-Chol/DOPE lipoplexes for gene delivery studied by circular dichroism and other biophysical techniques. https://doi.org/10.1016/j.bpc.2007.02.003

Ciani, L., Ristori, S., Salvati, A., Calamai, L., & Martini, G. (2004). DOTAP/DOPE and DC-Chol/DOPE lipoplexes for gene delivery: zeta potential measurements and electron spin resonance spectra. https://doi.org/10.1016/j.bbamem.2004.04.003

Clark, G. J., Silveira, P. A., Hogarth, P. M., & Hart, D. N. J. (2019). The cell surface phenotype of human dendritic cells. Seminars in Cell & Developmental Biology, 86, 3–14. https://doi.org/10.1016/j.semcdb.2018.02.013

Conde, J., Langer, R., & Rueff, J. (2023). mRNA therapy at the convergence of genetics and nanomedicine. Nature Nanotechnology 2023 18:6, 18(6), 537–540. https://doi.org/10.1038/s41565-023-01347-w

Coombes, B. K., & Mahony, J. B. (2001). Dendritic cell discoveries provide new insight into the cellular immunobiology of DNA vaccines. Immunology Letters, 78(2), 103–111. https://doi.org/10.1016/S0165-2478(01)00242-5

Cote, B., Rao, D., Alany, R. G., Kwon, G. S., & Alani, A. W. G. (2019). Lymphatic changes in cancer and drug delivery to the lymphatics in solid tumors. In Advanced Drug Delivery Reviews (Vol. 144, pp. 16–34). Elsevier B.V. https://doi.org/10.1016/j.addr.2019.08.009

Cruz, L. J., Tacken, P. J., Rueda, F., Domingo, J. C., Albericio, F., & Figdor, C. G. (2012). Targeting nanoparticles to dendritic cells for immunotherapy. In Methods in Enzymology (Vol. 509, pp. 143–163). Academic Press Inc. https://doi.org/10.1016/B978-0-12-391858-1.00008-3

Daugimont, L., Baron, N., Vandermeulen, G., Pavselj, N., Miklavcic, D., Jullien, M. C., Cabodevila, G., Mir, L. M., & Préat, V. (2010). Hollow microneedle arrays for intradermal drug delivery and DNA electroporation. Journal of Membrane Biology, 236(1), 117–125. https://doi.org/10.1007/s00232-010-9283-0

Davidson, S., Coles, M., Thomas, T., Kollias, G., Ludewig, B., Turley, S., Brenner, M., & Buckley, C. D. (2021). Fibroblasts as immune regulators in infection, inflammation and cancer. In Nature Reviews Immunology (Vol. 21, Issue 11, pp. 704–717). Nature Research. https://doi.org/10.1038/s41577-021-00540-z

Davis, B. S., Chang, G.-J. J., Cropp, B., Roehrig, J. T., Martin, D. A., Mitchell, C. J., Bowen, R., & Bunning, M. L. (2001). West Nile Virus Recombinant DNA Vaccine Protects Mouse and Horse from Virus Challenge and Expresses *In Vitro* a Noninfectious Recombinant Antigen That Can Be Used in Enzyme-Linked Immunosorbent Assays. Journal of Virology, 75(9), 4040–4047. https://doi.org/10.1128/jvi.75.9.4040-4047.2001

Degors, I. M. S., Wang, C., Rehman, Z. U., & Zuhorn, I. S. (2019). Carriers break barriers in drug delivery: endocytosis and endosomal escape of gene delivery vectors. Accounts of Chemical Research, 52(7), 1750–1760. https://doi.org/10.1021/ACS.ACCOUNTS.9B00177

den Hartog, G., van Binnendijk, R., Buisman, A. M., Berbers, G. A. M., & van der Klis, F. R. M. (2020). Immune surveillance for vaccine-preventable diseases. Expert Review of Vaccines, 19(4), 327–339. https://doi.org/10.1080/14760584.2020.1745071

Dengjel, J., Schoor, O., Fischer, R., Reich, M., Kraus, M., Müller, M., Kreymborg, K., Altenberend, F., Brandenburg, J., Kalbacher, H., Brock, R., Driessen, C., Rammensee, H. G., & Stevanovic, S. (2005). Autophagy promotes MHC class II presentation of peptides from intracellular source proteins. Proceedings of the National Academy of Sciences of the United States of America, 102(22), 7922–7927. https://doi.org/10.1073/PNAS.0501190102/SUPPL_FILE/01190FIG6.JPG

Dey, A., Chozhavel Rajanathan, T. M., Chandra, H., Pericherla, H. P. R., Kumar, S., Choonia, H. S., Bajpai, M., Singh, A. K., Sinha, A., Saini, G., Dalal, P., Vandriwala, S., Raheem, M. A., Divate, R. D., Navlani, N. L., Sharma, V., Parikh, A., Prasath, S., Sankar Rao, M., & Maithal, K. (2021). Immunogenic potential of DNA vaccine candidate, ZyCoV-D against SARS-CoV-2 in animal models. Vaccine, 39(30), 4108. https://doi.org/10.1016/J.VACCINE.2021.05.098

Diebold, S. S., Cotten, M., Koch, N., & Zenke, M. (2001a). MHC class II presentation of endogenously expressed antigens by transfected dendritic cells. Gene Therapy, 8(6), 487–493. https://doi.org/10.1038/sj.gt.3301433

Diebold, S. S., Cotten, M., Koch, N., & Zenke, M. (2001b). MHC class II presentation of endogenously expressed antigens by transfected dendritic cells. In Gene Therapy (Vol. 8). www.nature.com/gt

Dockrell, H. M., & Smith, S. G. (2017). What Have We Learnt about BCG Vaccination in the Last 20 Years? Frontiers in Immunology, 8(SEP), 1134. https://doi.org/10.3389/FIMMU.2017.01134

Donahue, N. D., Acar, H., & Wilhelm, S. (2019). Concepts of nanoparticle cellular uptake, intracellular trafficking, and kinetics in nanomedicine. In Advanced Drug Delivery Reviews (Vol. 143, pp. 68–96). Elsevier B.V. https://doi.org/10.1016/j.addr.2019.04.008

Drabick, J. J., Glasspool-Malone, J., Somiari, S., King, A., & Malone, R. W. (2001). Cutaneous transfection and immune responses to intradermal nucleic acid vaccination are significantly enhanced by *in vivo* electropermeabilization. Molecular Therapy, 3(2), 249–255. https://doi.org/10.1006/mthe.2000.0257

Du, Z., Munye, M. M., Tagalakis, A. D., Manunta, M. D. I., & Hart, S. L. (2014). The Role of the helper lipid on the DNA transfection efficiency of lipopolyplex formulations. Scientific Reports, 4. https://doi.org/10.1038/srep07107

Elnekave, M., Furmanov, K., & Hovav, A. H. (2011). Intradermal naked plasmid DNA immunization: Mechanisms of action. In Expert Review of Vaccines (Vol. 10, Issue 8, pp. 1169–1182). https://doi.org/10.1586/erv.11.66

Emi, N., Nagy, A., Castenmiller, C., Lozano Vigario, F., Sparrius, R., van Capel, T. M. M., de Haas, A. M., van Kooyk, Y., van Ree, R., Tas, S. W., Geijtenbeek, B. H., Jiskoot, W., Sl, B., & de Jong, E. C. (2022). Special Topic Cluster Uptake Kinetics Of Liposomal Formulations of Differing Charge Influences Development of *in Vivo* Dendritic Cell Immunotherapy. Journal of Pharmaceutical Sciences, 111, 1081–1091. https://doi.org/10.1016/j.xphs.2022.01.022

Ewert, K. K., Ahmad, A., Evans, H. M., & Safinya, C. R. (2005). Cationic lipid-DNA complexes for non-viral gene therapy: Relating supramolecular structures to cellular pathways. In Expert Opinion on Biological Therapy (Vol. 5, Issue 1, pp. 33–53). https://doi.org/10.1517/14712598.5.1.33

Faurez, F., Dory, D., le Moigne, V., Gravier, R., & Jestin, A. (2010). Biosafety of DNA vaccines: New generation of DNA vectors and current knowledge on the fate of plasmids after injection. Vaccine, 28, 3888–3895. https://doi.org/10.1016/j.vaccine.2010.03.040

Feikin, D. R., Higdon, M. M., Abu-Raddad, L. J., Andrews, N., Araos, R., Goldberg, Y., Groome, M. J., Huppert, A., O'Brien, K. L., Smith, P. G., Wilder-Smith, A., Zeger, S., Deloria Knoll, M., & Patel, M. K. (2022). Duration of effectiveness of vaccines against SARS-CoV-2 infection and COVID-19 disease: results of a systematic review and meta-regression. Lancet (London, England), 399(10328), 924. https://doi.org/10.1016/S0140-6736(22)00152-0

Felgner, P. L. (1997). Nonviral strategies for gene therapy. Scientific American, 276(6), 102–106. https://doi.org/10.1038/scientificamerican0697-102

Foged, C., Brodin, B., Frokjaer, S., & Sundblad, A. (2005). Particle size and surface charge affect particle uptake by human dendritic cells in an *in vitro* model. International Journal of Pharmaceutics, 298(2), 315–322. https://doi.org/10.1016/j.ijpharm.2005.03.035

Foldvari, M., Babiuk^, S., & Badea, I. (2006). DNA Delivery for Vaccination and Therapeutics Through the Skin. In Current Drug Delivery (Vol. 3).

Foroozandeh, P., & Aziz, A. A. (n.d.). Insight into Cellular Uptake and Intracellular Trafficking of Nanoparticles. https://doi.org/10.1186/s11671-018-2728-6

Francis, J. E., Skakic, I., Dekiwadia, C., Shukla, R., Taki, A. C., Walduck, A., & Smooker, P. M. (2020). Solid lipid nanoparticle carrier platform containing synthetic TLR4 agonist mediates non-viral DNA vaccine delivery. Vaccines, 8(3), 1–16. https://doi.org/10.3390/vaccines8030551

Fus-Kujawa, A., Prus, P., Bajdak-Rusinek, K., Teper, P., Gawron, K., Kowalczuk, A., & Sieron, A. L. (2021). An Overview of Methods and Tools for Transfection of Eukaryotic Cells *in vitro*. In Frontiers in Bioengineering and Biotechnology (Vol. 9). Frontiers Media S.A. https://doi.org/10.3389/fbioe.2021.701031

Gamvrellis, A., Leong, D., Hanley, J. C., Xiang, S. D., Mottram, P., & Plebanski, M. (2004). Vaccines that facilitate antigen entry into dendritic cells. Immunology and Cell Biology, 82(5), 506–516. https://doi.org/10.1111/j.0818-9641.2004.01271.x

Gao, J. Q., Chen, Y. Z., Yao, X. L., Tabata, Y., & Nakagawa, S. (2010). Gene carriers and transfection systems used in the recombination of dendritic cells for effective cancer immunotherapy. In Clinical and Developmental Immunology (Vol. 2010). https://doi.org/10.1155/2010/565643

Garaiova, Z., Strand, S. P., Reitan, N. K., Lélu, S., Størset, S. Ø., Berg, K., Malmo, J., Folasire, O., Bjørkøy, A., & Davies, C. D. L. (2012). Cellular uptake of DNA-chitosan nanoparticles: The role of clathrin-and caveolae-mediated

pathways. International Journal of Biological Macromolecules, 51, 1043–1051. https://doi.org/10.1016/j.ijbiomac.2012.08.016

Garu, A., Moku, G., Gulla, S. K., & Chaudhuri, A. (2016a). Genetic immunization with *in vivo* dendritic cell-targeting liposomal DNA vaccine carrier induces long-lasting antitumor immune response. Molecular Therapy, 24(2), 385–397. https://doi.org/10.1038/mt.2015.215

Garu, A., Moku, G., Gulla, S. K., & Chaudhuri, A. (2016b). Genetic Immunization With *In Vivo* Dendritic Cell-targeting Liposomal DNA Vaccine Carrier Induces Long-lasting Antitumor Immune Response. Molecular Therapy, 24(2), 385. https://doi.org/10.1038/MT.2015.215

Ghasemiyeh, P., & Mohammadi-Samani, S. (2018). Solid lipid nanoparticles and nanostructured lipid carriers as novel drug delivery systems: applications, advantages and disadvantages. In Research in Pharmaceutical Sciences (Vol. 13, Issue 4).

Gómez-Aguado, I., Rodríguez-Castejón, J., Vicente-Pascual, M., Rodríguez-Gascón, A., Pozo-Rodríguez, A. del, & Aspiazu, M. Á. S. (2020). Nucleic Acid Delivery by Solid Lipid Nanoparticles Containing Switchable Lipids: Plasmid DNA vs. Messenger RNA. Molecules, 25(24). https://doi.org/10.3390/MOLECULES25245995

Goodnow, C. C., Vinuesa, C. G., Randall, K. L., MacKay, F., & Brink, R. (2010). Control systems and decision making for antibody production. In Nature Immunology (Vol. 11, Issue 8, pp. 681–688). https://doi.org/10.1038/ni.1900

Goyal, K., & Huang, L. (1995). Gene Therapy Using Dc-Chol Liposomes. Journal of Liposome Research, 5(1), 49–60. https://doi.org/10.3109/08982109509039907

Grabowska, A. M., Kircheis, R., Kumari, R., Clarke, P., McKenzie, A., Hughes, J., Mayne, C., Desai, A., Sasso, L., Watson, S. A., & Alexander, C. (2015). Systemic *in vivo* delivery of siRNA to tumours using combination of polyethyleneimine and transferrin-polyethyleneimine conjugates. Biomaterials Science, 3(11), 1439–1448. https://doi.org/10.1039/c5bm00101c

Grosenbaugh, D. A., Leard, A. T., Bergman, P. J., Klein, M. K., Meleo, K., Susaneck, S., Hess, P. R., Jankowski, M. K., Jones, P. D., Leibman, N. F., Johnson, M. H., Kurzman, I. D., & Wolchok, J. D. (2011). Safety and efficacy of a xenogeneic DNA vaccine encoding for human tyrosinase as adjunctive treatment for oral malignant melanoma in dogs following surgical excision of the primary tumor. American Journal of Veterinary Research, 72(12), 1631–1638. https://doi.org/10.2460/AJVR.72.12.1631

Gutiérrez-Martínez, E., Planès, R., Anselmi, G., Reynolds, M., Menezes, S., Adiko, A. C., Saveanu, L., & Guermonprez, P. (2015). Cross-presentation of cell-associated antigens by MHC class I in dendritic cell subsets. In Frontiers in Immunology (Vol. 6, Issue JUL). Frontiers Research Foundation. https://doi.org/10.3389/fimmu.2015.00363

Hanahan, D., & Weinberg, R. A. (2011). Hallmarks of cancer: The next generation. Cell, 144(5), 646–674. https://doi.org/10.1016/J.CELL.2011.02.013/ATTACHMENT/68024D79-3A9C-46C4-930B-640934F11E2E/MMC1.PDF

Hartner, A. M., Li, X., Echeverria-Londono, S., Roth, J., Abbas, K., Auzenbergs, M., de Villiers, M. J., Ferrari, M. J., Fraser, K., Fu, H., Hallett, T., Hinsley, W., Jit, M., Karachaliou, A., Moore, S. M., Nayagam, S., Papadopoulos, T., Perkins, T. A., Portnoy, A., … Gaythorpe, K. A. M. (2024). Estimating the health effects of COVID-19-related immunisation disruptions in 112 countries during 2020–30: a modelling study. The Lancet Global Health, 12(4), e563–e571. https://doi.org/10.1016/S2214-109X(23)00603-4

Hatakeyama, H., Ito, E., Akita, H., Oishi, M., Nagasaki, Y., Futaki, S., & Harashima, H. (2009). A pH-sensitive fusogenic peptide facilitates endosomal escape and greatly enhances the gene silencing of siRNA-containing nanoparticles *in vitro* and *in vivo*. https://doi.org/10.1016/j.jconrel.2009.06.008

He, H., Suryawanshi, H., Morozov, P., us Gay-Mimbrera, J., del Duca, E., Je Kim, H., Kameyama, N., Estrada, Y., Der, E., Krueger, J. G., Ruano, J., Tuschl, T., Guttman-Yassky, E., York, N., ordoba, C., Graphical Abstract, S., Pharma, L., Lilly, E., Tanabe, M., & Biosciences, A. (2020). Single-cell transcriptome analysis of human skin identifies novel fibroblast subpopulation and enrichment of immune subsets in atopic dermatitis. J Allergy Clin Immunol, 145, 1615–1643. https://doi.org/10.1016/j.jaci.2020.01.042

Henriksen-Lacey, M., Christensen, D., Bramwell, V. W., Lindenstrøm, T., Agger, E. M., Andersen, P., & Perrie, Y. (2010a). Liposomal cationic charge and antigen adsorption are important properties for the efficient deposition of antigen at the injection site and ability of the vaccine to induce a CMI response. Journal of Controlled Release : Official Journal of the Controlled Release Society, 145(2), 102–108. https://doi.org/10.1016/J.JCONREL.2010.03.027

Henriksen-Lacey, M., Christensen, D., Bramwell, V. W., Lindenstrøm, T., Agger, E. M., Andersen, P., & Perrie, Y. (2010b). Liposomal cationic charge and antigen adsorption are important properties for the efficient deposition of antigen at the injection site and ability of the vaccine to induce a CMI response. https://doi.org/10.1016/j.jconrel.2010.03.027

Highly Efficient Transfection of Dendritic Cells Derived from Esophageal Squamous Cell Carcinoma Patient: Optimization with Green Fluorescent Protein and Validation with Tumor RNA as a Tool for Immuno-genetherapy. (n.d.). Retrieved January 6, 2020, from http://www.ijbiotech.com/article_7097.html

Hinuma, S., Fujita, K., & Kuroda, S. (2022). Specific Binding and Endocytosis of Liposomes to HEK293T Cells via Myrisoylated Pre-S1 Peptide Bound to Sodium Taurocholate Cotransporting Polypeptide. Vaccines, 10(12). https://doi.org/10.3390/vaccines10122050

Ho, J. K., White, P. J., & Pouton, C. W. (2018). Self-Crosslinking Lipopeptide/DNA/PEGylated Particles: A New Platform for DNA Vaccination Designed for Assembly in Aqueous Solution. Molecular Therapy: Nucleic Acid, 12, 504–517. https://doi.org/10.1016/j.omtn.2018.05.025

Hong, E., & Dobrovolskaia, M. A. (2019). Addressing barriers to effective cancer immunotherapy with nanotechnology: achievements, challenges, and roadmap to the next generation of nanoimmunotherapeutics. In Advanced Drug Delivery Reviews (Vol. 141, pp. 3–22). Elsevier B.V. https://doi.org/10.1016/j.addr.2018.01.005

Huebner, S., Battersby, B. J., Grimm, R., & Cevc, G. (1999). Lipid-DNA Complex Formation: Reorganization and Rupture of Lipid Vesicles in the Presence of DNA As Observed by Cryoelectron Microscopy. https://doi.org/10.1016/S0006-3495(99)77467-9

Inamdar, S., Tylek, T., Thumsi, A., Suresh, A. P., Jaggarapu, M. M. C. S., Halim, M., Mantri, S., Esrafili, A., Ng, N. D., Schmitzer, E., Lintecum, K., de Ávila, C., Fryer, J. D., Xu, Y., Spiller, K. L., & Acharya, A. P. (2023). Biomaterial mediated simultaneous delivery of spermine and alpha ketoglutarate modulate metabolism and innate immune cell phenotype in sepsis mouse models. Biomaterials, 293, 121973. https://doi.org/10.1016/J.BIOMATERIALS.2022.121973

Inoh, Y., Nagai, M., Matsushita, K., Nakanishi, M., & Furuno, T. (2017a). Gene transfection efficiency into dendritic cells is influenced by the size of cationic liposomes/DNA complexes. European Journal of Pharmaceutical Sciences, 102, 230–236. https://doi.org/10.1016/j.ejps.2017.03.023

Inoh, Y., Nagai, M., Matsushita, K., Nakanishi, M., & Furuno, T. (2017b). Gene transfection efficiency into dendritic cells is influenced by the size of cationic liposomes/DNA complexes. European Journal of Pharmaceutical Sciences, 102, 230–236. https://doi.org/10.1016/J.EJPS.2017.03.023

Irvine, A. S., Trinder, P. K. E., Laughton, D. L., Ketteringham, H., McDermott, R. H., Reid, S. C. H., Haines, A. M. R., Amir, A., Husain, R., Doshi, R., Young, L. S., & Mountain, A. (2000a). Efficient nonviral transfection of dendritic cells and their use for *in vivo* immunization. Nature Biotechnology, 18(12), 1273–1278. https://doi.org/10.1038/82383

Irvine, A. S., Trinder, P. K. E., Laughton, D. L., Ketteringham, H., McDermott, R. H., Reid, S. C. H., Haines, A. M. R., Amir, A., Husain, R., Doshi, R., Young, L. S., & Mountain, A. (2000b). Efficient nonviral transfection of dendritic cells and their use for *in vivo* immunization. Nature Biotechnology, 18(12), 1273–1278. https://doi.org/10.1038/82383

Israel, L. L., Lellouche, E., Ostrovsky, S., Yarmiayev, V., Bechor, M., Michaeli, S., & Lellouche, J. P. (2015). Acute *in Vivo* Toxicity Mitigation of PEI-Coated Maghemite Nanoparticles Using Controlled Oxidation and Surface Modifications toward siRNA Delivery. ACS Applied Materials and Interfaces, 7(28), 15240–15255. https://doi.org/10.1021/acsami.5b02743

Issekutz, A. C., & Issekutz, T. B. (2002). The Role of E-Selectin, P-Selectin, and Very Late Activation Antigen-4 in T Lymphocyte Migration to Dermal Inflammation. The Journal of Immunology, 168(4), 1934–1939. https://doi.org/10.4049/jimmunol.168.4.1934

Iversen, T.-G., Skotland, T., & Sandvig, K. (2011). Endocytosis and intracellular transport of nanoparticles: Present knowledge and need for future studies. Nano Today, 6, 176–185. https://doi.org/10.1016/j.nantod.2011.02.003

Jackson, D. G. (2009). Immunological functions of hyaluronan and its receptors in the lymphatics. In Immunological Reviews (Vol. 230, Issue 1, pp. 216–231). https://doi.org/10.1111/j.1600-065X.2009.00803.x

Jackson, L. A., Anderson, E. J., Rouphael, N. G., Roberts, P. C., Makhene, M., Coler, R. N., McCullough, M. P., Chappell, J. D., Denison, M. R., Stevens, L. J.,

Pruijssers, A. J., McDermott, A., Flach, B., Doria-Rose, N. A., Corbett, K. S., Morabito, K. M., O'Dell, S., Schmidt, S. D., Phillip A. Swanson, I., … Beigel, J. H. (2020). An mRNA Vaccine against SARS-CoV-2 — Preliminary Report. The New England Journal of Medicine, 383(20), 1920–1931. https://doi.org/10.1056/NEJMOA2022483

Johnson, D. B., Estrada, M. v., Salgado, R., Sanchez, V., Doxie, D. B., Opalenik, S. R., Vilgelm, A. E., Feld, E., Johnson, A. S., Greenplate, A. R., Sanders, M. E., Lovly, C. M., Frederick, D. T., Kelley, M. C., Richmond, A., Irish, J. M., Shyr, Y., Sullivan, R. J., Puzanov, I., … Balko, J. M. (2016). Melanoma-specific MHC-II expression represents a tumour-autonomous phenotype and predicts response to anti-PD-1/PD-L1 therapy. Nature Communications, 7. https://doi.org/10.1038/ncomms10582

Joon Sig Choi, Eun Jung Lee, Hyung Suk Jang, & Jong Sang Park. (2001a). New Cationic Liposomes for Gene Transfer into Mammalian Cells with High Efficiency and Low Toxicity. Bioconjugate Chemistry, 12(1), 108–113. https://doi.org/10.1021/BC000081O

Joon Sig Choi, Eun Jung Lee, Hyung Suk Jang, & Jong Sang Park. (2001b). New Cationic Liposomes for Gene Transfer into Mammalian Cells with High Efficiency and Low Toxicity. Bioconjugate Chemistry, 12(1), 108–113. https://doi.org/10.1021/BC000081O

Joon Sig Choi, Eun Jung Lee, Hyung Suk Jang, & Jong Sang Park. (2001c). New Cationic Liposomes for Gene Transfer into Mammalian Cells with High Efficiency and Low Toxicity. Bioconjugate Chemistry, 12(1), 108–113. https://doi.org/10.1021/BC000081O

Joseph, A., Itskovitz-Cooper, N., Samira, S., Flasterstein, O., Eliyahu, H., Simberg, D., Goldwaser, I., Barenholz, Y., & Kedar, E. (2006). A new intranasal influenza vaccine based on a novel polycationic lipid—ceramide carbamoyl-spermine (CCS): I. Immunogenicity and efficacy studies in mice. Vaccine, 24(18), 3990–4006. https://doi.org/10.1016/J.VACCINE.2005.12.017

Ju, J., Huan, M. L., Wan, N., Qiu, H., Zhou, S. Y., & Zhang, B. le. (2015). Novel cholesterol-based cationic lipids as transfecting agents of DNA for efficient gene delivery. International Journal of Molecular Sciences, 16(3), 5666–5681. https://doi.org/10.3390/ijms16035666

Kambayashi, T., Allenspach, E. J., Chang, J. T., Zou, T., Shoag, J. E., Reiner, S. L., Caton, A. J., & Koretzky, G. A. (2009). Inducible MHC Class II Expression by Mast Cells Supports Effector and Regulatory T Cell Activation. The Journal of Immunology, 182(8), 4686–4695. https://doi.org/10.4049/jimmunol.0803180

Kawakami, S., Sato, A., Nishikawa, M., Yamashita, F., & Hashida, M. (2000). Mannose receptor-mediated gene transfer into macrophages using novel mannosylated cationic liposomes. Gene Therapy 2000 7:4, 7(4), 292–299. https://doi.org/10.1038/sj.gt.3301089

Ke, L., Cai, P., Wu, Y., & Chen, X. (2020). Polymeric Nonviral Gene Delivery Systems for Cancer Immunotherapy. Advanced Therapeutics, 3(6). https://doi.org/10.1002/adtp.201900213

Ke, X., Howard, G. P., Tang, H., Cheng, B., Saung, M. T., Santos, J. L., & Mao, H. Q. (2019). Physical and chemical profiles of nanoparticles for lymphatic

targeting. In Advanced Drug Delivery Reviews (Vols. 151–152, pp. 72–93). Elsevier B.V. https://doi.org/10.1016/j.addr.2019.09.005

Kearns, M. D., Patel, Y. N., & Savva, M. (2010). Physicochemical characteristics associated with transfection of cationic cholesterol-based gene delivery vectors in the presence of DOPE. Chemistry and Physics of Lipids, 163, 755–764. https://doi.org/10.1016/j.chemphyslip.2010.08.001

Keller, M., Jorgensen, M. R., Perouzel, E., & Miller, A. D. (2003). Thermodynamic aspects and biological profile of CDAN/DOPE and DC-Chol/DOPE lipoplexes. Biochemistry, 42(20), 6067–6077. https://doi.org/10.1021/BI0274219

Kelly, C., Jefferies, C., & Cryan, S.-A. (2011). Targeted Liposomal Drug Delivery to Monocytes and Macrophages. Journal of Drug Delivery, 2011, 1–11. https://doi.org/10.1155/2011/727241

Khalid, K., & Poh, C. L. (2023). The development of DNA vaccines against SARS-CoV-2. In Advances in Medical Sciences (Vol. 68, Issue 2, pp. 213–226). Medical University of Bialystok. https://doi.org/10.1016/j.advms.2023.05.003

Khalil, I. A., Kogure, K., Akita, H., & Harashima, H. (2006). Uptake pathways and subsequent intracellular trafficking in nonviral gene delivery. In Pharmacological Reviews (Vol. 58, Issue 1, pp. 32–45). https://doi.org/10.1124/pr.58.1.8

Khobragade, A., Bhate, S., Ramaiah, V., Deshpande, S., Giri, K., Phophle, H., Supe, P., Godara, I., Revanna, R., Nagarkar, R., Sanmukhani, J., Dey, A., Rajanathan, T. M. C., Kansagra, K., & Koradia, P. (2022). Efficacy, safety, and immunogenicity of the DNA SARS-CoV-2 vaccine (ZyCoV-D): the interim efficacy results of a phase 3, randomised, double-blind, placebo-controlled study in India. The Lancet, 399(10332), 1313–1321. https://doi.org/10.1016/S0140-6736(22)00151-9

Khosravi-Maharlooei, M., Pakyari, M., Jalili, R. B., Salimi-Elizei, S., Lai, J. C. Y., Poormasjedi-Meibod, M., Kilani, R. T., Dutz, J., & Ghahary, A. (2016). Tolerogenic effect of mouse fibroblasts on dendritic cells. Immunology, 148(1), 22–33. https://doi.org/10.1111/IMM.12584

Kis-Toth, K., Szanto, A., Thai, T.-H., & Tsokos, G. C. (2011). Cytosolic DNA-Activated Human Dendritic Cells Are Potent Activators of the Adaptive Immune Response. The Journal of Immunology, 187(3), 1222–1234. https://doi.org/10.4049/jimmunol.1100469

Klicznik, M. M., Szenes-Nagy, A. B., Campbell, D. J., & Gratz, I. K. (2018). Taking the lead-how keratinocytes orchestrate skin T cell immunity. https://doi.org/10.1016/j.imlet.2018.06.009

Kolašinac, R., Kleusch, C., Braun, T., Merkel, R., & Csiszár, A. (2018). Deciphering the functional composition of fusogenic liposomes. International Journal of Molecular Sciences, 19(2). https://doi.org/10.3390/ijms19020346

Košmrlj, A., Jha, A. K., Huseby, E. S., Kardar, M., & Chakraborty, A. K. (2008). How the thymus designs antigen-specific and self-tolerant T cell receptor

sequences. Proceedings of the National Academy of Sciences of the United States of America, 105(43), 16671–16676. https://doi.org/10.1073/PNAS.0808081105/SUPPL_FILE/0808081105SI.PDF

Kulkarni, J. A., Layne Myhre, J., Chen, S., Yi Tam, Y. C., Danescu, A., Richman, J. M., & Cullis, P. R. (2016). Design of lipid nanoparticles for *in vitro* and *in vivo* delivery of plasmid DNA. https://doi.org/10.1016/j.nano.2016.12.014

Kumar, A., Wonganan, P., Sandoval, M. A., Li, X., Zhu, S., & Cui, Z. (2012). Microneedle-mediated transcutaneous immunization with plasmid DNA coated on cationic PLGA nanoparticles. https://doi.org/10.1016/j.jconrel.2012.08.011

Kumbhari, A., Egelston, C. A., Lee, P. P., & Kim, P. S. (2020). Mature Dendritic Cells May Promote High-Avidity Tuning of Vaccine T Cell Responses. Frontiers in Immunology, 11. https://doi.org/10.3389/fimmu.2020.584680

Lallow, E. O., Jhumur, N. C., Ahmed, I., Kudchodkar, S. B., Roberts, C. C., Jeong, M., Melnik, J. M., Park, S. H., Muthumani, K., Shan, J. W., Zahn, J. D., Shreiber, D. I., Singer, J. P., Park, Y. K., Maslow, J. N., & Lin, H. (2021). Novel suction-based *in vivo* cutaneous DNA transfection platform. Science Advances, 7(45), 611. https://doi.org/10.1126/SCIADV.ABJ0611/SUPPL_FILE/SCIADV.ABJ0611_MOVIE_S1.ZIP

Lane, P., Traunecker, A., Hubele, S., Inui, S., Lanzavecchia, A., & Gray, D. (1992). Activated human T cells express a ligand for the human B cell-

associated antigen CD40 which participates in T cell-dependent activation of B lymphocytes. European Journal of Immunology, 22(10), 2573–2578. https://doi.org/10.1002/EJI.1830221016

Lane, R. S., Femel, J., Breazeale, A. P., Loo, C. P., Thibault, G., Kaempf, A., Mori, M., Tsujikawa, T., Chang, Y. H., & Lund, A. W. (2018). IFNγ-activated dermal lymphatic vessels inhibit cytotoxic T cells in melanoma and inflamed skin. J. Exp. Med, 215, 3057–3074. https://doi.org/10.1084/jem.20180654

Layek, B., Lipp, L., & Singh, J. (2015). APC targeted micelle for enhanced intradermal delivery of hepatitis B DNA vaccine. Journal of Controlled Release, 207, 143–153. https://doi.org/10.1016/J.JCONREL.2015.04.014

Li, M., Yang, L., Wang, C., Cui, M., Wen, Z., Liao, Z., Han, Z., Zhao, Y., Lang, B., Chen, H., Qian, J., Shu, Y., Zeng, X., & Sun, C. (2023). Rapid Induction of Long-Lasting Systemic and Mucosal Immunity via Thermostable Microneedle-Mediated Chitosan Oligosaccharide-Encapsulated DNA Nanoparticles. ACS Nano, 17(23), 24200–24217. https://doi.org/10.1021/acsnano.3c09521

Li, Z., Wang, J., O'Hagan, M. P., Huang, F., Xia, F., & Willner, I. (2023). Dynamic Fusion of Nucleic Acid Functionalized Nano-/Micro-Cell-Like Containments: From Basic Concepts to Applications. ACS Nano, 17(16), 15308–15327. https://doi.org/10.1021/ACSNANO.3C04415

Li, Z., Zhang, Y., Zhu, D., Li, S., Yu, X., Zhao, Y., Ouyang, X., Xie, Z., & Li, L. (2017). Transporting carriers for intracellular targeting delivery via non-

endocytic uptake pathways. In Drug Delivery (Vol. 24, pp. 45–55). Taylor and Francis Ltd. https://doi.org/10.1080/10717544.2017.1391889

Liao, J.-F., Lee, J.-C., Lin, C.-K., Wei, K.-C., Chen, P.-Y., & Yang, H.-W. (2017). Self-Assembly DNA Polyplex Vaccine inside Dissolving Microneedles for High-Potency Intradermal Vaccination. Theranostics, 7, 10. https://doi.org/10.7150/thno.19894

Lin, A. J., Slack, N. L., Ahmad, A., Koltover, I., George, C. X., Samuel, C. E., & Safinya, C. R. (2000). Structure and structure-function studies of lipid/plasmid DNA complexes. Journal of Drug Targeting, 8(1), 13–27. https://doi.org/10.3109/10611860009009206

Liu, B., Li, A., Xu, J., & Cui, Y. (2022). Single-Cell Transcriptional Analysis Deciphers the Inflammatory Response of Skin-Resident Stromal Cells. In Frontiers in Surgery (Vol. 9). Frontiers Media S.A. https://doi.org/10.3389/fsurg.2022.935107

Liu, C., Zhang, L., Zhu, W., Guo, R., Sun, H., Chen, X., & Deng, N. (n.d.). Barriers and Strategies of Cationic Liposomes for Cancer Gene Therapy. https://doi.org/10.1016/j.omtm.2020.07.015

Liu, M. A. (2019). A Comparison of Plasmid DNA and mRNA as Vaccine Technologies. Vaccines, 7(2). https://doi.org/10.3390/VACCINES7020037

Lopez, S., Gomez, E., Torres, M., Pozo, D., Fernandez, T., Ariza, A., Sanz, M., Blanca, M., and Mayorga, C. (2015). Betalactam antibiotics affect human dendritic cells maturation through MAPK/NFkB systems. Role in allergic

reactions to drugs. Toxicology and Applied Pharmacology 288 (3) 289-299. https://doi.org/10.1016/j.taap.2015.08.001

Lorenz, C., Fotin-Mleczek, M., Roth, G., Becker, C., Dam, T. C., Verdurmen, W. P. R., Brock, R., Probst, J., & Schlake, T. (2011). Protein expression from exogenous mRNA: Uptake by receptor-mediated endocytosis and trafficking via the lysosomal pathway. RNA Biology, 8(4). https://doi.org/10.4161/rna.8.4.15394

Lu, B., Lim, J. M., Yu, B., Song, S., Neeli, P., Sobhani, N., K, P., Bonam, S. R., Kurapati, R., Zheng, J., & Chai, D. (2024). The next-generation DNA vaccine platforms and delivery systems: advances, challenges and prospects. Frontiers in Immunology, 15, 1332939. https://doi.org/10.3389/FIMMU.2024.1332939/BIBTEX

Luiz, M. T., Dutra, J. A. P., Tofani, L. B., de Araújo, J. T. C., di Filippo, L. D., Marchetti, J. M., & Chorilli, M. (2022). Targeted Liposomes: A Nonviral Gene Delivery System for Cancer Therapy. In Pharmaceutics (Vol. 14, Issue 4). MDPI. https://doi.org/10.3390/pharmaceutics14040821

Lund, A. W., Medler, T. R., Leachman, S. A., & Coussens, L. M. (n.d.). Lymphatic Vessels, Infl ammation, and Immunity in Skin Cancer. https://doi.org/10.1158/2159-8290.CD-15-0023

Maitani, Y., Igarashi, S., Sato, M., & Hattori, Y. (2007). Cationic liposome (DC-Chol/DOPE = 1:2) and a modified ethanol injection method to prepare liposomes, increased gene expression. International Journal of Pharmaceutics, 342, 33–39. https://doi.org/10.1016/j.ijpharm.2007.04.035

Mao, S., Sun, W., & Kissel, T. (2009). Chitosan-based formulations for delivery of DNA and siRNA ☆. Advanced Drug Delivery Reviews, 62, 12–27. https://doi.org/10.1016/j.addr.2009.08.004

Marani, M., Katul, G. G., Pan, W. K., & Parolari, A. J. (2021). Intensity and frequency of extreme novel epidemics. PNAS. https://doi.org/10.1073/pnas.2105482118/-/DCSupplemental

Margolis, N., Markovits, E., & Markel, G. (2019). Reprogramming lymphocytes for the treatment of melanoma: From biology to therapy. In Advanced Drug Delivery Reviews (Vol. 141, pp. 104–124). Elsevier B.V. https://doi.org/10.1016/j.addr.2019.06.005

Markov, O. O., Mironova, N. L., Maslov, M. A., Petukhov, I. A., Morozova, N. G., Vlassov, V. v., & Zenkova, M. A. (2012). Novel cationic liposomes provide highly efficient delivery of DNA and RNA into dendritic cell progenitors and their immature offsets. Journal of Controlled Release, 160(2), 200–210. https://doi.org/10.1016/J.JCONREL.2011.11.034

Mccaffrey, J., Mccrudden, C. M., Ali, A. A., Massey, A. S., Mcbride, J. W., Mccrudden, M. T. C., Vicente-Perez, E. M., Coulter, J. A., Robson, T., Donnelly, R. F., & Mccarthy, H. O. (2016). Transcending epithelial and intracellular biological barriers; a prototype DNA delivery device. https://doi.org/10.1016/j.jconrel.2016.02.023

McGill, A. R., Markoutsa, E., Mayilsamy, K., Green, R., Sivakumar, K., Mohapatra, S., & Mohapatra, S. S. (2023). Acetate-encapsulated Linolenic

Acid Liposomes Reduce SARS-CoV-2 and RSV Infection. Viruses, 15(7), 1429. https://doi.org/10.3390/V15071429/S1

Mohammed, J., Beura, L. K., Bobr, A., Astry, B., Chicoine, B., Kashem, S. W., Welty, N. E., Igyártó, B. Z., Wijeyesinghe, S., Thompson, E. A., Matte, C., Bartholin, L., Kaplan, A., Sheppard, D., Bridges, A. G., Shlomchik, W. D., Masopust, D., & Kaplan, D. H. (2016). Stromal cells control the epithelial residence of DCs and memory T cells by regulated activation of TGF-β. Nature Immunology, 17(4), 414–421. https://doi.org/10.1038/ni.3396

Mónica Bravo-Anaya, L., Gricelda Fernández-Solís, K., Rosselgong, J., Luz, J., Nano-Rodríguez, E., Carvajal, F., & Rinaudo, M. (2019). Chitosan-DNA polyelectrolyte complex: Influence of chitosan characteristics and mechanism of complex formation. https://doi.org/10.1016/j.ijbiomac.2019.01.008

Montes-Gómez, A. E., García-Cordero, J., Marcial-Juárez, E., Shrivastava, G., Visoso-Carvajal, G., Juárez-Delgado, F. J., Flores-Romo, L., Sanchez-Torres, M. C., Santos-Argumedo, L., Bustos-Arriaga, J., & Cedillo-Barrón, L. (2020a). Crosstalk Between Dermal Fibroblasts and Dendritic Cells During Dengue Virus Infection. Frontiers in Immunology, 11, 538240. https://doi.org/10.3389/FIMMU.2020.538240/BIBTEX

Montes-Gómez, A. E., García-Cordero, J., Marcial-Juárez, E., Shrivastava, G., Visoso-Carvajal, G., Juárez-Delgado, F. J., Flores-Romo, L., Sanchez-Torres, M. C., Santos-Argumedo, L., Bustos-Arriaga, J., & Cedillo-Barrón, L. (2020b). Crosstalk Between Dermal Fibroblasts and Dendritic Cells During Dengue Virus Infection. Frontiers in Immunology, 11. https://doi.org/10.3389/fimmu.2020.538240

Morin, S., Simard, M., Rioux, G., Julien, P., & Pouliot, R. (2022). Alpha-Linolenic Acid Modulates T Cell Incorporation in a 3D Tissue-Engineered Psoriatic Skin Model. Cells, 11(9), 1513. https://doi.org/10.3390/CELLS11091513/S1

Mosmann, T. R., & Sad, S. (n.d.). The expanding universe subsets: Thl, Th2 and.

Muñoz-Úbeda, M., Rodríguez-Pulido, A., Nogales, A., Martín-Molina, A., Aicart, E., & Junquera, E. (2010). Effect of lipid composition on the structure and theoretical phase diagrams of DC-Chol/DOPE-DNA lipoplexes. Biomacromolecules, 11(12), 3332–3340. https://doi.org/10.1021/BM1008124/ASSET/IMAGES/LARGE/BM-2010-008124_0007.JPEG

Nam, K., Kim, T., Kim, Y. M., Yang, K., Choe, D., Mensah, L. B., Choi, K. Y., & Roh, Y. H. (2019). Size-controlled synthesis of polymerized DNA nanoparticles for targeted anticancer drug delivery. Chemical Communications, 55(34), 4905–4908. https://doi.org/10.1039/c9cc01442j

Natoli, G., & Ostuni, R. (2019). Adaptation and memory in immune responses. Nature Immunology 2019 20:7, 20(7), 783–792. https://doi.org/10.1038/s41590-019-0399-9

Nguyen, A. v., & Soulika, A. M. (2019). The dynamics of the skin's immune system. In International Journal of Molecular Sciences (Vol. 20, Issue 8). MDPI AG. https://doi.org/10.3390/ijms20081811

Nguyen-Hoai, T., Kobelt, D., Hohn, O., Vu, M. D., Schlag, P. M., Dörken, B., Norley, S., Lipp, M., Walther, W., Pezzutto, A., & Westermann, J. (2012). HER2/neu DNA vaccination by intradermal gene delivery in a mouse tumor model: Gene gun is superior to jet injector in inducing ctl responses and protective immunity. OncoImmunology, 1(9), 1537–1545. https://doi.org/10.4161/ONCI.22563/ASSET/B229F906-A8E5-4F15-869B-164496F2F465/ASSETS/IMAGES/LARGE/KONI_A_10922563_F0005.JPG

Niu, L., Chu, L. Y., Burton, S. A., Hansen, K. J., & Panyam, J. (2018). Intradermal delivery of vaccine nanoparticles using hollow microneedle array generates enhanced and balanced immune response. https://doi.org/10.1016/j.jconrel.2018.12.026

Nitsch, A., Haralambiev, L., Einenkel, R., Muzzio, D., Zygmunt, M., Ekkernkamp, A., Burchardt, M., and Stope, M. (2019). Determination of *In Vitro* Membrane Permeability by Analysis of Intracellular and Extracellular Fluorescein Signals in Renal Cells. In Vivo 33(6) 1767-1771. https://doi.org/10.21873/invivo.11667

Noguchi, M., Sasada, T., & Itoh, K. (2013). Personalized peptide vaccination: A new approach for advanced cancer as therapeutic cancer vaccine. Cancer Immunology, Immunotherapy, 62(5), 919–929. https://doi.org/10.1007/S00262-012-1379-1/TABLES/2

Noris, M., Benigni, A., & Remuzzi, G. (n.d.). The case of complement activation in COVID-19 multiorgan impact. https://doi.org/10.1016/j.kint.2020.05.013

Noval, M. G., Kaczmarek, M. E., Koide, A., Rodriguez-Rodriguez, B. A., Louie, P., Tada, T., Hattori, T., Panchenko, T., Romero, L. A., Teng, K. W., Bazley, A., de Vries, M., Samanovic, M. I., Weiser, J. N., Aifantis, I., Cangiarella, J., Mulligan, M. J., Desvignes, L., Dittmann, M., … Stapleford, K. A. (2021). Antibody isotype diversity against SARS-CoV-2 is associated with differential serum neutralization capacities. Scientific Reports, 11(1). https://doi.org/10.1038/s41598-021-84913-3

Ohue-Kitano, R., Yasuoka, Y., Goto, T., Kitamura, N., Park, S. B., Kishino, S., Kimura, I., Kasubuchi, M., Takahashi, H., Li, Y., Yeh, Y. S., Jheng, H. F., Iwase, M., Tanaka, M., Masuda, S., Inoue, T., Yamakage, H., Kusakabe, T., Tani, F., … Kawada, T. (2018). A-Linolenic acid–derived metabolites from gut lactic acid bacteria induce differentiation of anti-inflammatory M2 macrophages through G protein-coupled receptor 40. FASEB Journal, 32(1), 304–318. https://doi.org/10.1096/FJ.201700273R/-/DC1

Paez-Perez, M., Russell, I. A., Cicuta, P., & di Michele, L. (2022). Modulating membrane fusion through the design of fusogenic DNA circuits and bilayer composition. Soft Matter, 18(37), 7035. https://doi.org/10.1039/D2SM00863G

Palumbo, R. N., Zhong, X., & Wang, C. (2012). Polymer-mediated DNA vaccine delivery via bystander cells requires a proper balance between transfection efficiency and cytotoxicity. Journal of Controlled Release, 157(1), 86–93. https://doi.org/10.1016/J.JCONREL.2011.08.037

Park, S., Matte-Martone, C., Gonzalez, D. G., Lathrop, E. A., May, D. P., Pineda, C. M., Moore, J. L., Boucher, J. D., Marsh, E., Schmitter-Sánchez, A., Cockburn, K., Markova, O., Bellaïche, Y., & Greco, V. (2021). Skin-resident immune cells actively coordinate their distribution with epidermal cells

during homeostasis. Nature Cell Biology, 23(5), 476–484. https://doi.org/10.1038/s41556-021-00670-5

Perche, F., Benvegnu, T., Berchel, M., Lebegue, L., Pichon, C., Jaffrès, P. A., & Midoux, P. (2011). Enhancement of dendritic cells transfection *in vivo* and of vaccination against B16F10 melanoma with mannosylated histidylated lipopolyplexes loaded with tumor antigen messenger RNA. Nanomedicine: Nanotechnology, Biology and Medicine, 7(4), 445–453. https://doi.org/10.1016/J.NANO.2010.12.010

Perrie, Y., McNeil, S., & Vangala, A. (2003). Liposome-mediated DNA immunisation via the subcutaneous route. Journal of Drug Targeting, 11(8–10), 555–563. https://doi.org/10.1080/10611860410001670071

Pielenhofer, J., Sohl, J., Windbergs, M., Langguth, P., & Radsak, M. P. (2020). Current Progress in Particle-Based Systems for Transdermal Vaccine Delivery. Frontiers in Immunology, 11, 266. https://doi.org/10.3389/fimmu.2020.00266

Piipponen, M., Li, D., & Xu Landén, N. (n.d.). Molecular Sciences The Immune Functions of Keratinocytes in Skin Wound Healing. https://doi.org/10.3390/ijms21228790

Pink, D. L., Loruthai, O., Ziolek, R. M., Wasutrasawat, P., Terry, A. E., Lawrence, M. J., & Lorenz, C. D. (2019). On the Structure of Solid Lipid Nanoparticles. Small, 15(45). https://doi.org/10.1002/smll.201903156

Plank, C., Mechtler, K., Szoka, F. C., & Wagner, E. (1996). Activation of the complement system by synthetic DNA complexes: A potential barrier for intravenous gene delivery. Human Gene Therapy, 7(12), 1437–1446. https://doi.org/10.1089/hum.1996.7.12-1437

Polack, F. P., Thomas, S. J., Kitchin, N., Absalon, J., Gurtman, A., Lockhart, S., Perez, J. L., Marc, G. P., Moreira, E. D., Zerbini, C., Bailey, R., Swanson, K. A., Roychoudhury, S., Koury, K., Li, P., Kalina, W. v., Cooper, D., Robert W. Frenck, Jr., Hammitt, L. L., … Gruber, W. C. (2020). Safety and Efficacy of the BNT162b2 mRNA Covid-19 Vaccine. The New England Journal of Medicine, 383(27), 2603–2615. https://doi.org/10.1056/NEJMOA2034577

Pozzi, D., Amenitsch, H., Caminiti, R., & Caracciolo, G. (2006). How lipid hydration and temperature affect the structure of DC-Chol-DOPE/DNA lipoplexes. https://doi.org/10.1016/j.cplett.2006.02.106

Pradeu, T., & Cooper, E. L. (2012). The danger theory: 20 years later. Frontiers in Immunology, 3(SEP), 31824. https://doi.org/10.3389/FIMMU.2012.00287/BIBTEX

Priddle, H., Grabowska, A., Morris, T., Clarke, P. A., McKenzie, A. J., Sottile, V., Denning, C., Young, L., & Watson, S. (2009). Bioluminescence imaging of human embryonic stem cells transplanted *in vivo* in murine and chick models. Cloning and Stem Cells, 11(2), 259–267. https://doi.org/10.1089/clo.2008.0056

Proietti, E., Rossini, S., Grohmann, U., & Mondanelli, G. (2020a). Polyamines and Kynurenines at the Intersection of Immune Modulation.

Trends in Immunology, 41(11), 1037–1050.
https://doi.org/10.1016/J.IT.2020.09.007

Proietti, E., Rossini, S., Grohmann, U., & Mondanelli, G. (2020b). Polyamines and Kynurenines at the Intersection of Immune Modulation. Trends in Immunology, 41, 1037–1050.
https://doi.org/10.1016/j.it.2020.09.007

Qin, Y., Rouatbi, N., Wang, J. T.-W., Baker, R., Spicer, J., Walters, A. A., & Al-Jamal, K. T. (2024). Plasmid DNA ionisable lipid nanoparticles as non-inert carriers and potent immune activators for cancer immunotherapy. Journal of Controlled Release, 369, 251–265.
https://doi.org/10.1016/j.jconrel.2024.03.018

Qiu, Y., Guo, L., Zhang, S., Xu, B., Gao, Y., Hu, Y., Hou, J., Bai, B., Shen, H., & Mao, P. (2016). DNA-based vaccination against hepatitis B virus using dissolving microneedle arrays adjuvanted by cationic liposomes and CpG ODN. Drug Delivery, 23(7), 2391–2398.
https://doi.org/10.3109/10717544.2014.992497

Rädler, J. O., Koltover, I., Salditt, T., & Safinya, C. R. (1997). Structure of DNA-Cationic Liposome Complexes: DNA Intercalation in Multilamellar Membranes in Distinct Interhelical Packing Regimes. In New Series (Vol. 275, Issue 5301).

Ramamoorth, M., & Narvekar, A. (2015). Non viral vectors in gene therapy - An overview. In Journal of Clinical and Diagnostic Research (Vol. 9, Issue 1, pp. GE01–GE06). Journal of Clinical and Diagnostic Research.
https://doi.org/10.7860/JCDR/2015/10443.5394

Ramezani, M., Khoshhamdam, M., Dehshahri, A., & Malaekeh-Nikouei, B. (2009a). The influence of size, lipid composition and bilayer fluidity of cationic liposomes on the transfection efficiency of nanolipoplexes. Colloids and Surfaces B: Biointerfaces, 72(1), 1–5. https://doi.org/10.1016/j.colsurfb.2009.03.018

Ramezani, M., Khoshhamdam, M., Dehshahri, A., & Malaekeh-Nikouei, B. (2009b). The influence of size, lipid composition and bilayer fluidity of cationic liposomes on the transfection efficiency of nanolipoplexes. Colloids and Surfaces B: Biointerfaces, 72, 1–5. https://doi.org/10.1016/j.colsurfb.2009.03.018

Randolph, G. J., Angeli, V., & Swartz, M. A. (2005). Dendritic-cell trafficking to lymph nodes through lymphatic vessels. In Nature Reviews Immunology (Vol. 5, Issue 8, pp. 617–628). https://doi.org/10.1038/nri1670

Raphael, I., Nalawade, S., Eagar, T. N., & Forsthuber, T. G. (2014). T cell subsets and their signature cytokines in autoimmune and inflammatory diseases. https://doi.org/10.1016/j.cyto.2014.09.011

Reddy, S. T., van der Vlies, A. J., Simeoni, E., Angeli, V., Randolph, G. J., O'Neil, C. P., Lee, L. K., Swartz, M. A., & Hubbell, J. A. (2007). Exploiting lymphatic transport and complement activation in nanoparticle vaccines. Nature Biotechnology, 25(10), 1159–1164. https://doi.org/10.1038/nbt1332

Redondo-Morata, L., Giannotti, M. I., & Sanz, F. (2012). Influence of cholesterol on the phase transition of lipid bilayers: A temperature-

controlled force spectroscopy study. Langmuir, 28(35), 12851–12860. https://doi.org/10.1021/LA302620T

Ren, Y., Jiang, X., Pan, D., & Mao, H.-Q. (n.d.). Charge Density and Molecular Weight of Polyphosphoramidate Gene Carrier Are Key Parameters Influencing Its DNA Compaction Ability and Transfection Efficiency. https://doi.org/10.1021/bm1009574

Richard, I., Thibault, M., de Crescenzo, G., Buschmann, M. D., & Lavertu, M. (2013). Ionization Behavior of Chitosan and Chitosan–DNA Polyplexes Indicate That Chitosan Has a Similar Capability to Induce a Proton-Sponge Effect as PEI. Biomacromolecules, 14(6), 1732–1740. https://doi.org/10.1021/bm4000713

Richmond, J. M., Bangari, D. S., Essien, K. I., Currimbhoy, S. D., Groom, J. R., Pandya, A. G., Youd, M. E., Luster, A. D., & Harris, J. E. (2017). Keratinocyte-Derived Chemokines Orchestrate T-Cell Positioning in the Epidermis during Vitiligo and May Serve as Biomarkers of Disease. Journal of Investigative Dermatology, 350–358. https://doi.org/10.1016/j.jid.2016.09.016

Rinaldi, E., & Baggi, F. (2018). LYVE-1 is “on stage” now: an emerging player in dendritic cell docking to lymphatic endothelial cells. Cellular and Molecular Immunology, 15(7), 663–665. https://doi.org/10.1038/cmi.2017.126

Roche, P. A., & Furuta, K. (2015). The ins and outs of MHC class II-mediated antigen processing and presentation. In Nature Reviews

Immunology (Vol. 15, Issue 4, pp. 203–216). Nature Publishing Group. https://doi.org/10.1038/nri3818

Rodríguez-Pulido, A., Ortega, F., Llorca, O., Aicart, E., & Junquera, E. (2008). A Physicochemical Characterization of the Interaction between DC-Chol/DOPE Cationic Liposomes and DNA. Journal of Physical Chemistry B, 112(39), 12555–12565. https://doi.org/10.1021/JP804066T

Rodway, L. A., Pauls, S. D., Pascoe, C. D., Aukema, H. M., Taylor, C. G., & Zahradka, P. (2023). Distinct effects of α-linolenic acid and docosahexaenoic acid on the expression of genes related to cholesterol metabolism and the response to infection in THP-1 monocytes and immune cells of obese humans. Biomedicine & Pharmacotherapy, 159, 114167. https://doi.org/10.1016/J.BIOPHA.2022.114167

Roth, G., Picece V., Ou, B., Luo, W., Pulendran, B., and Appel, E. (2022). Designing spatial and temporal control of vaccine responses. Nature Reviews Materials 7, 174-195. https://doi.org/10.1038/s41578-021-00372-2

Rotte, A. (2019). Combination of CTLA-4 and PD-1 blockers for treatment of cancer. Journal of Experimental and Clinical Cancer Research, 38(1), 1-12. BioMed Central Ltd. https://doi.org/10.1186/s13046-019-1259-z

Rovere, P., Vallinoto, C., Bondanza, A., Crosti, M. C., Rescigno, M., Ricciardi-Castagnoli, P., Rugarli, C., & Manfredi, A. A. (1998). Cutting Edge: Bystander Apoptosis Triggers Dendritic Cell Maturation and Antigen-Presenting Function. The Journal of Immunology, 161(9), 4467–4471. https://doi.org/10.4049/jimmunol.161.9.4467

Rughetti, A., Biffoni, M., Sabbatucci, M., Rahimi, H., Pellicciotta, I., Fattorossi, A., Pierelli, L., Scambia, G., Lavitrano, M., Frati, L., & Nuti, M. (2000). Transfected human dendritic cells to induce antitumor immunity. Gene Therapy, 7(17), 1458–1466. https://doi.org/10.1038/sj.gt.3301266

Saad, S., Hasan, N., Siddiqui, L., Beg, S., Ali, A., Gupta, A., Jain, G. K., & Ahmad, F. J. (2023). Novel gamma linoleic acid encased in situ lipogel for augmented anti-tumor efficacy against solid tumor: *In vitro* and *in vivo* evaluation. Journal of Drug Delivery Science and Technology, 87, 104768. https://doi.org/10.1016/J.JDDST.2023.104768

Saalbach, A., Klein, C., Sleeman, J., Sack, U., Kauer, F., Gebhardt, C., Averbeck, M., Anderegg, U., & Simon, J. C. (2007). Dermal Fibroblasts Induce Maturation of Dendritic Cells. The Journal of Immunology, 178(8), 4966–4974. https://doi.org/10.4049/jimmunol.178.8.4966

Sabado, R. L., Babcock, E., Kavanagh, D. G., Tjomsland, V., Walker, B. D., Lifson, J. D., Bhardwaj, N., & Larsson, M. (2007). Pathways utilized by dendritic cells for binding, uptake, processing and presentation of antigens derived from HIV-1. European Journal of Immunology, 37(7), 1752–1763. https://doi.org/10.1002/eji.200636981

Saremi, S. S., Shahryari, M., Ghoorchian, R., Eshaghian, H., Jalali, S. A., Nikpoor, A. R., Jafari, M. R., & Badiee, A. (2018). The role of nanoliposome bilayer composition containing soluble leishmania antigen on maturation and activation of dendritic cells. Iranian Journal of Basic Medical Sciences, 21(5), 536–545. https://doi.org/10.22038/IJBMS.2018.25976.6391

Schnyder, J. L., Garcia Garrido, H. M., de Pijper, C. A., Daams, J. G., Stijnis, C., Goorhuis, A., & Grobusch, M. P. (2021). Comparison of equivalent fractional vaccine doses delivered by intradermal and intramuscular or subcutaneous routes: A systematic review. https://doi.org/10.1016/j.tmaid.2021.102007

Segura, E., Albiston, A. L., Wicks, I. P., Yeen Chai, S., & Villadangos, J. A. (2009). Different cross-presentation pathways in steady-state and inflammatory dendritic cells. In PNAS December 1 (Vol. 106). www.pnas.orgcgidoi10.1073pnas.0910295106

Semple, S. C., Harasym, T. O., Clow, K. A., Ansell, S. M., Klimuk, S. K., & Hope, M. J. (2005). Immunogenicity and Rapid Blood Clearance of Liposomes Containing Polyethylene Glycol-Lipid Conjugates and Nucleic Acid. Journal of Pharmacology and Experimental Therapeutics, 312(3), 1020–1026. https://doi.org/10.1124/JPET.104.078113

Seok, H., Noh, J. Y., Lee, Y., Kim, S. J., Song, C. S., & Kim, Y. C. (2017). Effective humoral immune response from a H1N1 DNA vaccine delivered to the skin by microneedles coated with PLGA-based cationic nanoparticles. https://doi.org/10.1016/j.jconrel.2017.04.027

Seok, H. Y., Noh, J. Y., Lee, D. Y., Kim, S. J., Song, C. S., & Kim, Y. C. (2017). Effective humoral immune response from a H1N1 DNA vaccine delivered to the skin by microneedles coated with PLGA-based cationic nanoparticles. Journal of Controlled Release, 265, 66–74. https://doi.org/10.1016/j.jconrel.2017.04.027

Sharma, D., Arora, S., Singh, J., & Layek, B. (2021). A review of the tortuous path of nonviral gene delivery and recent progress. International Journal of Biological Macromolecules, 183, 2055–2073. https://doi.org/10.1016/j.ijbiomac.2021.05.192

Shrestha, P., & Stoeber, B. (2018). Fluid absorption by skin tissue during intradermal injections through hollow microneedles. Scientific Reports, 8(1). https://doi.org/10.1038/s41598-018-32026-9

Siders, W. M., Vergillis, K., Johnson, C., Scheule, R. K., & Kaplan, J. M. (2002). Tumor Treatment with Complexes of Cationic Lipid and Noncoding Plasmid DNA Results in the Induction of Cytotoxic T Cells and Systemic Tumor Elimination. YMTHE, 6(4), 519–527. https://doi.org/10.1006/mthe.2002.0697

Simões, S., Filipe, A., Faneca, H., Mano, M., Penacho, N., Düzgünes, N., & de Lima, M. P. (2005). Cationic liposomes for gene delivery. In Expert Opinion on Drug Delivery (Vol. 2, Issue 2, pp. 237–254). https://doi.org/10.1517/17425247.2.2.237

Smith, S. J., Rahman, C. v., Clarke, P. A., Ritchie, A. A., Gould, T. W., Ward, J. H., Shakesheff, K. M., Grundy, R. G., & Rahman, R. (2014). Surgical delivery of drug releasing poly(lactic-co-glycolic acid)/poly(ethylene glycol) paste with *in vivo* effects against glioblastoma. Annals of the Royal College of Surgeons of England, 96(7), 495–501. https://doi.org/10.1308/003588414X13946184903568

Smith, T. R. F., Patel, A., Ramos, S., Elwood, D., Zhu, X., Yan, J., Gary, E. N., Walker, S. N., Schultheis, K., Purwar, M., Xu, Z., Walters, J., Bhojnagarwala, P.,

Yang, M., Chokkalingam, N., Pezzoli, P., Parzych, E., Reuschel, E. L., Doan, A., … Broderick, K. E. (2020). Immunogenicity of a DNA vaccine candidate for COVID-19. Nature Communications, 11(1). https://doi.org/10.1038/s41467-020-16505-0

Smith, T. R., Schultheis, K., Kiosses, W. B., Amante, D. H., Mendoza, J. M., Stone, J. C., McCoy, J. R., Sardesai, N. Y., & Broderick, K. E. (2014). DNA vaccination strategy targets epidermal dendritic cells, initiating their migration and induction of a host immune response. Molecular Therapy Methods and Clinical Development, 1, 14054. https://doi.org/10.1038/mtm.2014.54

So, R. B., Li, G., Brentville, V., Daly, J. M., & Dixon, J. E. (2024). Combined biolistic and cell penetrating peptide delivery for the development of scalable intradermal DNA vaccines. Journal of Controlled Release, 367, 209–222. https://doi.org/10.1016/j.jconrel.2024.01.031

Soema, P. C., Willems, G. J., Jiskoot, W., Amorij, J. P., & Kersten, G. F. (2015). Predicting the influence of liposomal lipid composition on liposome size, zeta potential and liposome-induced dendritic cell maturation using a design of experiments approach. European Journal of Pharmaceutics and Biopharmaceutics, 94, 427–435. https://doi.org/10.1016/j.ejpb.2015.06.026

Sonoda, J., Mizoguchi, I., Inoue, S., Watanabe, A., Sekine, A., Yamagishi, M., Miyakawa, S., Yamaguchi, N., Horio, E., Katahira, Y., Hasegawa, H., Hasegawa, T., Yamashita, K., & Yoshimoto, T. (2023). A Promising Needle-Free Pyro-Drive Jet Injector for Augmentation of Immunity by Intradermal Injection as a Physical Adjuvant. In International Journal of Molecular

Sciences (Vol. 24, Issue 10). Multidisciplinary Digital Publishing Institute (MDPI). https://doi.org/10.3390/ijms24109094

Sousa, D. A., Gaspar, R., Ferreira, C. J. O., Baltazar, F., Rodrigues, L. R., & Silva, B. F. B. (2022). *In Vitro* CRISPR/Cas9 Transfection and Gene-Editing Mediated by Multivalent Cationic Liposome–DNA Complexes. Pharmaceutics, 14(5). https://doi.org/10.3390/pharmaceutics14051087

Stepanenko, A. A., & Heng, H. H. (2017). Transient and stable vector transfection: Pitfalls, off-target effects, artifacts. In Mutation Research - Reviews in Mutation Research (Vol. 773, pp. 91–103). Elsevier B.V. https://doi.org/10.1016/j.mrrev.2017.05.002

Stewart, L., Manvell, M., Hillery, E., Etheridge, C. J., Cooper, R. G., Stark, H., Van-Heel, M., Preuss, M., Alton, E. W. F. W., & Miller, A. D. (2001). Physico-chemical analysis of cationic liposome–DNA complexes (lipoplexes) with respect to *in vitro* and *in vivo* gene delivery efficiency. Journal of the Chemical Society, Perkin Transactions 2, 4, 624–632. https://doi.org/10.1039/B005992G

Stunova, A., & Vistejnova, L. (2018). Dermal fibroblasts-A heterogeneous population with regulatory function in wound healing. https://doi.org/10.1016/j.cytogfr.2018.01.003

Sun, D., & Lu, Z. R. (2023). Structure and Function of Cationic and Ionizable Lipids for Nucleic Acid Delivery. In Pharmaceutical Research (Vol. 40, Issue 1, pp. 27–46). Springer. https://doi.org/10.1007/s11095-022-03460-2

Sun, J., Niu, K., Fu, H., Li, H., Li, Y., & Yang, W. (2016). Autoimmune regulator expression in DC2.4 cells regulates the NF-κB signaling and cytokine expression of the toll-like receptor 3 pathway. International Journal of Molecular Sciences, 17(12). https://doi.org/10.3390/ijms17122002

Sun, X., Zeng, L., & Huang, Y. (2019). Transcutaneous delivery of DNA/mRNA for cancer therapeutic vaccination. Journal of Gene Medicine, 21(7). https://doi.org/10.1002/JGM.3089

Tada, R., Hidaka, A., Iwase, N., Takahashi, S., Yamakita, Y., Iwata, T., Muto, S., Sato, E., Takayama, N., Honjo, E., Kiyono, H., Kunisawa, J., Aramaki, Y., & Boyaka, P. N. (2015). Intranasal Immunization with DOTAP Cationic Liposomes Combined with DC-Cholesterol Induces Potent Antigen-Specific Mucosal and Systemic Immune Responses in Mice. PLOS ONE, 10(10), e0139785. https://doi.org/10.1371/JOURNAL.PONE.0139785

Tamburini, B. A., Burchill, M. A., & Kedl, R. M. (2014). Antigen capture and archiving by lymphatic endothelial cells following vaccination or viral infection. Nature Communications, 5. https://doi.org/10.1038/ncomms4989

Tan, P. H., Beutelspacher, S. C., Wang, Y. H., McClure, M. O., Ritter, M. A., Lombardi, G., & George, A. J. T. (2005). Immunolipoplexes: An efficient, nonviral alternative for transfection of human dendritic cells with potential for clinical vaccination. Molecular Therapy, 11(5), 790–800. https://doi.org/10.1016/j.ymthe.2004.12.009

Tao, P., Mahalingam, M., Marasa, B. S., Zhang, Z., Chopra, A. K., & Rao, V. B. (n.d.). *In vitro* and *in vivo* delivery of genes and proteins using the bacteriophage T4 DNA packaging machine. https://doi.org/10.1073/pnas.1300867110

ten Broeke, T., Wubbolts, R., & Stoorvogel, W. (2013). MHC class II antigen presentation by dendritic cells regulated through endosomal sorting. Cold Spring Harbor Perspectives in Biology, 5(12). https://doi.org/10.1101/cshperspect.a016873

Terry, T. L., Givens, B. E., Adamcakova-Dodd, A., Thorne, P. S., Rodgers, V. G. J., & Salem, A. K. (2021). Encapsulating Polyethyleneimine-DNA Nanoplexes into PEGylated Biodegradable Microparticles Increases Transgene Expression *In Vitro* and Reduces Inflammatory Responses *In Vivo*. AAPS PharmSciTech, 22(2). https://doi.org/10.1208/s12249-021-01932-z

Thaiss, C. A., Semmling, V., Franken, L., Wagner, H., & Kurts, C. (2011). Chemokines: A new dendritic cell signal fort cell activation. Frontiers in Immunology, 2(AUG). https://doi.org/10.3389/fimmu.2011.00031

Thamphiwatana, S., Gao, W., Obonyo, M., & Zhang, L. (2014). *In vivo* treatment of Helicobacter pylori infection with liposomal linolenic acid reduces colonization andameliorates inflammation. Proceedings of the National Academy of Sciences of the United States of America, 111(49), 17600–17605. https://doi.org/10.1073/PNAS.1418230111/ASSET/D27AB091-5961-49B8-831A-C87623D79487/ASSETS/GRAPHIC/PNAS.1418230111FIG05.JPEG

Thomas, C. E., Ehrhardt, A., & Kay, M. A. (2003). Progress and problems with the use of viral vectors for gene therapy. In Nature Reviews Genetics (Vol. 4, Issue 5, pp. 346–358). https://doi.org/10.1038/nrg1066

Thongbamrer, C., Roobsoong, W., Sattabongkot, J., Opanasopit, P., & Yingyongnarongkul, B. ek. (2022a). Serum Compatible Spermine-Based Cationic Lipids with Nonidentical Hydrocarbon Tails Mediate High Transfection Efficiency. ChemBioChem, 23(6), e202100672. https://doi.org/10.1002/CBIC.202100672

Thongbamrer, C., Roobsoong, W., Sattabongkot, J., Opanasopit, P., & Yingyongnarongkul, B. ek. (2022b). Serum Compatible Spermine-Based Cationic Lipids with Nonidentical Hydrocarbon Tails Mediate High Transfection Efficiency. ChemBioChem, 23(6), e202100672. https://doi.org/10.1002/CBIC.202100672

Todorova, B., Adam, L., Culina, S., Boisgard, R., Martinon, F., Cosma, A., Ustav, M., Kortulewski, T., Grand, R. le, & Chapon, C. (2017). Electroporation as a vaccine delivery system and a natural adjuvant to intradermal administration of plasmid DNA in macaques. Scientific Reports, 7(1). https://doi.org/10.1038/s41598-017-04547-2

Tom, R., Bisson, L., & Durocher, Y. (2008). Transfection of adherent HEK293-EBNA1 cells in a six-well plate with branched PEI for production of recombinant proteins. Cold Spring Harbor Protocols, 3(3). https://doi.org/10.1101/pdb.prot4978

Tozuka, M., Oka, T., Jounai, N., Egawa, G., Ishii, K. J., Kabashima, K., & Takeshita, F. (n.d.). Efficient antigen delivery to the draining lymph nodes is

a key component in the immunogenic pathway of the intradermal vaccine. https://doi.org/10.1016/j.jdermsci.2015.11.008

Travieso, T., Li, J., Mahesh, S., Mello, J. D. F. R. E., & Blasi, M. (2022). The use of viral vectors in vaccine development. In npj Vaccines (Vol. 7, Issue 1). Nature Research. https://doi.org/10.1038/s41541-022-00503-y

Tresset, G., Cheong, W. C. D., & Lam, Y. M. (2007). Role of multivalent cations in the self-assembly of phospholipid-DNA complexes. Journal of Physical Chemistry B, 111(51), 14233–14238. https://doi.org/10.1021/jp0762830

Tretiakova, D. S., & Vodovozova, E. L. (2022). Liposomes as Adjuvants and Vaccine Delivery Systems. In Biochemistry (Moscow) Supplement Series A: Membrane and Cell Biology (Vol. 16, Issue 1). Pleiades Publishing. https://doi.org/10.1134/S1990747822020076

Trimzi, M. A., Ham, Y.-B., Han, H.-K., & Lee, B.-J. (2021). A Needle-Free Jet Injection System for Controlled Release and Repeated Biopharmaceutical Delivery. https://doi.org/10.3390/pharmaceutics

Tuomela, M., Malm, M., Wallen, M., Stanescu, I., Krohn, K., & Peterson, P. (2004). Biodistribution and general safety of a naked DNA plasmid, GTU ®-MultiHIV, in a rat, using a quantitative PCR method. https://doi.org/10.1016/j.vaccine.2004.08.004

Turell, M. J., Bunning, M., Ludwig, G. v., Ortman, B., Chang, J., Speaker, T., Spielman, A., McLean, R., Komar, N., Gates, R., McNamara, T., Creekmore, T.,

Farley, L., & Mitchell, C. J. (2003). DNA Vaccine for West Nile Virus Infection in Fish Crows (Corvus ossifragus). Emerging Infectious Diseases, 9(9), 1077. https://doi.org/10.3201/EID0909.030025

Varga, C. M., Tedford, N. C., Thomas, M., Klibanov, A. M., Griffith, L. G., & Lauffenburger, D. A. (2005). Quantitative comparison of polyethylenimine formulations and adenoviral vectors in terms of intracellular gene delivery processes. Gene Therapy, 12(13), 1023–1032. https://doi.org/10.1038/sj.gt.3302495

Veera, V., Satya, N., Lakshmi, A., Pammi, · S V N, Lakshmi Venkata, ·, Priya Bhatraju, K., Lakshmi, ·, & Ruddaraju, K. (n.d.). A Comprehensive Review on Novel Liposomal Methodologies, Commercial Formulations, Clinical Trials and Patents. https://doi.org/10.1007/s12668-022-00941-x

Vij, M., Natarajan, P., Pattnaik, B. R., Alam, S., Gupta, N., Santhiya, D., Sharma, R., Singh, A., Ansari, K. M., Gokhale, R. S., Natarajan, V. T., & Ganguli, M. (2016). Non-invasive topical delivery of plasmid DNA to the skin using a peptide carrier. Journal of Controlled Release, 222, 159–168. https://doi.org/10.1016/j.jconrel.2015.12.017

Wahane, A., Waghmode, A., Kapphahn, A., Dhuri, K., Gupta, A., & Bahal, R. (2020). Role of lipid-based and polymer-based non-viral vectors in nucleic acid delivery for next-generation gene therapy. In Molecules (Vol. 25, Issue 12). MDPI AG. https://doi.org/10.3390/molecules25122866

Wang, X. N., McGovern, N., Gunawan, M., Richardson, C., Windebank, M., Siah, T. W., Lim, H. Y., Fink, K., Li, J. L. Y., Ng, L. G., Ginhoux, F., Angeli, V., Collin, M., & Haniffa, M. (2014). A three-dimensional atlas of human dermal

leukocytes, lymphatics, and blood vessels. Journal of Investigative Dermatology, 134(4), 965–974. https://doi.org/10.1038/jid.2013.481

Wang, Y., Wu, S., Wang, L., Wang, Y., Liu, D., Fu, Y., & Xie, Y. (2022). The Activity of Liposomal Linolenic Acid Against Helicobacter pylori *In Vitro* and Its Impact on Human Fecal Bacteria. Frontiers in Cellular and Infection Microbiology, 12, 865320. https://doi.org/10.3389/FCIMB.2022.865320/BIBTEX

Weisblum, Y., Schmidt, F., Zhang, F., DaSilva, J., Poston, D., Lorenzi, J. C. C., Muecksch, F., Rutkowska, M., Hoffmann, H. H., Michailidis, E., Gaebler, C., Agudelo, M., Cho, A., Wang, Z., Gazumyan, A., Cipolla, M., Luchsinger, L., Hillyer, C. D., Caskey, M., … Bieniasz, P. D. (2020). Escape from neutralizing antibodies by SARS-CoV-2 spike protein variants. ELife, 9, 1. https://doi.org/10.7554/ELIFE.61312

Xie, L., Yang, Y., Meng, J., Wen, T., Liu, J., & Xu, H. (2019). Cationic polysaccharide spermine-pullulan drives tumor associated macrophage towards M1 phenotype to inhibit tumor progression. International Journal of Biological Macromolecules, 123, 1012–1019. https://doi.org/10.1016/J.IJBIOMAC.2018.11.089

Xu, X., Prens, E., Florencia, E., Leenen, P., Boon, L., Asmawidjaja, P., Mus, A. M., & Lubberts, E. (2021). Interleukin-17A Drives IL-19 and IL-24 Expression in Skin Stromal Cells Regulating Keratinocyte Proliferation. Frontiers in Immunology, 12. https://doi.org/10.3389/fimmu.2021.719562

Xue, W., Brentville, V. A., Symonds, P., Cook, K. W., Yagita, H., Metheringham, R. L., Durrant, L. G., Xue, W., Brentville, V. A., Symonds, P., Cook, K. W., Yagita, H., Metheringham, R. L., & Durrant, L. G. (2016). SCIB1, a huIgG1 antibody DNA vaccination, combined with PD-1 blockade induced efficient therapy of poorly immunogenic tumors. Oncotarget, 7(50), 83088–83100. https://doi.org/10.18632/ONCOTARGET.13070

Yang, J.-P., & Huang, L. (1997). Overcoming the inhibitory effect of serum on lipofection by increasing the charge ratio of cationic liposome to DNA. In Gene Therapy (Vol. 4).

Yang, S., Chen, J., Zhao, D., Han, D., & Chen, X. (2012a). Comparative study on preparative methods of DC-Chol/DOPE liposomes and formulation optimization by determining encapsulation efficiency. International Journal of Pharmaceutics, 434(1–2), 155–160. https://doi.org/10.1016/j.ijpharm.2012.05.041

Yang, S., Chen, J., Zhao, D., Han, D., & Chen, X. (2012b). Pharmaceutical Nanotechnology Comparative study on preparative methods of DC-Chol/DOPE liposomes and formulation optimization by determining encapsulation efficiency. International Journal of Pharmaceutics, 434, 155–160. https://doi.org/10.1016/j.ijpharm.2012.05.041

Yang, S. ye, Zheng, Y., Chen, J. yin, Zhang, Q. yang, Zhao, D., Han, D. en, & Chen, X. jing. (2013). Comprehensive study of cationic liposomes composed of DC-Chol and cholesterol with different mole ratios for gene transfection. Colloids and Surfaces B: Biointerfaces, 101, 6–13. https://doi.org/10.1016/J.COLSURFB.2012.05.032

Yang, S.-Y., Zheng, Y., Chen, J.-Y., Zhang, Q.-Y., Zhao, D., Han, D.-E., & Chen, X.-J. (2013). Comprehensive study of cationic liposomes composed of DC-Chol and cholesterol with different mole ratios for gene transfection. Colloids and Surfaces B: Biointerfaces, 101, 6–13. https://doi.org/10.1016/j.colsurfb.2012.05.032

Yang, Y., Chen, Y., Li, D., Lin, S., Chen, H., Wu, W., & Zhang, W. (2023). Linolenic acid conjugated chitosan micelles for improving the oral absorption of doxorubicin via fatty acid transporter. Carbohydrate Polymers, 300, 120233. https://doi.org/10.1016/J.CARBPOL.2022.120233

Yi, W.-J., Zhang, Q.-F., Zhang, J., Liu, Q., Ren, L., Chen, Q.-M., Guo, L., & Yu, X.-Q. (2013). Cyclen-based lipidic oligomers as potential gene delivery vehicles. https://doi.org/10.1016/j.actbio.2013.12.010

Yuba, E., Kojima, C., Sakaguchi, N., Harada, A., Koiwai, K., & Kono, K. (2008). Gene delivery to dendritic cells mediated by complexes of lipoplexes and pH-sensitive fusogenic polymer-modified liposomes. Journal of Controlled Release, 130(1), 77–83. https://doi.org/10.1016/J.JCONREL.2008.05.007

Zakrewsky, M., Kumar, S., & Mitragotri, S. (2015). Nucleic acid delivery into skin for the treatment of skin disease: Proofs-of-concept, potential impact, and remaining challenges. https://doi.org/10.1016/j.jconrel.2015.09.017

Zhang, Z., Mateus, J., Coelho, C. H., Dan, J. M., Moderbacher, C. R., Gálvez, R. I., Cortes, F. H., Grifoni, A., Tarke, A., Chang, J., Escarrega, E. A., Kim, C., Goodwin, B., Bloom, N. I., Frazier, A., Weiskopf, D., Sette, A., & Crotty, S.

(2022). Humoral and cellular immune memory to four COVID-19 vaccines. Cell, 185(14), 2434-2451.e17. https://doi.org/10.1016/j.cell.2022.05.022

Zhao, Z., Ma, X., Zhang, R., Hu, F., Zhang, T., Liu, Y., Han, M. H., You, F., Yang, Y., & Zheng, W. (2021). A novel liposome-polymer hybrid nanoparticles delivering a multi-epitope self-replication DNA vaccine and its preliminary immune evaluation in experimental animals. Nanomedicine: Nanotechnology, Biology and Medicine, 35, 102338. https://doi.org/10.1016/j.nano.2020.102338

Zhdanov, R. I., Podobed, O. v, & Vlassov, V. v. (n.d.). Cationic lipid-DNA complexes-lipoplexes-for gene transfer and therapy. Retrieved May 2, 2024, from www.elsevier.com/locate/bioelechem

Zheng, L. I., Bandara, S. R., Tan, Z. I., & Leal, C. (2023). Lipid nanoparticle topology regulates endosomal escape and delivery of RNA to the cytoplasm. https://doi.org/10.1073/pnas

Zhigaltsev, I. v., & Cullis, P. R. (2023). Morphological Behavior of Liposomes and Lipid Nanoparticles. Langmuir, 39(9), 3185–3193. https://doi.org/10.1021/acs.langmuir.2c02794

Zou, Y., Zhou, Q., Zhao, Y., Zhi, D., Chen, H., Wang, R., Ju, B., & Zhang, S. (2022). Structure-activity relationships of pH-responsive and ionizable lipids for gene delivery. International Journal of Pharmaceutics, 617, 121596. https://doi.org/10.1016/j.ijpharm.2022.121596